

### **5.0 Synthesis of SPSBR Membrane, its Composites and Applications**

Available literature on proton exchange membrane synthesis show that the polymers used in synthesizing alternative membrane to Nafion<sup>®</sup> are either in powder or crystal form with low viscosity and high solubility in common organic solvents (Mokrini and Acosta, 2001; Smitha et al, 2003; Kim et al, 2003; Gao et al, 2003; Xing et al, 2004; Chen et al, 2004; Blackwell and Maurtiz, 2004; Jelcic et al, 2005; del Rio et al, 2005; Sangeetha, 2005). In this present study, polystyrene-butadiene rubber (PSBR), which is a copolymer of butadiene and styrene, combining both thermoplastic and rubbery phases, is selected for sulphonation to produce proton exchange membrane. PSBR is one of the most versatile copolymer rubber compounds in the world today (Karbochem report, 2007), with high molecular weight, and due to its excellent abrasion resistance and under a well tailored degree of sulphonation, is expected to yield PEM of good ion conductivity with low and acceptable methanol crossover suitable for fuel cell application. PSBR rubber has high viscosity compared to the powder/crystal polymer, making it difficult to control the sulphonation reaction. Therefore it is necessary to conduct a preliminary investigation into this rubber to confirm its viability as an alternative polymer for proton exchange membrane synthesis. The preliminary investigation conducted on this rubber included testing of: solubility of the rubber in different solvents, effect of weight of rubber on degree of sulphonation, choice of sulphonating agents and effect of stirring speed on the sulphonation reaction. Other factors such as: effects of concentration of the sulphonating agent, sulphonation time and sulphonation temperatures were investigated. The synthesized membrane was then blended with carbon nanoballs to produce polystyrene butadiene rubber-CNBs composite membrane with the aim of improving its qualities for fuel cell applications. This section, therefore, presents the results and discussion of results of various investigations conducted on the composite membrane

synthesis from polystyrene butadiene rubber and carbon nanoballs for proton exchange membrane fuel cell application.

### **5.1 Preliminary investigation**

Sulphonation is an important process that can be used to render polymers proton conductive and hydrophilic in nature. The sulphonation of inexpensive and locally available polymer PSBR was conducted using different sulphonating agents such as: sulphuric acid, fuming sulphuric acid, mixture of fuming sulphuric acid and sulphuric acid, acetylsulphate and chlorosulphonic acid as sulphonating agents to determine which of them would be suitable for the sulphonation of PSBR. Also investigated was the solubility of the polymer in different solvents, the effect of the weight of the polymer, stirring speed and sulphonation time on the degree of sulphonation. Results obtained for various analyses on the sulphonated rubber are reproducible.

#### **5.1.1 Solubility of PSBR**

Prior to the sulphonation process, PSBR was dissolved in different solvents. The results obtained are presented in Table 5.1 and indicate that PSBR is insoluble in polar aprotic solvents such as Dimethyl formamide (DMF), Dimethyl acetate (DMAc) and Dimethyl sulphoxide (DMSO). Among the chlorinated solvents listed in Table 5.1, PSBR is only soluble in  $C_2H_4Cl_2$  and shows partial solubility at high temperature ( $< 120\text{ }^\circ\text{C}$ ) to others. The solubility of Sulphonated Polystyrene Butadiene Rubber (SPSBR) in different solvents was also investigated and the results are shown in Table 5.1. SPSBR also shows solubility with  $C_2H_4Cl_2$  and  $CDCl_3$  and at a high temperature ( $< 120\text{ }^\circ\text{C}$ ) it is soluble in  $CH_2Cl_2$ . The solubility differences between the PSBR and SPSBR can be attributed to the sulphonic acid group introduced to the polymer, which causes changes in the polarity

of the polymers and intermolecular forces relating to the hydrogen bond (Gao et al., 2003). Therefore,  $C_2H_4Cl_2$  was the solvent chosen for the dissolution of the rubber, because of its strong affinity with the rubber, and also because of its availability and reasonable cost, while  $CDCl_3$  was used to dissolve the sulphonated samples for  $^1H$ NMR analysis.

Table 5.1: Solubility of PSBR and SPSBR

Polymer	DMF	DMAc	DMSO	$CHCl_3$	$CH_2Cl_2$	$C_2H_4Cl_2$	PE	$C_8H_{10}$	$CDCl_3$
<b>PSBR</b>	-	-	-	±	±	+	-	±	±
<b>SPSBR</b>	-	-	±	±	+Δ	+	-	±	+

Soluble (+); insoluble (-); soluble at high temperature (+Δ); swelling or partially soluble (±), PE = Petroleum Ether

### 5.1.2 Choice of sulphonating agents

Different sulphonating agents such as concentrated sulphuric acid, fuming sulphuric acid, trimethylsilyl chlorosulphonate, sulphur trioxide-triethyl phosphate complex, chlorosulphonic acid (Zonquo et al, 2006) and acetyl sulphate (Smitha et al, 2003) have been used to carry out the sulphonation process on polymer materials. The selection of working sulphonating agents depends strictly on their compatibility with the polymer in question, their film forming property and the mechanical strength of the resulting sulphonated polymer (Smitha et al, 2003). Amongst these agents, concentrated sulphuric acid, chlorosulphonic acid and acetylsulphate have been employed especially for polymers with aryl backbones where the  $SO_3H$  group is attached to the aromatic ring (Smitha et al, 2003). Table 5.2 shows the results of different sulphonating agents employed in this research in terms of sulphonation time, degree of sulphonation and ion exchange capacity.

Table 5.2: Effects of sulphonating agents and sulphonation time on the degree of sulphonation

	<b>Sulphonating Agents</b>							
	<b>ClSO<sub>3</sub>H</b>		<b>H<sub>2</sub>SO<sub>4</sub></b>		<b>F-HSO<sub>4</sub>H</b>		<b>H/F (60/40) (%)</b>	
<b>Time (hrs)</b>	4	12	4	12	4	12	4	12
<b>Sc (%)</b>	0.37	0.80	0.17	0.31	0.33	0.63	0.04	0.19
<b>DS (%)</b>	7.65	16.12	3.37	6.17	6.57	12.64	0.79	3.77
<b>IEC (mmol/g)</b>	0.463	1	0.213	0.338	0.413	0.788	0.05	0.238

Where: ClSO<sub>3</sub>H = chlorosulphonic acid; H<sub>2</sub>SO<sub>4</sub> = sulphuric acid; F-H<sub>2</sub>SO<sub>4</sub>H = fuming sulphuric acid; H/F = mixture sulphuric acid and fuming sulphuric acid; Sc = Sulphur content; DS = degree of sulphonation and IEC = ion exchange capacity.

Table 5.2 continued

	<b>Sulphonating Agents</b>			
	<b>H/F (40/60) (%)</b>		<b>AcSO<sub>4</sub>H</b>	
<b>Time (hrs)</b>	4	12	4	12
<b>Sc (%)</b>	0.10	0.27	0.18	0.55
<b>DS (%)</b>	1.98	5.37	3.57	11.02
<b>IEC (mmol/g)</b>	0.125	0.388	0.225	0.688

Where: H/F = mixture of sulphuric acid and fuming sulphuric acid; AcSO<sub>4</sub>H = acetylsulphate; Sc = Sulphur content DS = degree of sulphonation and IEC = ion exchange capacity.

The results as presented in Table 5.2 show that PSBR has an affinity for all the sulphonating agents investigated, though some are more promising than others. In an equimolar amount (1.4 M/ml) of acids used for the sulphonation of PSBR at a constant stirring speed of 1000 rpm, a mixture of sulphuric acid and fuming sulphuric acid at ratio

60/40 and 40/60 (%) exhibited the lowest sulphur content ( $< 0.3\%$ ), DS ( $< 6\%$ ) and IEC ( $< 0.39\text{ mmol/g}$ ). This is followed by sulphuric acid, which also exhibited low sulphur content, degree of sulphonation and ion exchange capacity both at a short and prolonged time of sulphonation, probably due to hydrolytic desulphonation (Nobuhiru and Rogers, 1992; Daoust et al, 2001). Acetylsulphate and fuming sulphuric acid used at prolonged time of sulphonation demonstrated a relatively high value of DS, ie.11.02 and 12.64 % with IEC of 0.6875 and 0.7875 mmol/g, respectively. On the other hand, chlorosulphonic acid demonstrated the highest values of sulphur content, DS and IEC (0.80 %, 16.12 % and 1 mmol/g). This result therefore promotes chlorosulphonic acid as a sulphonating agent of choice for PSBR sulphonation since an appreciable amount and degree of sulphonation is crucial for the proton conductivity of the resulting polymer for proton exchange membrane (Zongwu et al, 2006, 2006; Larminie and Dicks, 2000)

### 5.1.3 FT – IR and $^1\text{HNMR}$ studies

In a bid to validate the choice of sulphonating agent and to confirm that  $\text{SO}_3\text{H}$  groups are present as a result of sulphonation,  $^1\text{HNMR}$  and FT-IR analysis were conducted and the results are presented in Figures 5.1 and 5.2. Figure 5.1 shows the  $^1\text{HNMR}$  spectra of different sulphonating agents, all the spectra indicating that all sulphonating agents investigated showed affinity for PSBR. The hump appearing between 4 and 5 ppm indicates the presence of sulphonic acid linkage on the aromatic phenyl ring which is lacking in the unsulphonated sample. The characteristically sharp peaks of the sulphonated as opposed to unsulphonated samples are the result of the influence of the acid group grafted on the polymer matrix. The strong deshielding effect of the phenyl ring serves to shift the protons bonded to it to very low fields in the region between 7 – 7.5 ppm. The deshielding effect of carbon-carbon double bond can be observed at 2 ppm,

while C = C proton at 1.70 ppm. As a result of a negligible neighbouring centre, the end chain methyl peaks appear at the position of a high field (0.23 - 0.88 ppm), which exhibited four bands of reduced intensity as against three – proton bands, possibly due either to the effect of the acid (Biemark et al, 1963) or the proton's resonance effect. Peaks at 2.30 ppm are attributed to the C<sub>6</sub>H<sub>5</sub> protons, while peaks at 1.30 ppm occur because of the CH<sub>2</sub> protons. But the peaks between 5 – 6 ppm should deshield the values of some typical terminal methylene groups of proton (Biemark et al, 1963). More importantly, the effect of the sulphonic acid linkage on the aromatic phenyl ring results in a new peak between 4 – 5 ppm; this is not present in the unsulphonated sample, thus confirming the successful attachment of the acid group on the polymer.

Figure 5.2 is the IR spectra of the synthesized membranes with respect to choice of sulphonating agent. All the spectra also show that the array of sulphonating agents investigated is able to sulphonate PSBR. The weak peak inside the rectangular box on each of the spectra represents the O-H vibration from the sulphonic acid group upon sulphonation. The changes in the combination vibrations around 1800 – 1650 cm<sup>-1</sup> (finger band) characterize the phenyl group (Mokrini and Acosta, 2001). The peak identified in the spectra between 1350 cm<sup>-1</sup> and 1360 cm<sup>-1</sup> correspond to the asymmetric stretching of S=O. The vibration of the phenyl ring, substituted with a sulphonated group and sulphonate anion attached to the phenyl ring, results in the absorbance between 950 and 1126 cm<sup>-1</sup> respectively in all the sulphonated spectra.



Figure 5.1:  $^1\text{H}$ NMR of different sulphonating agents: 1= unsulphonated; 2 = fuming sulphuric acid; 3= sulphuric acid; 4 = fuming sulphuric/sulphuric acid; 5 =acetylsulphate; 6 = chlorosulphonic acid

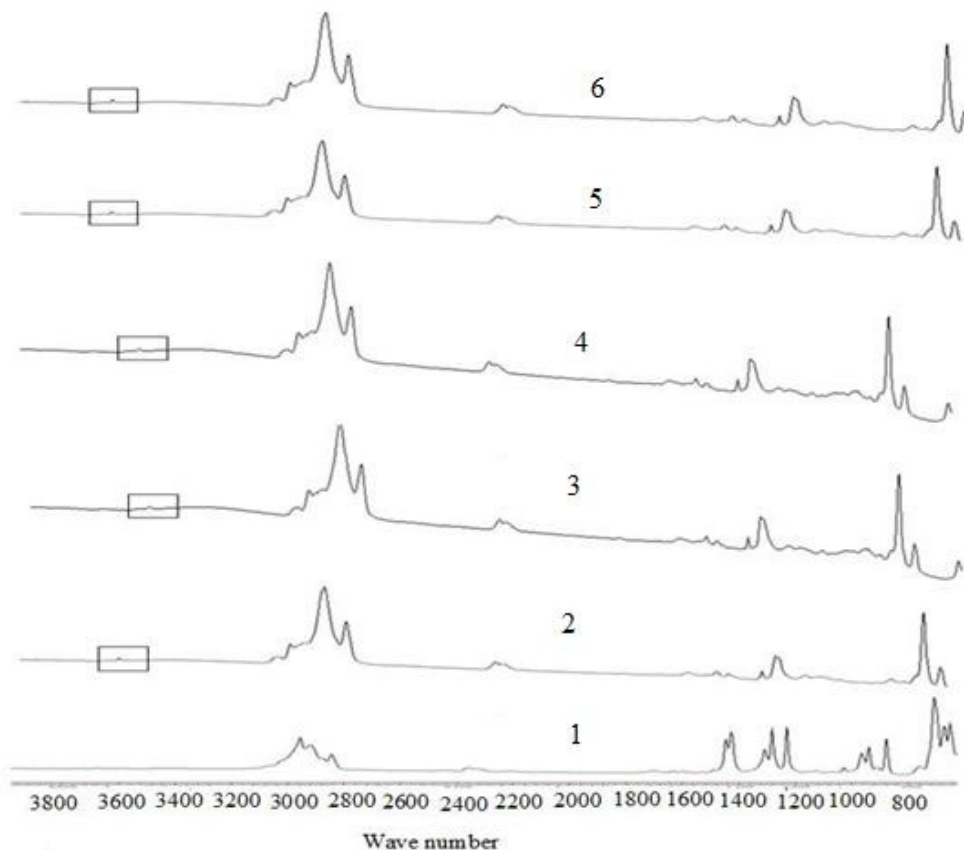


Figure 5.2: IR spectra of different sulphonating agents; 1= unsulphonated; 2 = fuming sulphuric acid; 3 = sulphuric acid; 4 = fuming sulphuric/sulphuric acids; 5 = acetylsulphate; 6 = chlorosulphonic acid

#### 5.1.4 Effect of the weight off polymer and sulphonation time

After the choice of chlorosulphonic acid as the sulphonating agent, the next task is to determine the weight of rubber that will produce a good degree of sulphonation; hence it is of paramount importance to investigate the effect of the weight of the polymer on the degree of sulphonation. The sulphur contents of the SPSBR at various weights of the polymer and sulphonation time and constant concentration of sulphonating agent and stirring speed were studied using an elemental analyzer. The results obtained revealed

the presence of sulphur in the SPSBR, which also confirms that the polymer was sulphonated by the sulphonating agent used. The low percentage of sulphur obtained in the samples can be attributed to the low concentration of acid used for sulphonation. The percentage of sulphur content in the SPSBR was used to evaluate the ion exchange capacity and degree of sulphonation of the polymer using equations 3.1 and 3.2 respectively.

Ion exchange capacity is the number of milli-equivalent of ions in 1g of the dry polymer; it is also used to calculate the degree of sulphonation of the polymer. In this work, the ion exchange capacity of the SPSBR is calculated from the sulphur content obtained by elemental analysis. It can be observed from Table 5.3 that the sulphonation time and weight of the polymer used at a constant concentration of acid affected the ion exchange of the sulphonated polymer. As the sulphonation time increases, the ion exchange capacity character of the SPSBR also increases 10 g PSBR giving maximum IEC values of 0.63mmol/g. Though the result obtained reveals low values of ion exchange capacity for the SPSBR, it is nevertheless an indication of the presence of the acid group in the polymer matrix. The acid group changes the property of the polymer from insulator to conductor, and thus gives it the power to conduct proton. The lower ion exchange capacity is also necessary to keep the quality of the membrane, i.e. reduce the swelling of the membrane, which occurs in a more stable membrane.

Table 5.3: Effect of sulphonation time and weight of polymer rubber on the ion exchange capacity of the sulphonated rubber at constant stirring speed of 1000 rpm

<b>Ion Exchange Capacity (IEC) (mmol/g) of Dry Membrane</b>						
<b>T (h)</b>	<b>5 g</b>	<b>10 g</b>	<b>15 g</b>	<b>20 g</b>	<b>25 g</b>	<b>30 g</b>
2	0.15	0.24	0.23	0.21	0.17	0.15
4	0.18	0.30	0.26	0.23	0.20	0.20
6	0.19	0.36	0.33	0.28	0.26	0.24
8	0.21	0.50	0.39	0.36	0.31	0.27
10	0.23	0.63	0.46	0.43	0.38	0.34

The degree of sulphonation, which indicates the average number of sulphonic groups that are present in the sulphonated polymers, was also investigated, using the results of the ion exchange capacity. The results, presented in Table 5.4, show a low degree of sulphonation due to a low concentration of acid used. A low concentration of acid was chosen for the purpose of the preliminary investigation of the polymer sulphonation and also to prevent the polymer from becoming soluble in water. Extensive sulphonation could lead to high solubility in water and a soluble membrane is mechanically weak and is not good for fuel cell applications (Xu, 2005; Sangeetha, 2005). Results obtained also show that the ratio of weight of polymer to acid (w/v) and sulphonation time affect the degree of sulphonation. As the sulphonation time increases, it in turn increases the degree of sulphonation, and as the weight of polymer increases, the degree of sulphonation decreases. As such the maximum degree of sulphonation (10.48 %) was achieved with 10 g PSBR in 10 hours of sulphonation and a constant stirring speed (1000rpm). The percentage increase of the degree of sulphonation between 10 and 30 g of polymer considered is of appreciable value, ie, of approximately 53 %. The results in Table 5.4 further reveal that an increase in degree of sulphonation with time increases the viscosity of the sulphonated rubber.

Table 5.4 Effect of sulphonation time and weight of polymer rubber on the degree of sulphonation and viscosity of the sulphonated rubber

Degree of Sulphonation (DS) (%) and Inherent Viscosity												
T	5g		10 g		15 g		20 g		25 g		30 g	
	DS	$\eta$	DS	$\eta$	DS	$\eta$	DS	$\eta$	DS	$\eta$	DS	$\eta$
2	2.39	0.36	3.86	0.41	3.70	0.41	3.37	0.39	2.72	0.37	2.39	0.36
4	2.88	0.37	4.85	0.49	4.19	0.42	3.70	0.41	3.21	0.38	3.21	0.38
6	3.04	0.37	5.85	0.53	5.35	0.51	4.52	0.43	4.19	0.42	3.86	0.41
8	3.37	0.39	8.23	0.61	6.36	0.57	5.85	0.55	5.02	0.46	4.36	0.44
10	3.70	0.41	10.48	0.66	7.54	0.63	7.03	0.62	6.19	0.50	5.52	0.46

Where T = time in hrs; DS = degree of sulphonation in % and  $\eta$  = inherent viscosity in dl g<sup>-1</sup>

### 5.1.5 FT – IR and <sup>1</sup>H NMR studies

The weak broad band that appears in sulphonated polystyrene butadiene rubber (SPSBR) spectra at 3573 cm<sup>-1</sup>, as shown in Figure 5.3, represents the O-H vibration from the sulphonic acid group upon sulphonation which increases with an increase in DS. The peak identified in the spectra at 1346 Cm<sup>-1</sup> is due to the asymmetric stretching of the S=O band. The symmetric vibration of this bond affects the characteristic splint at 1309 – 1235 cm<sup>-1</sup> which also confirms the attachment of the sulphonic group. The peaks identified at 2846, 2919 and 3027 cm<sup>-1</sup> for both the PSBR and SPSBR are the bands for C-H, C-C and C=C, while the aromatic C=C and C-C were identified at 1649 and 1494 cm<sup>-1</sup> respectively (Biemark et al, 1963; Silverstein et al 1991). No significant change was observed at 700 and 759 cm<sup>-1</sup> within the region of the -C-H, which is out of plane deformation that indicates a reaction substitution type, probably due to the low concentration of acid. It suffices to note that the sharp band at 1450 cm<sup>-1</sup>, which is unique to PSBR, was reduced to a broad peak after sulphonation. This reduction increases with DS. This is attributed to the interaction of the sulphonic group that has been introduced, by reducing the C-H bending vibration intensity of the polymer chain and thereby promoting the appearance of a new peak at 1403 cm<sup>-1</sup>. Thus the results of the FT-IR

analysis clearly show the occurrence of sulphonation through the presence of the sulphonate group on the SPSBR.

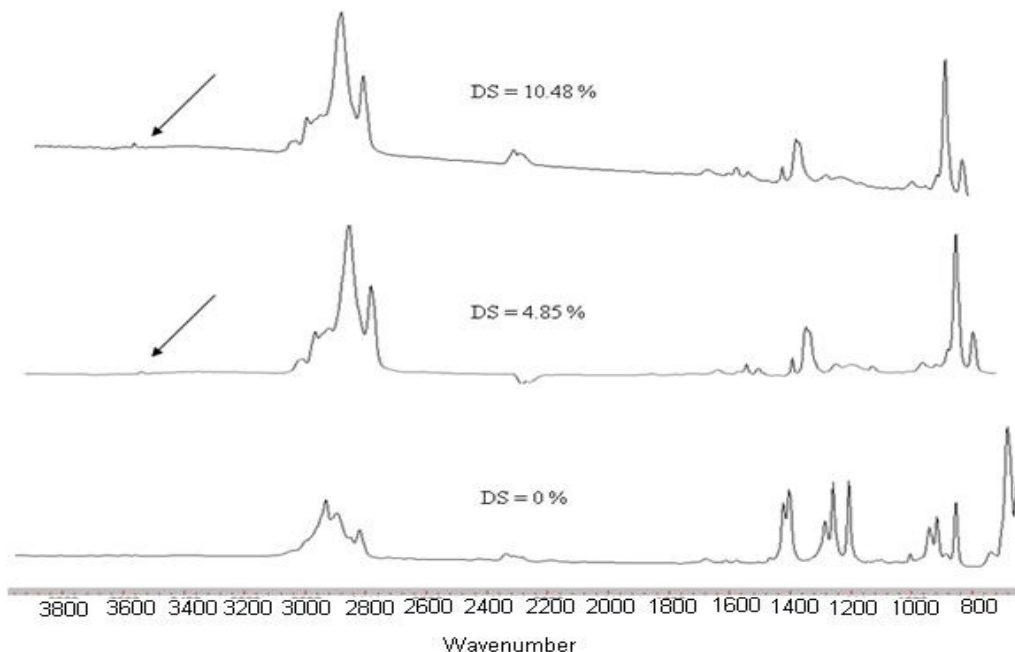


Figure 5.3: FT-IR spectra of: Unsulphonated PSBR and Sulphonated PSBR at different of degree of sulphonation

The  $^1\text{H}$  NMR spectra shown in Figure 5.4 indicate that there is no significant change in the signals at 7.3 and 7.6 ppm for the SPBR, representing an aromatic proton (Idibie, 2009). The only hump appearing between 4 and 5 ppm indicates the presence of sulphonic acid linkage on the aromatic benzene ring, confirming that the substitution is limited to the para-position of the phenyl ring (Nobuhiro and Roger, 1994). The increase in chemical shift (7.16 to 7.24) in the aromatic protons range is observed in the case of the SPSBR. This can be attributed to the stronger electron attracting the force of the sulphonic acid group (Idibie, 2009).

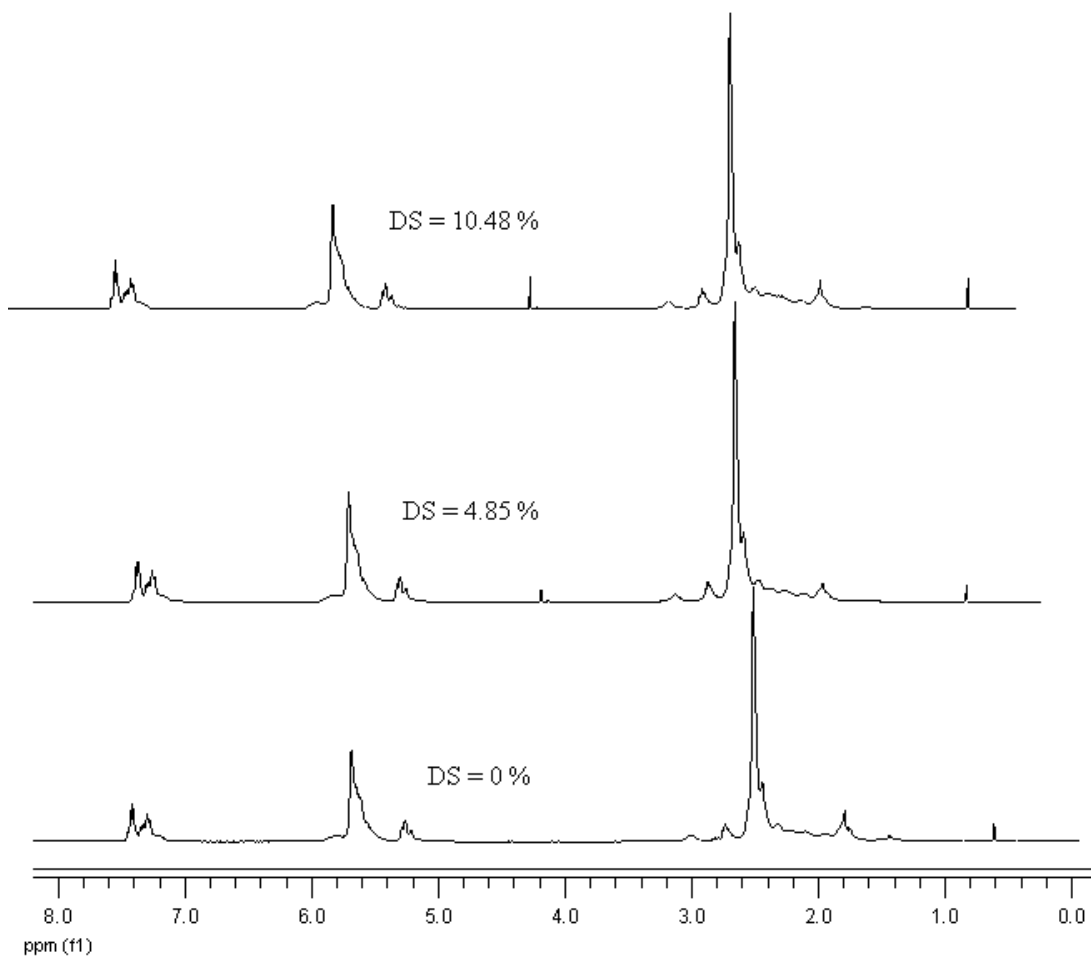


Figure 5.4:  $^1\text{H}$ NMR spectra of: Unsulphonated PSBR and Sulphonated PSBR

## 5.2 Optimization of Membrane Synthesis

In order to optimize the membrane synthesis, various factors such as: stirring speed, concentrations of sulphonating agent, sulphonation time, and sulphonation temperature were investigated. Results obtained as presented below show that each of these parameters influence the qualities of the membrane synthesized.

### 5.2.1 Effect of concentration of acid on the sulphonation of PSBR

The effects of acid concentration (0.4 – 2.0 M/ml) on DS and IEC at a constant sulphonation time of 10 hours, weight of PSBR of 10 g and stirring speed of 1000rpm were investigated and the results are presented in Table 5.5. Results from the table show

that IEC and DS increased with an increase in the acid concentration until 1.6 M/ml before the polymer experienced a decrease in IEC and DS at 1.8 and 2.0 M/ml respectively. The decrease in DS at a higher concentration of acid (above 1.6 M/ml) can be attributed to the high viscosity of rubber which tends to reduce its affinity for the sulphonating agent. A higher concentration of acid also resulted in scission and chemical degradation of the polymer chain (Xing et al., 2004) as shown in Figure 5.5, with the resulting consequence of a limited site for SO<sub>3</sub>H. The relationship between the optimum IEC and DS together with viscosity is illustrated in Figure 5.6.

Table 5.5: Effect of acid concentration on DS and IEC

Conc.	0.4	0.6	0.8	1.0	1.2	1.4	1.6	1.8	2.0
S <sub>c</sub>	1.32	1.76	2.27	2.35	2.49	2.88	3.68	3.39	3.13
IEC	0.412	0.552	0.711	0.735	0.779	0.903	1.150	1.062	0.977
DS	6.73	9.13	11.92	12.34	13.13	15.39	20.04	18.35	16.76

Where Conc. = Concentration (mol); S<sub>c</sub> = Sulphur content (%); IEC = Ion exchange capacity (mmol/g); DS = Degree of sulphonation (%)

Figure 5.6 indicates that the degree of sulphonation that the content of the acid groups presents in the polymer matrix is proportional to the ion exchange capacity, which in turn is proportional to the inherent viscosity of the resulting SPSBR. As IEC increases from 0.412 – 1.15 mmol/g, the DS correspondingly increases from 6.73 – 20.04 %. Since IEC is dependent on acid concentration (Zonquo et al, 2006), this implies that, as the ion exchange capacity increases, more of the SO<sub>3</sub>H group is attached to the polymer matrix, which will serve to increase the polymer hydrophilicity and promote proton mobility and conductivity of the resulting membrane (Zonguo et al, 2006; Smitha et al, 2003). In a bid to confirm the earlier claim during the preliminary investigation that DS influenced the

viscosity of the SPSBR, further tests were conducted on the SPSBR at different DS, as a result of the change in the concentration of the sulphonating acid.

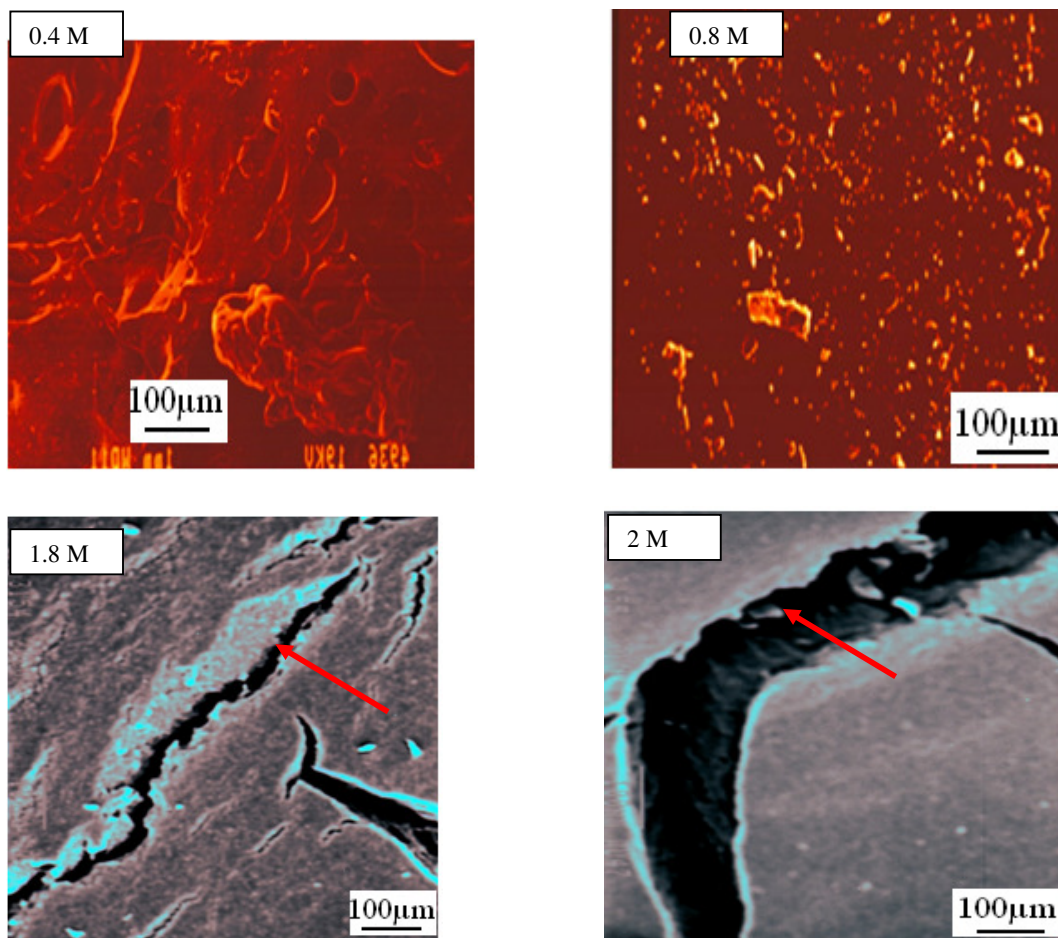


Figure 5.5: Effects of acid concentration on the morphology of the membrane

The effect of the DS on viscosity of SPSBR as shown in Figure 5.6 reveals that the increase in the DS increases the viscosity of the polymer. The DS value ranges from 6.73 – 20.04 % and thus increases the inherent viscosity from 0.58 – 0.8 dl/g. This is due to an increase in hydrogen– bonding interactions associated with the sulphonic acid group within the polymer matrix thereby increasing polymer viscosity. This result is also an indication that within the range of the DS studied, the polymer chain is not broken down

during the sulphonation process (Gao et al, 2003), but that it rather increases the polymer molecular weight.

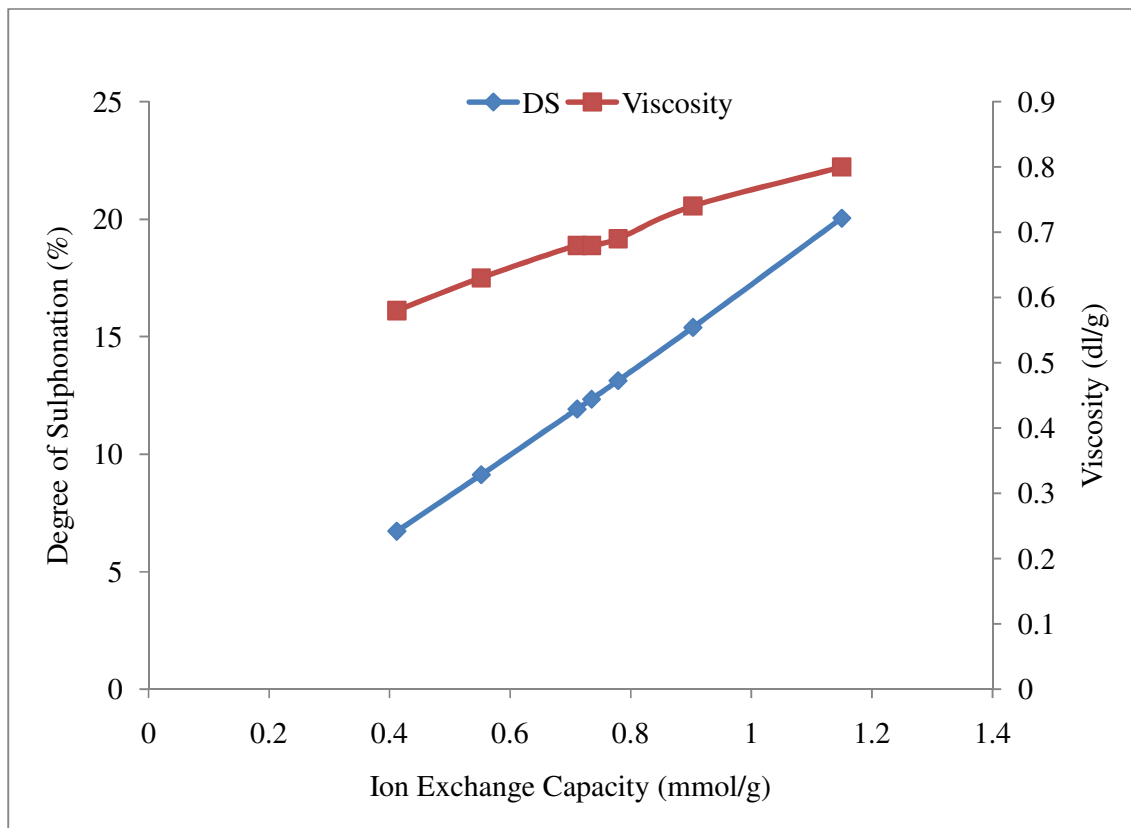


Figure 5.6: Relationship between ion exchange capacity, degree of sulphonation and viscosity

### 5.2.2 Effect of stirring speed

The effect of the stirring speed on the sulphonation of PSBR was investigated using the Heidolph MR3002 dual plate machine (ordered from Germany). This study is aimed at investigating the mass transfer behaviour of the sulphonic group on the aromatic ring of the sulphonated PSBR under a sulphonation time of 10 hrs and acid concentration of 1.6 M/ml. The dual plate is generally calibrated from 100 – 1500 rpm. Effects of stirring

speed on degree of sulphonation and ion exchange capacity of the PSBR are depicted in Figure 5.7

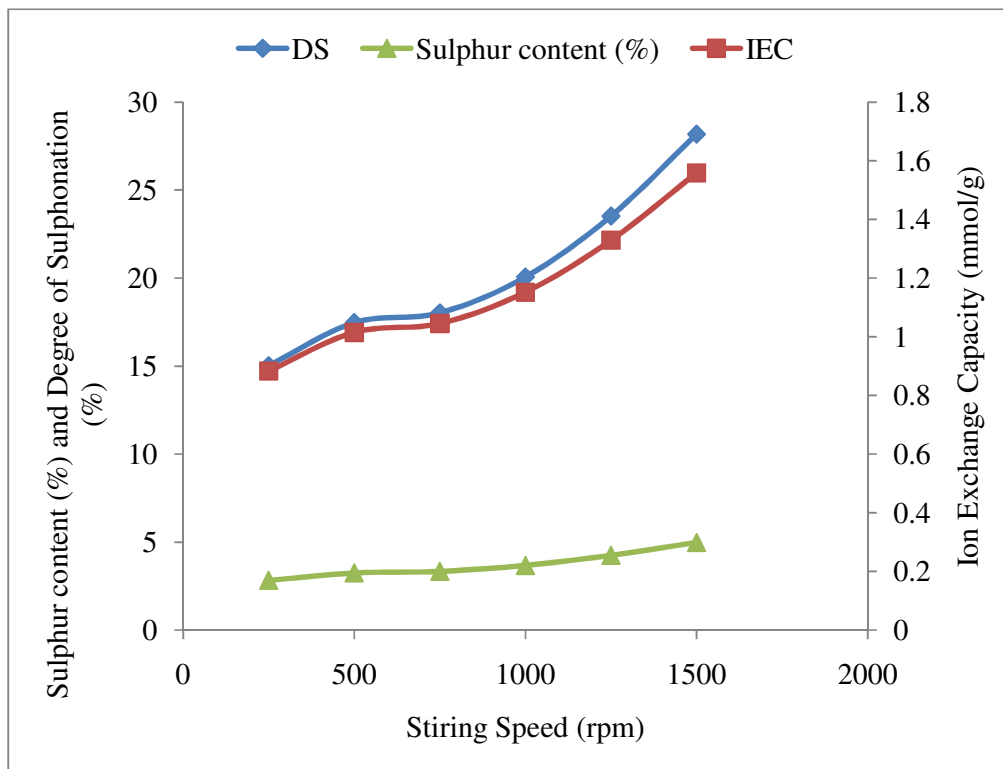


Figure 5.7: Effect of stirring speed on sulphonation of PSBR

The results as shown in Figure 5.7 reveal that the stirring speed is also a vital factor in the sulphonation of PSBR, as both degrees of sulphonation and ion exchange capacity increase with an increase in stirring speed. The graph clearly shows that there is a linear increase in degree of sulphonation and ion exchange capacity as the stirring speed increases until 1250 rpm before a very steep rise at 1500 rpm indicating that a high stirring speed favours the sulphonation reaction of PSBR. Figure 5.7 also shows the sulphur content in the sulphonated PSBR matrix deduced via elemental analysis together with the DS and IEC. The increase in DS and IEC as the stirring speed increases could be due to an increase in the rate of  $\text{SO}_3\text{H}$  distribution to the phenyl ring. This encourages

the sulphonation reaction of PSBR to proceed in a desired direction and to maintain a uniform distribution of  $\text{SO}_3\text{H}$  group, thus discouraging its local concentration that could in turn lead to polymer chain scission. Therefore a very high stirring speed of 1500 rpm is essential in the sulphonation of PSBR. Due to mechanical constraints, the stirring speed could not increase further.

### 5.2.3 Effect of time on sulphonation of PSBR

The effects of a sulphonation time at a constant weight of polymer (10 g), concentration of acid (1.6 M/ml) and stirring speed of 1500 rpm on the sulphonation of PSBR are presented in Figure 5.8. The result shows that an optimum time of sulphonation is needed during the sulphonation reaction of PSBR to achieve its optimum IEC and DS. The results in Figure 5.8 show the initial values of IEC and DS to be 0.784 mmol/g and 13.22 %, which increase with the time of sulphonation with an optimum realization of IEC value of 2.074 mmol/g and DS value of 39.38% in 24 hrs. If continued for more than 24 hrs, there is a steep decrease in both the IEC and DS values, and the progress after 36 hours is slow. This is an indication that prolonging the sulphonation time is unfavourable to PSBR, leading to a possible breakdown of the polymer chain with a reduction of the available site of attachment for the  $-\text{SO}_3\text{H}$  group and hence a decrease in the IEC and DS of the SPSBR.

The inherent viscosity of SPSBR as a function of time is also measured and the result is presented in Figure 5.9, showing that the viscosity of SPSBR is also dependent on the sulphonation time. It can be observed from Figure 5.9 that the best sulphonation time of 24 hrs gives a maximum value of 39.38 % of DS and 1.61 dl/g of inherent viscosity. Beyond 24 hrs of sulphonation time, the rubber is observed to decrease in DS and

inherent viscosity, where 36 hrs gives DS of 23.45 % with viscosity of 0.95 dl/g and 48 hrs gives 22.93% of DS and 0.84 dl/g of viscosity, respectively. Therefore, the sulphonation time of 24 hours is found to be favourable for PSBR sulphonation.

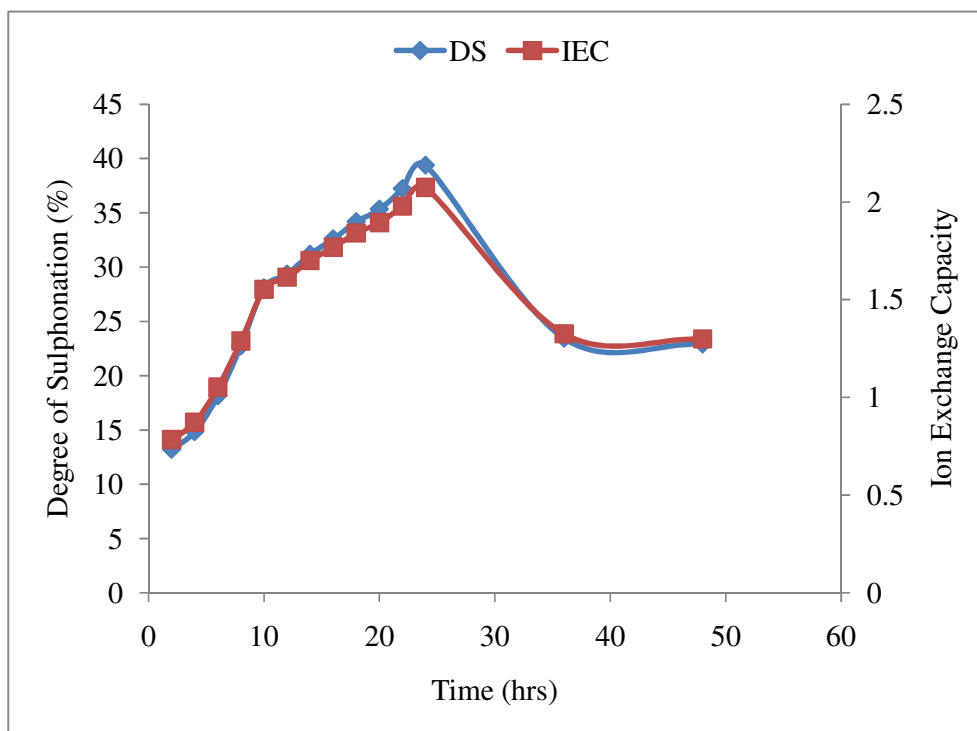


Figure 5.8: Effect of sulphonation time on IEC and DS

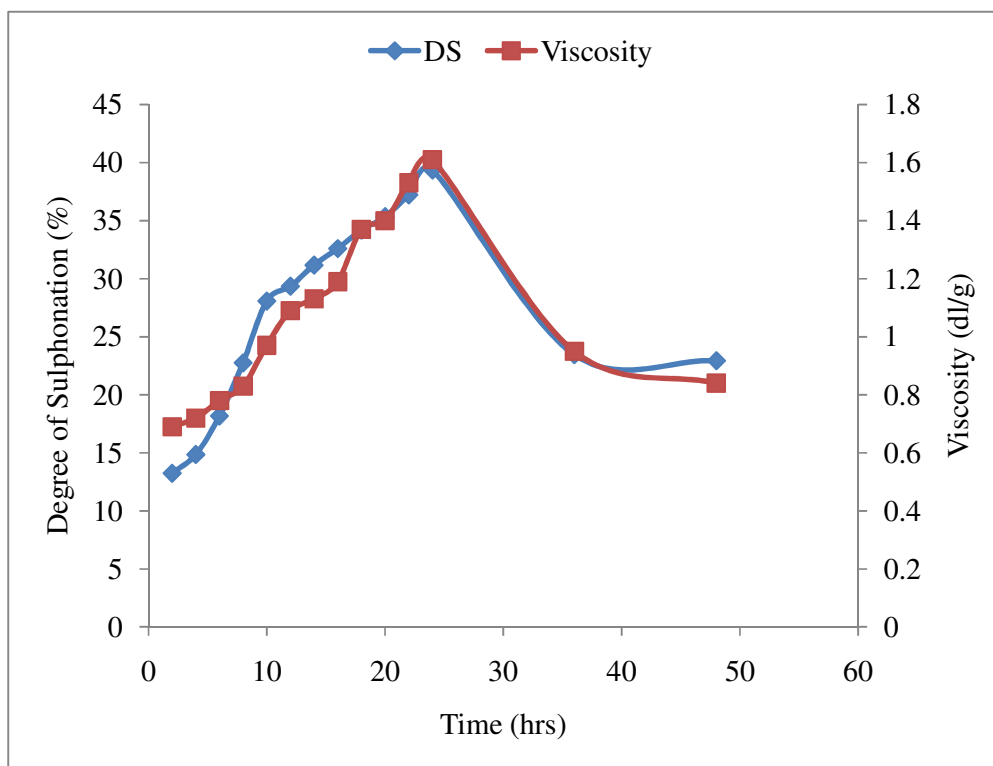


Figure 5.9: Degree of sulphonation and viscosity as a function of optimum reaction time

Figure 5.10 represents the effects of DS and IEC on the viscosity of SPSBR. The higher inherent viscosity values are achieved with an increase in sulphonation time over the initial viscosity of 0.28dl/g for the unsulphonated rubber.

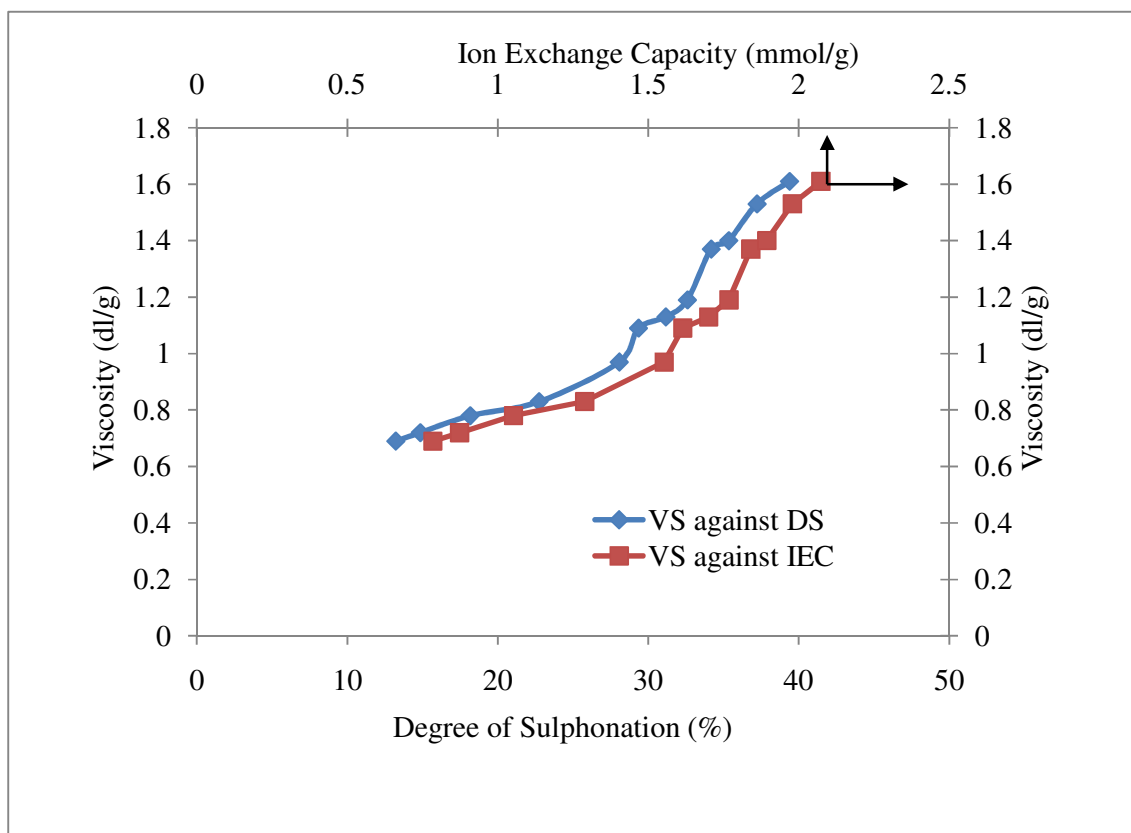


Figure 5.10: Effects of DS and IEC on viscosity of SPSBR

The high degree of sulphonation achieved as a result of increasing the sulphonation time is not due to an increase in molecular weight, but rather an increase in the ion content of the polymer solution. It can be seen in Figure 5.10 that increases in IEC led to an increase in the viscosity of the sulphonated polymer. This concept has also been investigated by Nazan's study of the synthesis and characterization of polyimides (2001), in which he discovered that the increase in viscosity is due to the increase in ion content of the polymer solution and not the molar mass increase.

**5.2.3.1 FT- IR analysis of effect of time on SPSBR**

The FT-IR Spectroscopy spectra on the effect of sulphonation time on DS as a function of sulphonation time on PSBR are shown in Figure 5.11. The weak band's at  $3573\text{ cm}^{-1}$  represent the O-H vibration from the sulphonic acid group upon sulphonation, which are slightly intensified with the sulphonation time. The bands appearing on the spectra at  $1364\text{ cm}^{-1}$  are attributed to the asymmetric stretching of S=O which show a gradual increase in intensity with time. The symmetric vibration of this bond affects the characteristic splint at  $1309 - 1200\text{ cm}^{-1}$ . As the DS increases with time, the symmetric and asymmetric stretching vibration resulting from the S=O group between  $1500 - 900\text{ cm}^{-1}$  increases significantly, while simultaneously increasing the intensity of the aromatic C=C and C-C at  $1649$  and  $1494\text{ cm}^{-1}$  and that of the non-aromatic at  $2846$  and  $2919\text{ cm}^{-1}$ , respectively. It is interesting to note the reduction on the sharp band at  $1500\text{ cm}^{-1}$  after sulphonation.

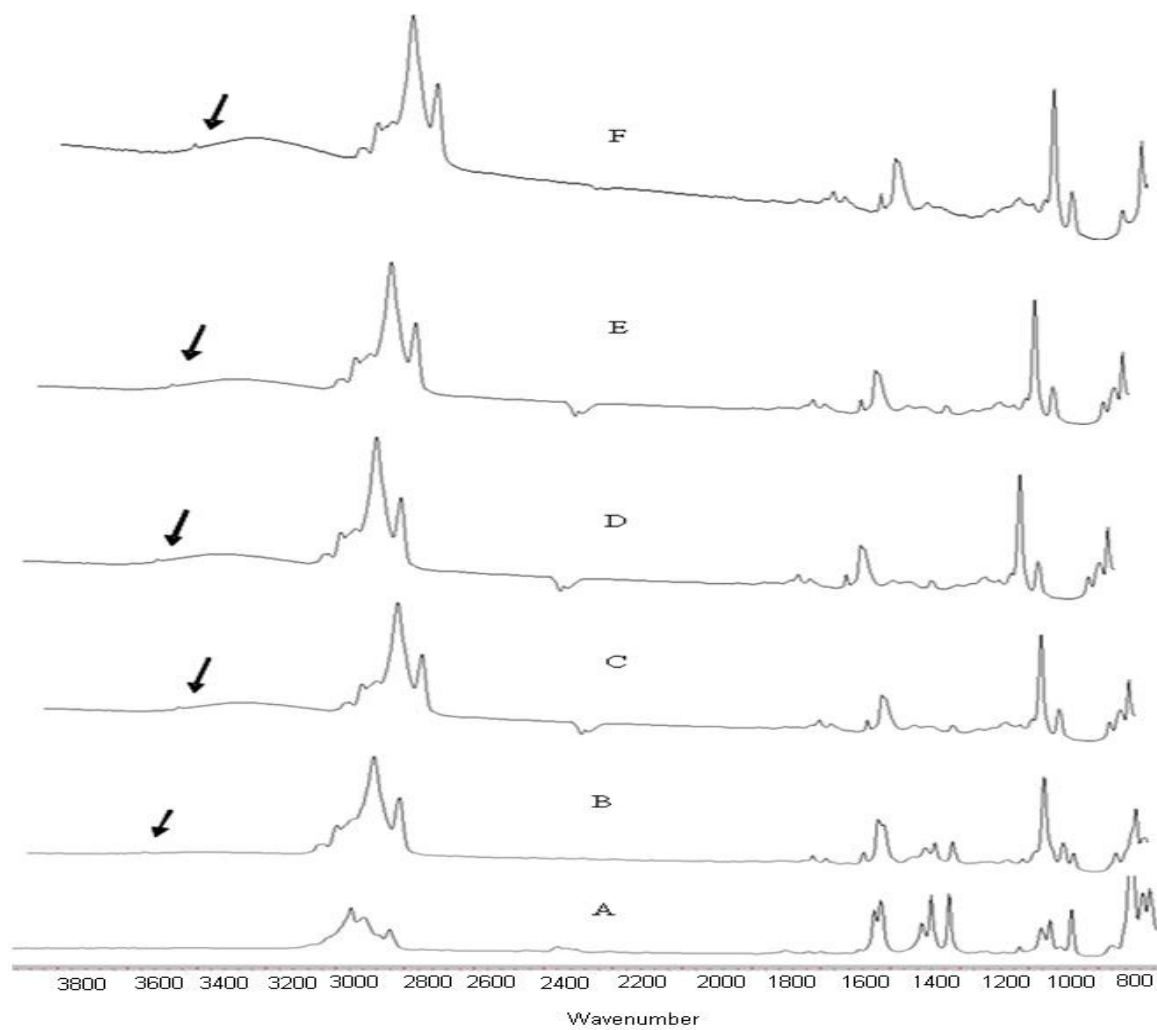
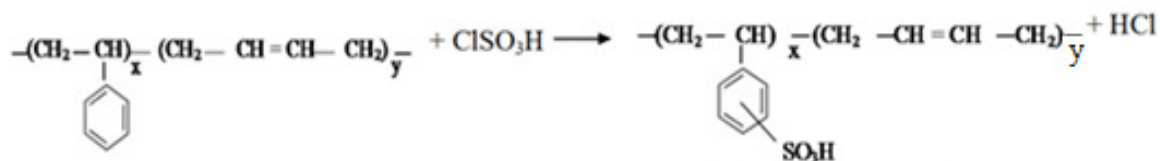


Figure 5.11: IR spectra of SPSBR where A = 0 hr; DS = 0 %, B = 8 hrs = 22.74 %, C = 10 hrs; DS = 28.07 %, D = 20 hrs; DS = 35.34 %, E = 22 hrs; DS = 37.23 %, F = 24 hrs; DS = 39.38 %

### 5.2.4 Effect of temperature on sulphonation of PSBR

Figures 5.12 and 5.13 respectively plot the IEC and DS at various temperatures. It can be observed from both figures that both the IEC and DS are influenced by the sulphonation temperature. Therefore, the graph of DS as a function of time at different temperatures, as shown in Figure 5.12, represents the sulphonation kinetics of polystyrene butadiene rubber in chlorosulphonic acid. The sulphonation kinetics in chlorosulphonic acid was measured at four constant temperatures (22°C, 35°C, 55°C and 75°C). The sulphonation reaction between polystyrene butadiene rubber and chlorosulphonic acid is shown in Scheme 5.1



Scheme 5.1: Sulphonation reaction of polystyrene butadiene rubber (Idibie, 2009)

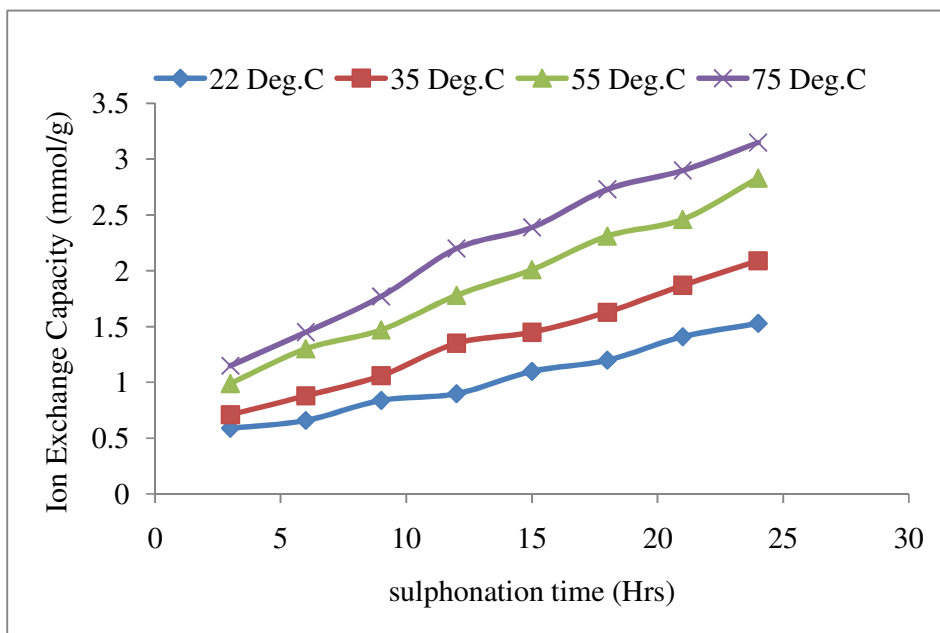


Figure 5.12: Effects of temperature on IEC of the sulphonated rubber

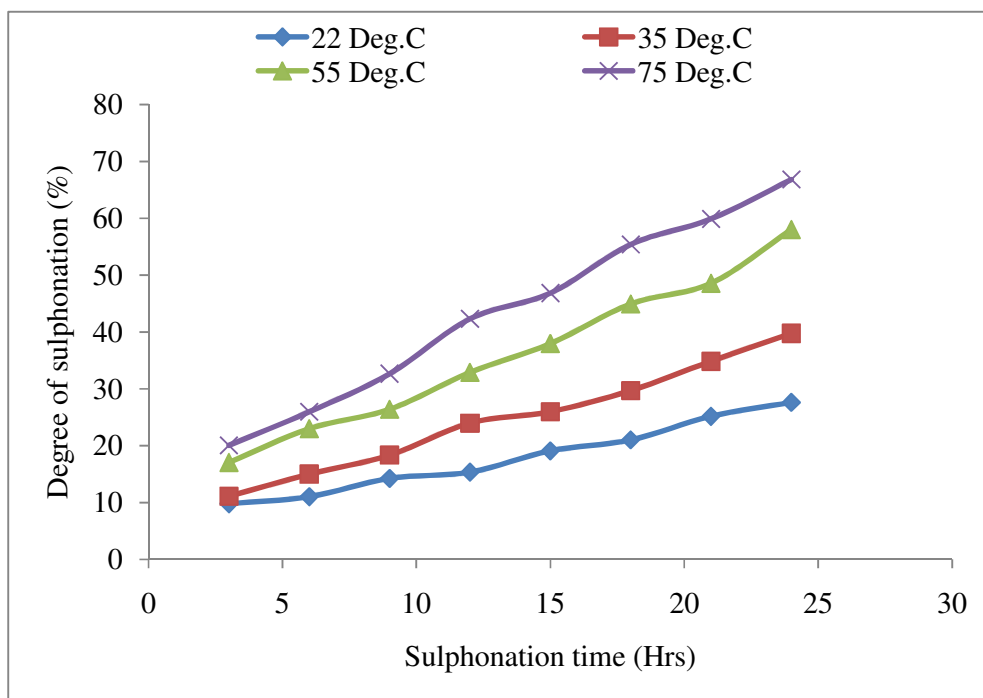


Figure 5.13: Effects of temperature DS on sulphonated rubber

Sulphonation is an electrophilic substitution reaction and the electron density of the active site of the phenyl ring determined the site for substitution, as detailed in Idibie (2009). Hence the sulphonation of polystyrene butadiene rubber takes place in the phenyl group. The phenyl ring has five equal positions for sulphonation with only one of the five protons on the ring being substituted as shown in scheme 5.1. According to the reaction scheme, there is the possibility of only one  $-SO_3H$  attaching itself to each of the repeating units; it is also possible that the  $-SO_3H$  group attached to the other ring at a higher temperature. The first possibility of substitution was considered in this study, because the substitution takes place at a low temperature.

### 5.3 Blending of SPBR with carbon nanoballs

One of the objectives of this research is to improve the quality (proton conductivity, water uptake, solvent uptake, porosity to solvent, thermal stability and fuel crossover) of the membrane synthesized from the locally available polystyrene butadiene rubber by blending it with carbon nanoparticles. Carbon nanoballs produced by non catalytic method is the nanoparticles of choice for the blend. 10 g of sulphonated polystyrene butadiene rubber was mixed with various quantities (0.1g, 0.2g, 0.3g and 0.4g) of carbon nanoballs to improve its qualities as a proton exchange membrane. High purity, low porosity and low degree of graphitization (low electrical conductivity) favour the choice of carbon nanoballs produced by the non-catalytic method.

The catalyst plays a major role in the production of carbon nanoparticles and ferrocene; the latter iron precursor is the catalyst employed in this work for carbon nanoparticles synthesis. It should be noted, however, that although the catalyst aids the growth of carbon nanoparticles, it also results in the formation of impurities on the carbon nanoparticles. Hence there is the need to remove the catalyst particles from the carbon nanoparticles before these can be used for any application. The common route for removing the catalyst impurities produced along with the carbon nanoparticles is to dissolve the particles in concentrated acid. The purification process usually results in the structural damage of carbon nanoparticles, and not all the catalyst remains present as the impurities are removed. Non usages of catalyst in the synthesis of carbon nanoballs ascertain the purity of the carbon nanoballs. CHN analysis of the carbon nanoballs also revealed that the materials contained 98% carbon and the remaining 2% comprised of hydrogen and trace amounts of oxygen. Apart from the effect of the purification process on the quality of the carbon nanoparticles, the membrane fortified with carbon nanoballs

will be used in Proton Exchange Membrane Fuel Cell (PEMFC). The by-products of the oxidation-redox reaction in the cell are heat and water, as shown in equations 1.1-1.3. Iron in the presence of water and air results in the formation of ferrous hydroxide ( $\text{Fe}(\text{OH})_2$ ), as shown in Equation 5.1 (Odigure et al, 2003):



The ferrous hydroxide is unstable in an oxygenated solution and it undergoes further oxidation to produce hydrated iron or rust as shown in Equation 5.2 (Odigure et al, 2003):



It can be deduced from Equations 5.1 and 5.2 that if iron is present in the carbon nanoballs blended with the membrane, there will be resultant rusting of the cell components. Another reason for favoring the choice of carbon nanoballs as nanoparticles for the blending is the low porosity exhibited by the synthesized carbon nanoballs. The surface area analysis of the carbon nanoballs is  $15\text{m}^2/\text{g}$ , which indicates that they had little or no porosity. The TEM image of the carbon nanoballs shown in Figure 4.5 indicates that only nanoballs of uniform diameter (average diameter = 150 nm) were produced and employed for the blending. Also, the carbon nanoballs used for the blending have a low degree of graphitization, which prevents the short circuiting of the cell. At a low degree of graphitization, carbon nanoballs exhibit poor electrical conductivity, hence blending the synthesized membrane with carbon nanoballs will only improve the qualities of the membrane. The effect of the carbon nanoballs on the water uptake, porosity, morphology, thermal stability and proton conductivity of the membrane were investigated and the results are presented.

## 5.4 Characterization of the Synthesized Membrane

Membranes synthesized from polystyrene butadiene using chlorosulphonic acid as the sulphonating agent were characterized to determine the physical, thermal and chemical properties of the sulphonated membrane. Various characterizations conducted on the synthesized membrane are presented below.

### 5.4.1 Morphological study of SPBR and SPSBR using SEM

Figure 5.14 shows the morphology of the unsulphonated and sulphonated rubber, using the AJSM 840 scanning electron microscope (SEM). It can be seen from Figure 5.14a that the unsulphonated rubber possesses a very porous and coarse morphology with irregular and large size domain which is typical of unsulphonated PSBR before modification and reduced significantly after modification. It can be observed from Figures 5.14 that the morphology of PSBR changes as DS increases from a porous base material to a dense material. The enhancement in the size of pores after sulphonation is revealed, and at high DS, pores become more adequate, appearing to have a uniform distribution throughout the membrane (Figure 5.14c and d), and thus ensuring a desirable and efficient proton conductivity (Smitha et al, 2003). The large number of pores as shown in Figure 5.14 on the surface of sulphonated PSBR is a promising indication of a large interfacial area between the hydrophobic and hydrophilic interface (Kreuer, 2001).

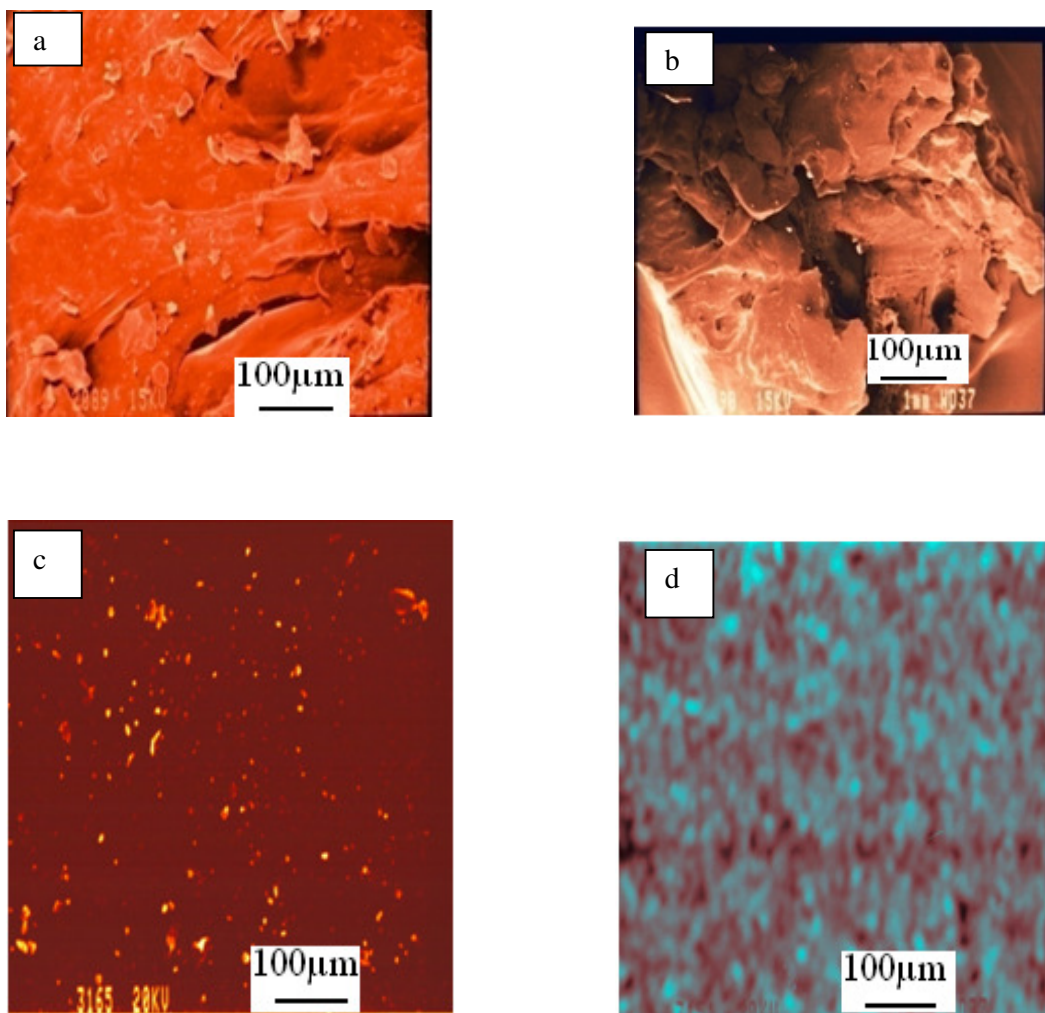


Figure 5.14: SEM images of (a) unsulphonated and (b) DS = 2.31% (c) DS = 7.54 % (d) DS = > 10 %

Carbon nanoballs were used as the proton conductive reinforcing material to produce SPSBR/CNBS composite membrane for proton exchange membrane. The morphology of the composite membranes at various mass of carbon nanoballs is presented in Figure 5.15. It can be seen from the Figure 5.15 that the CNBs are uniformly dispersed within the membrane, and that, as the mass of carbon nanoballs blended with the membrane increases, the denser the membrane becomes. The uniform distribution of the CNBs on the membrane can be attributed to the electrostatic force of attraction between the sulphonic group and CNBs. The average particles diameters in the polymer-CNBs

composite are in the ranges of 50-100nm. The particle size of dispersed CNBs on the synthesized membrane increases with the increase in the mass of CNBs blended with the polymer membrane.

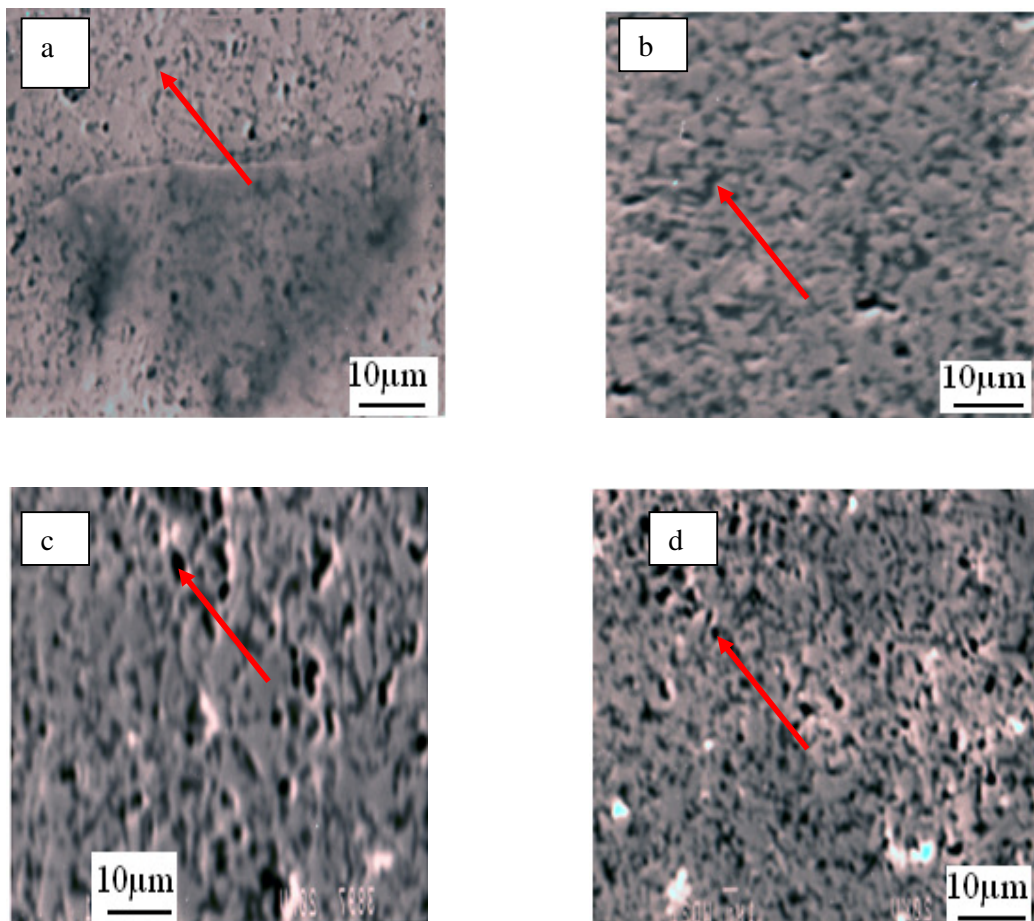


Figure 5.15: Morphology of sulphonated polystyrene butadiene rubber blended with carbon nanoballs (a) mass of CNBs = 0.1g, (b) mass of CNBs = 0.2g, (c) mass of CNBs = 0.3g and (d) mass of CNBs = 0.4g

In Figure 5.16, the cross sectional micrograph of the prepared composite membranes are shown as a function of mass of CNBs. It can also be seen here that the CNBs were not only distributed on the surface of the sulphonated rubber, but also inside the membrane pores.

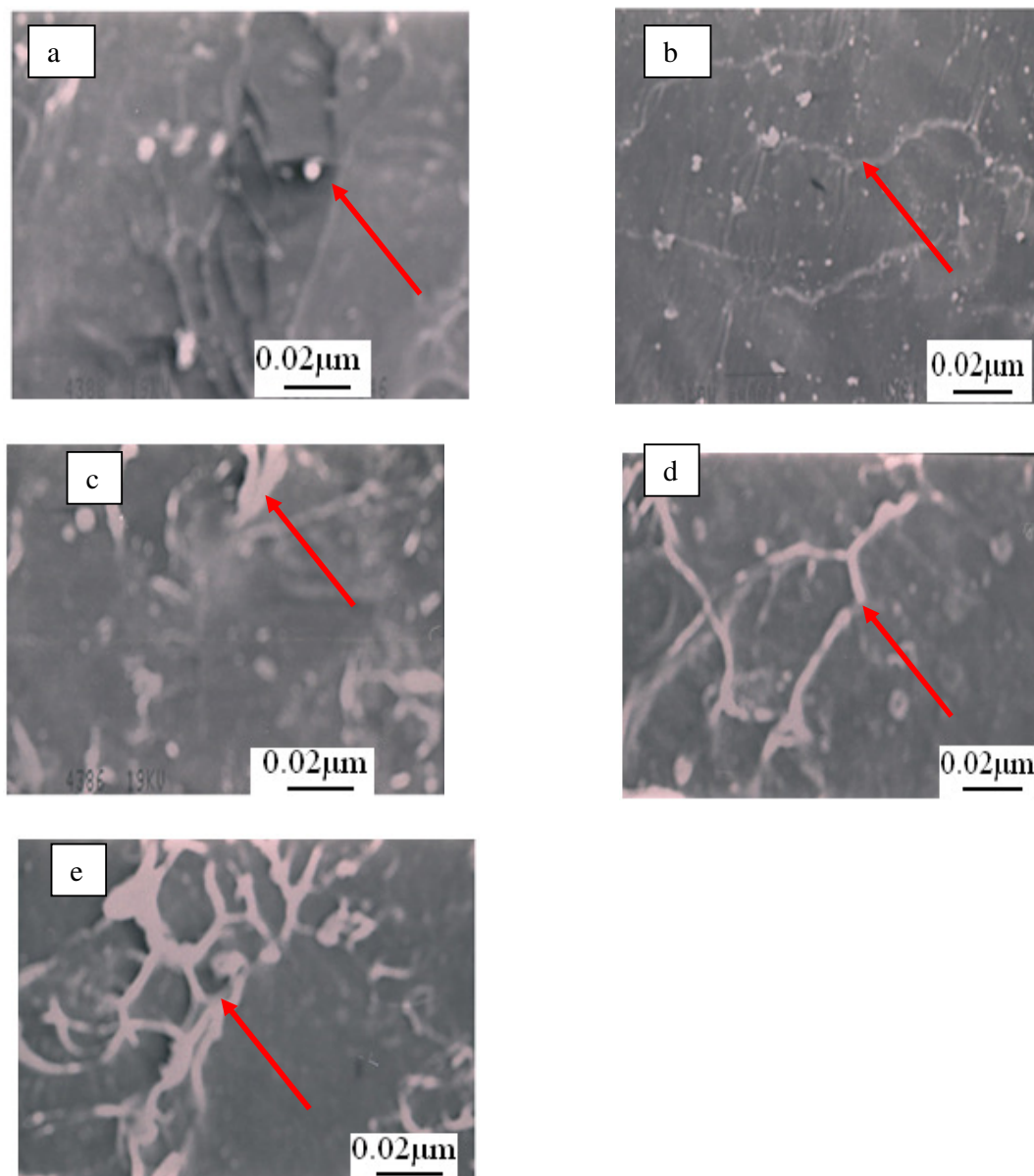


Figure 5.16: SEM micrographs of the composite membrane (a) non-blended membrane (mass of CNBs = 0g) (b) mass of CNBs = 0.1g, (c) mass of CNBs = 0.2g (d) mass of CNBs = 0.3g and (e) mass of CNBs = 0.4g)

The CNBs particles are located in the polymer cluster because of the smaller size of the CNBs when compared to that of polymer. Therefore the CNBs are entrapped in the polymer cluster which will result in an increase in the proton conducting property of the

composite membrane. The charge passage through the percolated sponge-like microstructure supplies the transport channels as shown in Figures 5.16 (Haubold et al, 2001). The affinity of the  $\text{SO}_3\text{H}$  group with the CNBs is further strengthened as the CNBs significantly aggregated the  $\text{SO}_3\text{H}$  group molecules thereby forming a net working ring, especially as the amount of CNBs used in the composite membranes increases. This is the phenomenon that will therefore improve the quality of the resulting membrane, and especially its ionic or proton conductivity.

#### **5.4.2 Problem of brittleness with SPSBR**

The PSBR was found to exhibit element of brittleness after its casting into a thin film. This could be associated with the plastic domain of the polymer, as polystyrene often exhibits crosslink characteristics. But, in a well tailored degree of sulphonation, the brittleness is resolved: it reduces as DS increases until it is completely overcome. It is therefore inferred that as increasing DS reduces the porous and coarse nature of the starting polymer to a dense polymer material, its mechanical property is correspondingly enhanced. At  $\text{DS} > 2.5 \%$  membrane brittleness was completely overcome up to DS of 55 % (Figure 5.17a – c); however the membrane showed signs of brittleness again at the highest DS ( $\text{DS} > 55 \%$ ), although with the highest level of ionic conductivity. Since PEM is required to balance the conductivity property with the mechanical properties, the membrane with a  $\text{DS} > 55 \%$  is considered unfit for proton exchange membrane fuel cell.

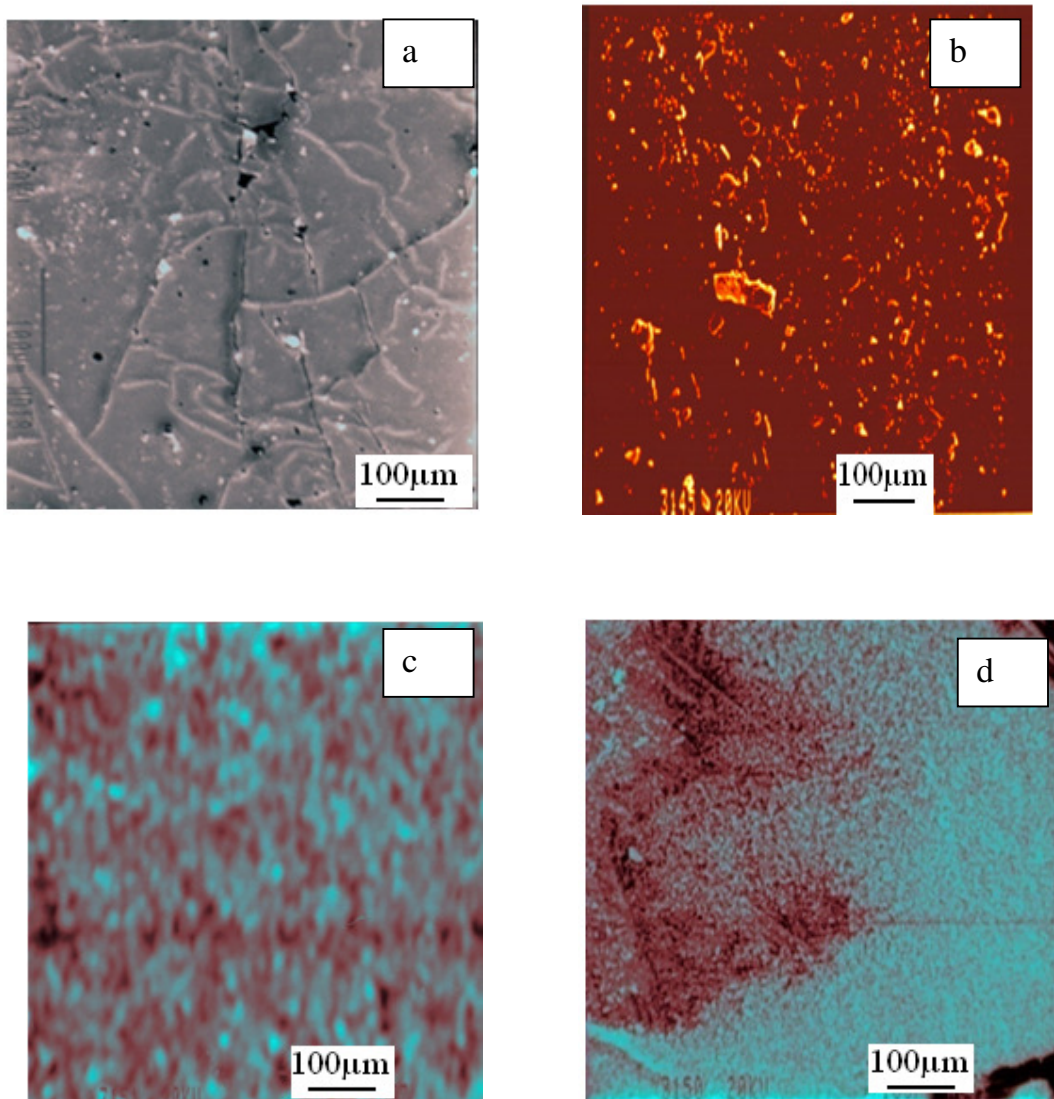


Figure 5.17: SEM images of (a) DS < 2.5 %; (b) DS = > 7 %; (c) DS = > 10 %; (d) DS > 55 %, respectively.

### 5.4.3 THERMAL STABILITY

The major factor militating against the use of Nafion<sup>®</sup> (the readily commercial available membrane in hydrogen fuel cell applications) is its thermal stability which, is in the ranges of 120-150°C. Consequently, this factor limits the operating temperature of fuel cell to about 80°C. The hydration of Nafion<sup>®</sup> must be high enough to give the membrane

sufficient conductivity; limiting the operating temperature to 80°C prevents the membrane from drying out. The difference between the ambient and operating temperature, therefore, makes it difficult to utilize the heat generated by the electrochemical reaction in hydrogen fuel cell (Ogaji et al, 2006). If the operating temperature of hydrogen fuel cells can be raised, the problems associated with heat generation/utilization and the current system will be solved. Therefore, the latest technology for the membrane development in hydrogen fuel cells application is aimed at synthesizing a mechanically stable membrane that can withstand a high temperature at low cost. In this work, differential scanning calorimeter (DSC), thermo gravimetric analysis (TGA) and differential thermal analysis (DTA) were used to analyze the thermal stability of the unsulphonated and sulphonated polystyrene butadiene rubber. Effects of concentrations of sulphonating agent, sulphonation time and degree of sulphonation on the thermal stability of the rubber were investigated and the results obtained were presented. Also the theoretical values of the degree of sulphonation were calculated from the TGA curves, on the assumption that the difference between the decomposition temperature ranges for the unsulphonated and sulphonated rubber is the result of the sulphonic group attached to the styrene group.

Because of the need for aqueous proton conductivity and the fact that Nafion<sup>®</sup> has a relatively low glass transition temperature ( $T_g \approx 110^\circ\text{C}$ ) (Yang et al, 2004) when it is hydrated, it is difficult to operate fuel cells at a high temperature as elucidated earlier. It is therefore important that the synthesized membrane has a higher glass transition temperature. The curves shown in Figures 5.18 and 5.19 reveal that polystyrene butadiene rubber is a highly thermo stable polymer with a glass transition temperature ( $T_g$ ) of about 198°C.  $T_g$  which is the temperature at which the polymer becomes brittle

on cooling and soft on heating, and is taken as the point of inflexion on the slope change of DSC curve. This implies that the styrene group where the  $\text{SO}_3\text{H}$  attached after sulphonation becomes weak and consequently results in the degradation of the group from the main chain (Gu et al, 2006). DSC curves show that  $T_g$  of the sulphonated membrane is in the range of  $201\text{-}224^\circ\text{C}$ , depending on the sulphonation time and degree of sulphonation. The final peak on the curve represents the final scission of the main chain of the membrane which is in the range of  $360 - 363^\circ\text{C}$  for sulphonated and unsulphonated rubber.

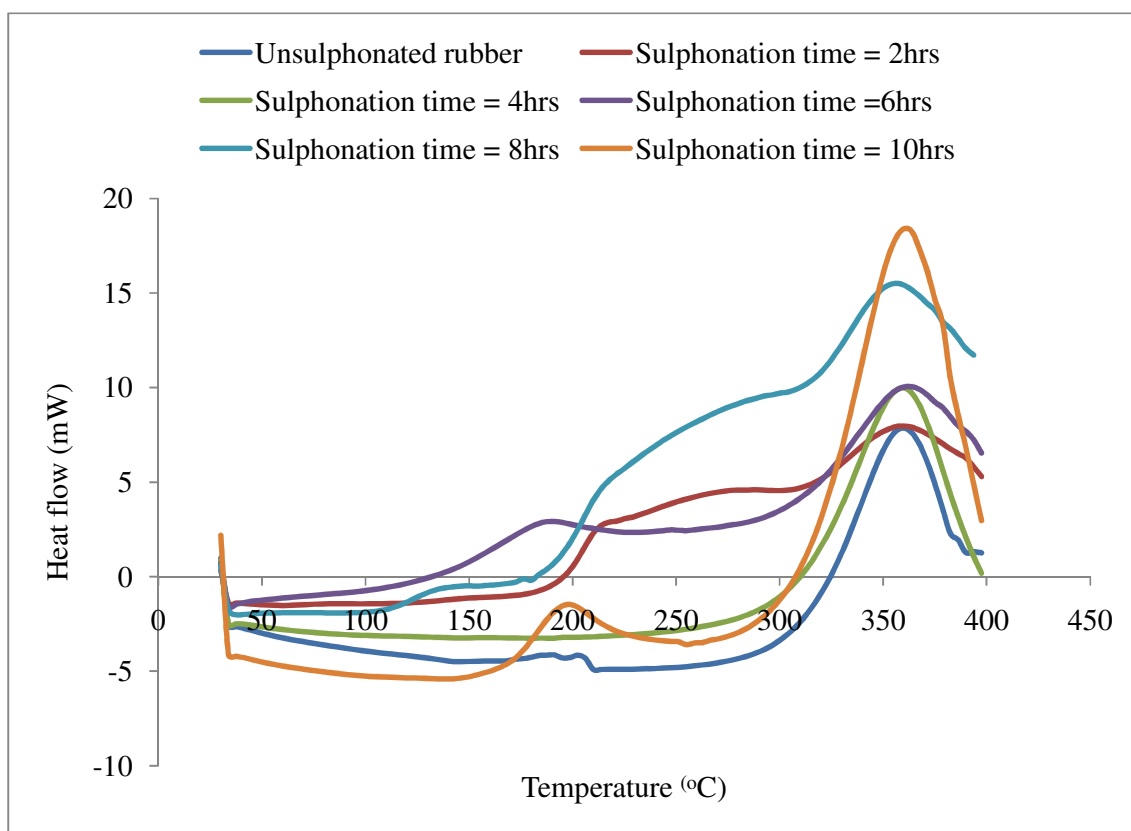


Figure 5.18: DSC curves of the unsulphonated and sulphonated rubber at different sulphonation time.

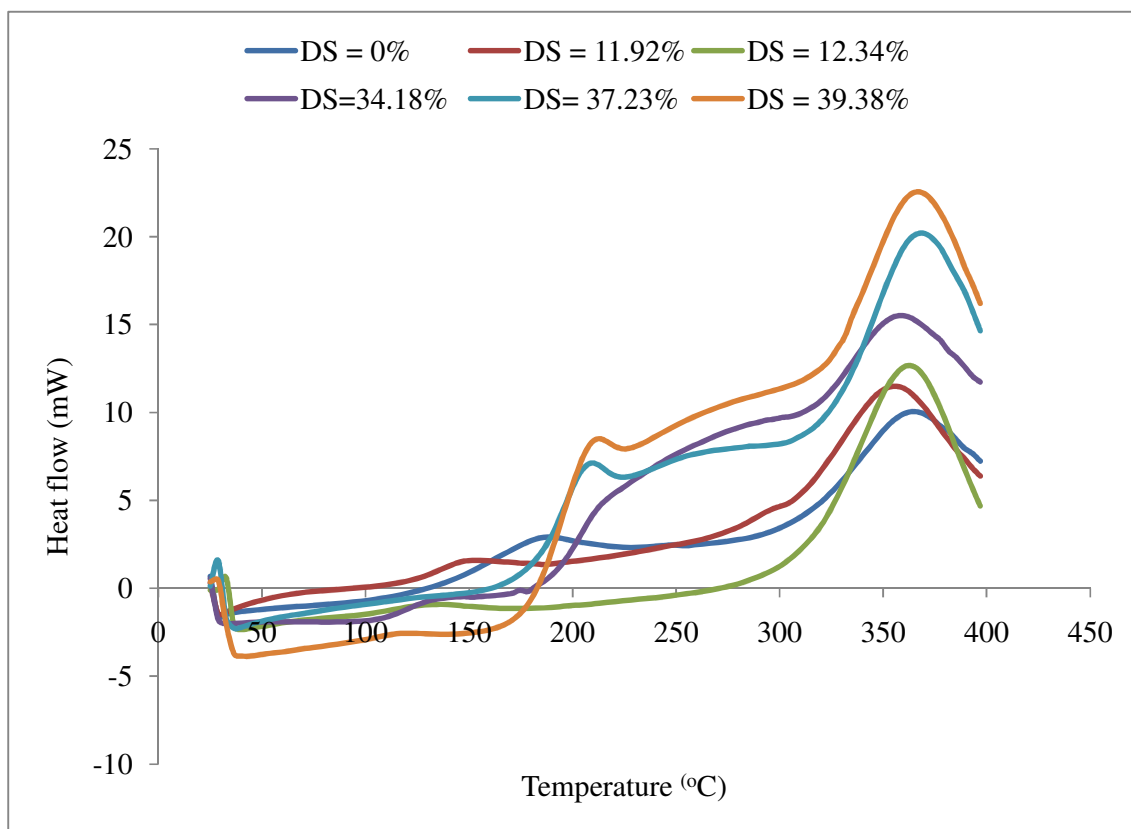


Figure 5.19: DSC curves of the unsulphonated and sulphonated rubber at different degrees of sulphonation.

Thermo gravimetric analysis (TGA) which determines a change in weight relative to temperature was also employed to investigate the thermal stability of the unsulphonated and sulphonated rubber at different degrees of sulphonation and sulphonation time. Three transitions in the loss in weight in three ranges of temperature can be observed in the TGA curves for both unsulphonated and sulphonated rubber. For unsulphonated rubber, the first transition in the range of 23.79°C-219.51°C as shown in Figures 5.20 and 5.21 can be attributed to the presence of moisture and some other additives used in the production of polystyrene butadiene rubber. It can be observed from the TGA curves that the drop in weight at these temperature ranges reduces as the degree of sulphonation

increases and this is an indication that the attached  $\text{SO}_3\text{H}$  group improved the strength of the rubber. The second drop in weight in the range of  $219.51^\circ\text{C}$ - $302.97^\circ\text{C}$  represents the thermal degradation of the styrene group attached to the butadiene, which is the main chain, while the third transition in the range of  $302.97^\circ\text{C}$ - $366^\circ\text{C}$  is ascribed to the thermal degradation of the main chain. It was also observed during the pretreatment of the samples in the presence of air that the sulphonated rubber does not undergo oxidation as the weight remains constant.

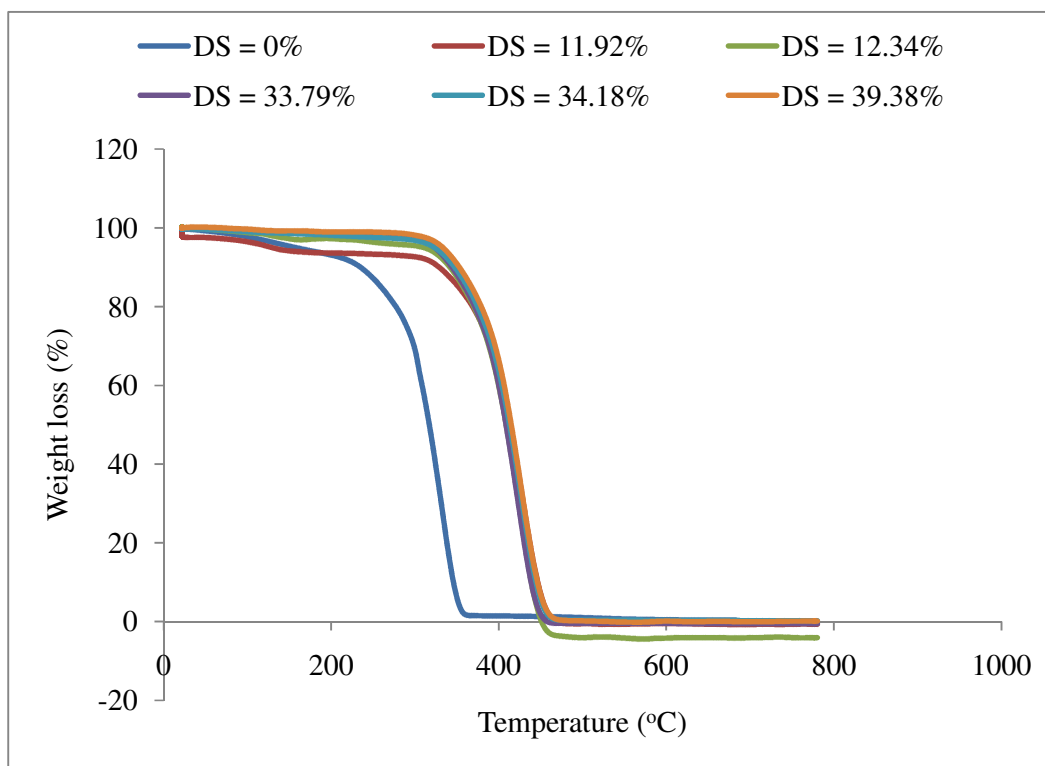


Figure 5.20: TGA curve of the unsulphonated and sulphonated rubber at different degrees of sulphonation

In the case of the sulphonated rubber the second weight loss step was around  $306.9^\circ\text{C}$ - $412^\circ\text{C}$ , depending on the degree of sulphonation which is mainly associated with the loss of the styrene-sulphonic group. The third weight loss step in the range of  $402.9^\circ\text{C}$ - $475.52^\circ\text{C}$  represents the decomposition of the main chain. It can be noticed from Figures



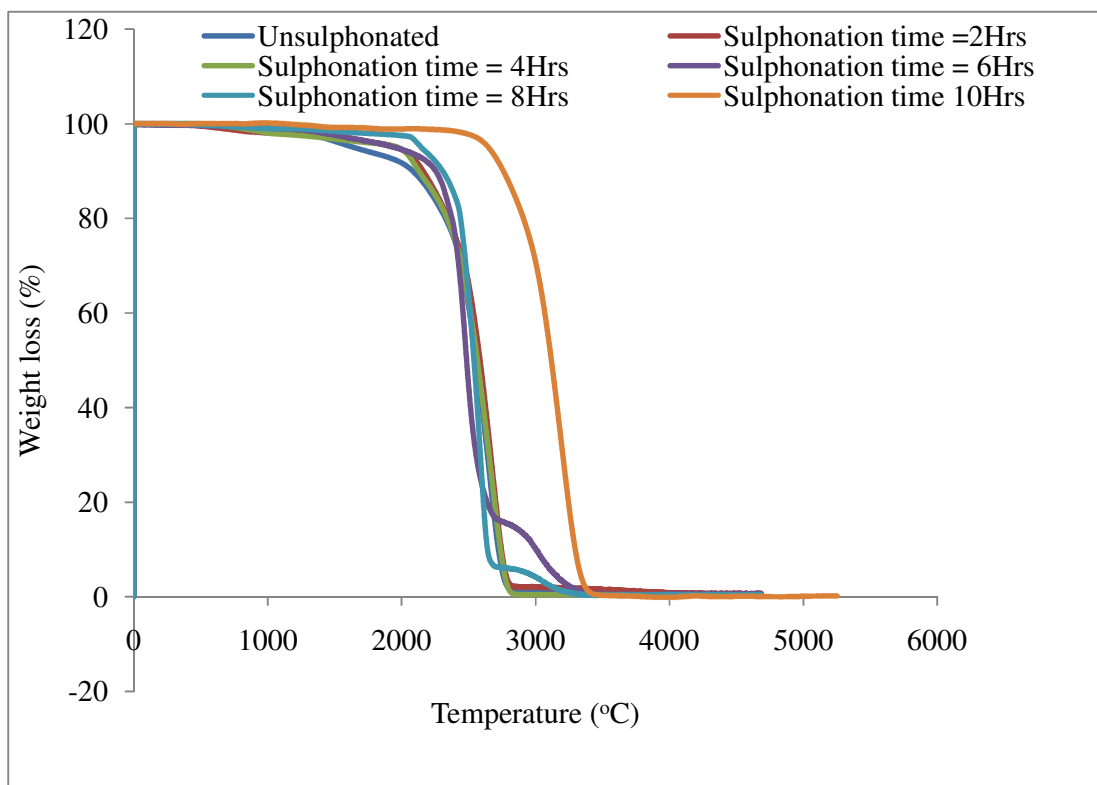


Figure 5.21: TGA curve of the unsulphonated and sulphonated rubber at different sulphonation time

Results obtained on the theoretical values of DS at various concentrations of acid are presented in Figure 5.22. The DS values calculated from the TGA, otherwise referred to as theoretical values, and at various concentrations of acid are presented in Figure 5.22. It could be observed from the results that there is a little variation between the experimental and theoretical values with the correlation coefficient of 0.9975 and standard deviation of 2.7094. These variations can be attributed to the fact that not all  $\text{SO}_3\text{H}$  groups attached to the styrene were degraded from the main chain (Gao et al, 2003). The variations can also be blamed on the fact that the TGA test is carried out under non equilibrium conditions and there is thus the possibility of a small amount of chain scission at the sulphonated styrene-butadiene linkage involved in the first step

degradation (Xing et al, 2004). Therefore the sulphonated membrane has an adequate thermal property in polymer electrolyte membrane fuel cell applications, since the thermal decomposition is above 120°C, being the maximum operating temperature of the PEMFC. DTA curves shown in Figure 5.23, also confirm the results of the thermal stability of the membrane, as shown in the TGA and DSC curves.

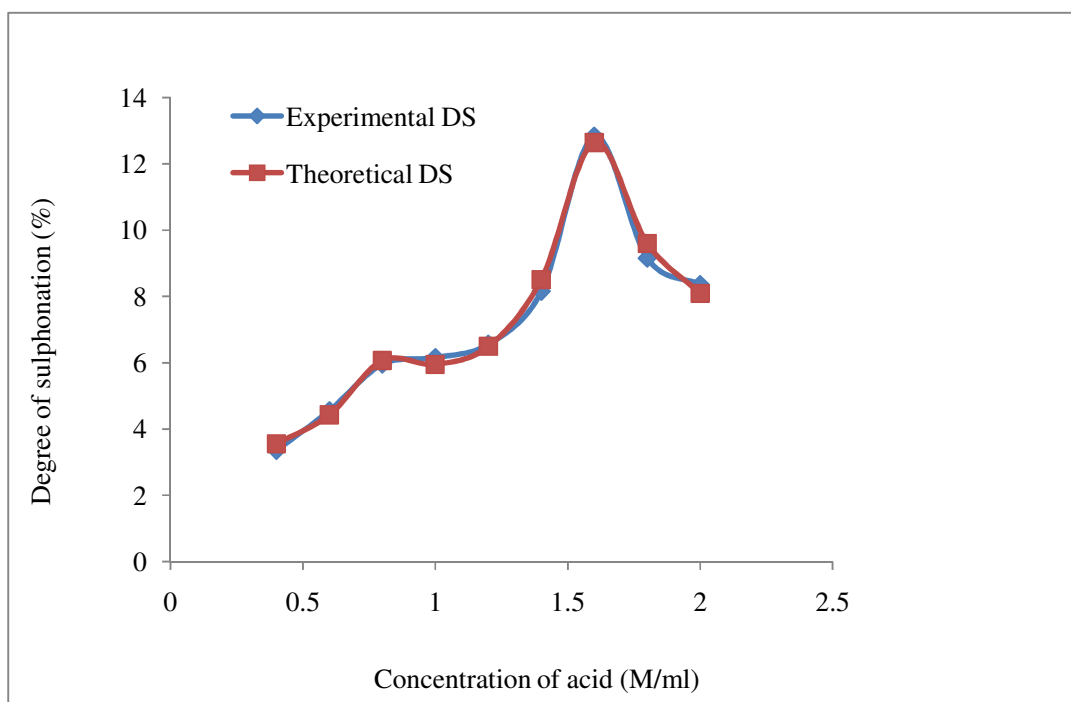


Figure 5.22: Experimental and Theoretical Degree of sulphonation at different concentration of acid

Figure 5.24 shows the TGA profiles of the synthesized membrane and the membrane modified with CNBs. The improvement in the thermal stability of the composite membranes as presented in Figure 5.24 can be attributed to the rigid electrostatic force of attraction between the  $\text{SO}_3\text{H}$  and network of CNBs in the composite. Results revealed that the mass of CNBs blended with the membrane is a contributing factor to improving the thermal stability of the membrane synthesized from PSBR. It can be observed from

the TGA profile shown in Figure 5.24 that the second weight loss step which represents the loss of the styrene group is in the range of 341-457.64, which increases with an increase in the mass of CNBs as compared to temperatures ranging around 306.9°C-412°C for the non blended membrane. The third weight loss step is in the range of 475.25°C- 554.72°C, representing the decomposition of the main chain, which also increases with the increase in mass of CNBs in the composite membranes.

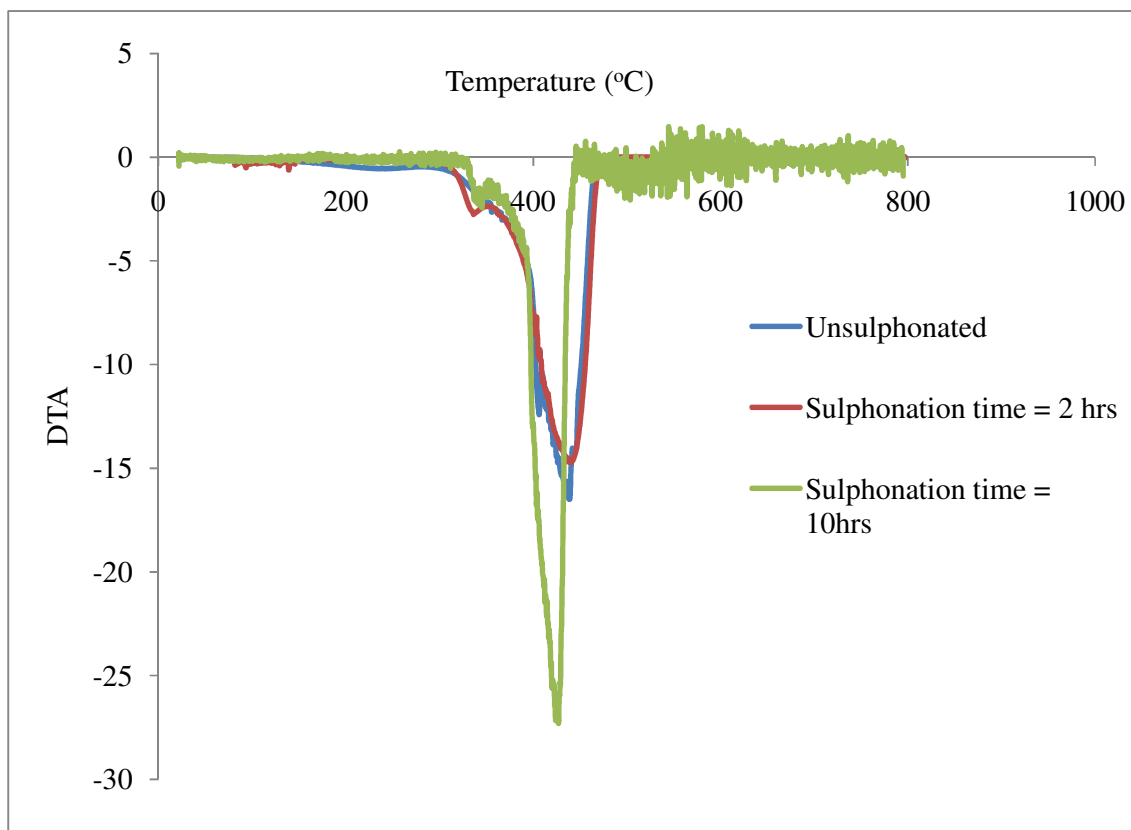


Figure 5.23: Differential thermal curve of sulphonated and unsulphonated polystyrene butadiene rubber at different sulphonation time.

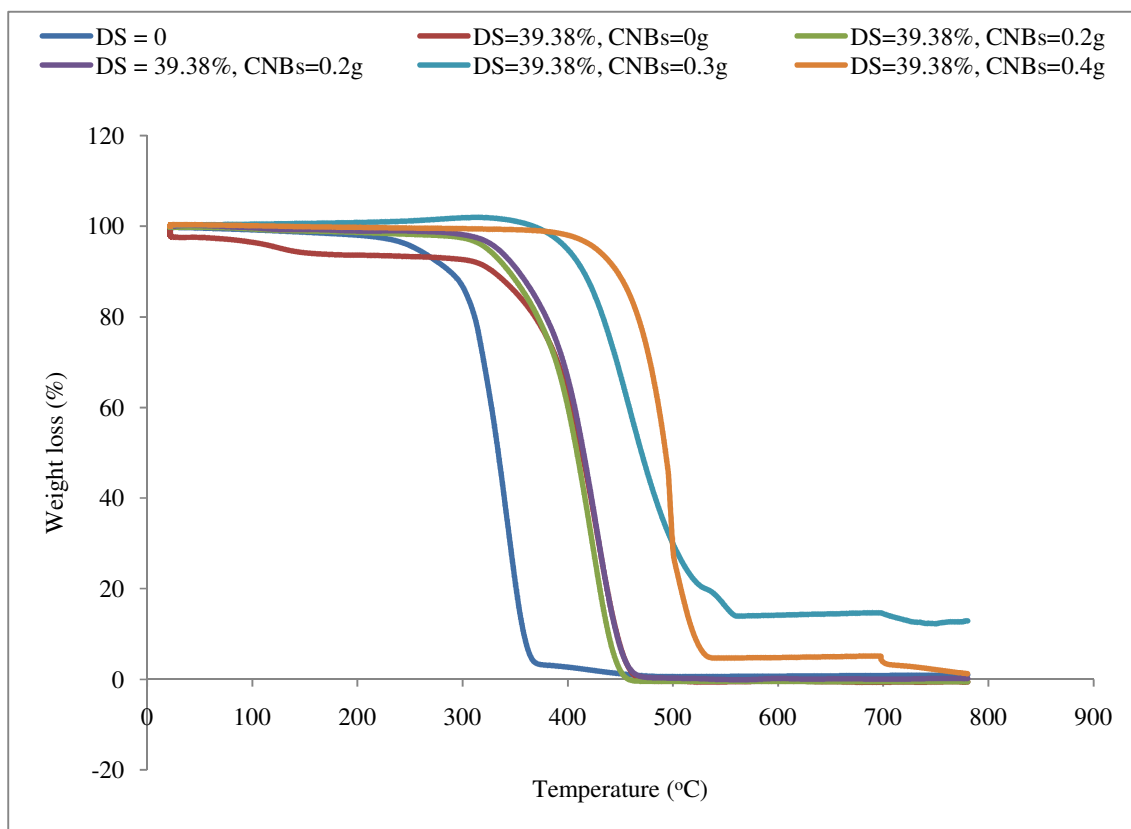


Figure 5.24: TGA profile of the SPSBR/CNBs composite membranes at different mass of blended CNBs

#### 5.4.4 Water uptake and water desorption capacity of the membrane

With respect to the electro-osmotic transport of water by the conduction ion and back diffusion of water once the gradient is established, the water uptake and physical dimension of the membrane become important among the special properties of the ion exchange membrane (Sangeetha et al, 2005). In this work a thin film of membrane of various thicknesses devoid of air was cast, using a laboratory scale casting machine. The water uptake and desorption capacity of the membrane at different thickness and temperature were investigated and the results obtained are presented.

Water uptake is the weight percent of water absorbed by the SPSBR membrane with respect to the weight of dry membrane (Sangeetha, 2005). Water molecules are necessary in the membrane because they provide the medium for the movement of ions, but an excess uptake of water can result in the swelling of the membrane and consequently affects the mechanical and conductivity properties. Results obtained on the water uptake at different degrees of sulphonation are shown in Figure 5.25. The degree of sulphonation (arising from the ion exchange capacity of the membrane) and water uptake contribute to the proton transport through the dense membrane (Basile et al., 2006). Better water uptake facilitates better proton conductivity of the membrane (Constamagna and Srinivasan, 2001). In a sulphonic acid based membrane, the proton conductivity depends on the number of available acid groups best expressed as degree of sulphonation and water contents in the membrane (Mokrini et al, 2006). Therefore, the higher the degree of sulphonation the better the abilities of the membrane to absorb water and cause proton dissociation and mobility. It is therefore important to note that proton conduction in sulphonic acid membranes is due to proton hopping from one sulphonic group to another (Grothus mechanism) (Mahreni et al, 2009). In the presence of water, both the proton and the sulphonic groups are in the solvated form, and it is recognized to greatly facilitate the hopping mechanism, for instance a specific conductivity of about 0.1 S/cm has been reported for a fully hydrated Nafion membrane at 80°C (Costamagna and Srinivasan, 2001). Thus maximum water uptake by the electrolyte membrane is vital for proton exchange membrane fuel cell to attain its highest performance (Costamagna and Srinivasan, 2001).

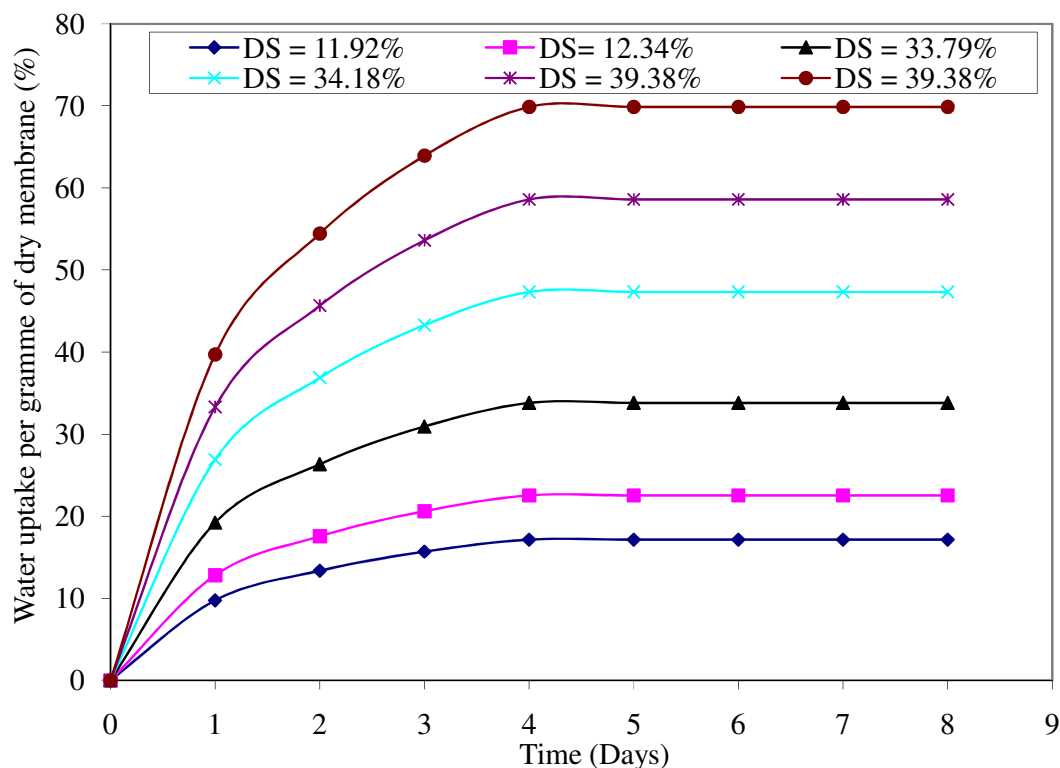


Figure 5.25: Water uptake at different degrees of sulphonation

Results obtained on the variation of water uptake at different thickness of the membrane at 9.4 % degree of sulphonation as shown in Figure 5.26 revealed that the water uptake increases as the thickness of the membrane decreases. The maximum water uptakes at different thickness of membrane are 60.33% for membrane thickness of 0.12mm, 54.29% for 0.16mm, 46.59% for 0.22mm, 41.49% for 0.33mm and 16.67% for membrane of thickness of 0.42mm. Results also show that all the membranes attained their saturation points on the fifth day, except for the membrane with thickness 0.12 and 0.16mm, which attained their water saturation point on the sixth day. The membrane ability to absorb water was high for the first day, followed by gradual water uptake towards saturation point. This trend in the results is in agreement with those obtained by Sangeetha (2005), while investigating the conductivity and solvent uptake of polystyrene triblock polymer. Also, the increase in water uptake with reduction can be probably due

to the fact that thinner membrane possesses low resistance to flow with fast molecular diffusion.

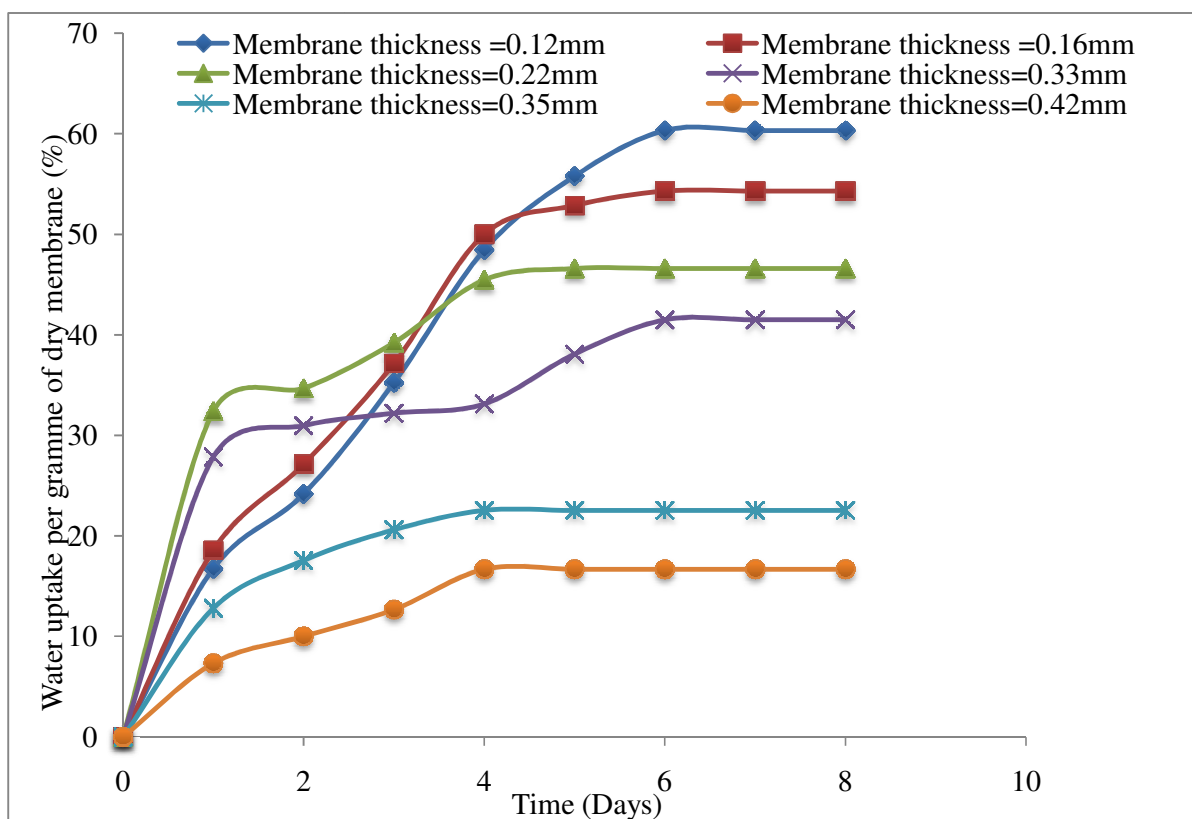


Figure 5.26: Water uptake at different membrane thickness

The result obtained regarding the effects of the temperature on the water uptake ability of the membrane is presented in Figure 5.28. Results revealed that as the temperature increases, the percentage of water uptake also increases, Sangeetha (2005) attributed the increase in water uptake with increase in temperature to hydrophilic property of the membrane which, increase as the temperature increases and consequently aid the water uptake ability of the membrane. Results also revealed that the time required by the membrane to attain its saturation decreases as the temperature increases. The comparison of the water uptake ability of synthesized membrane with that of Nafion<sup>®</sup> shows that the synthesized membrane has better water uptake ability than Nafion<sup>®</sup> which was reported

to be in the ranges of 30 - 36 % by weight (Sangeetha, 2005; Ni et al, 2006). It was noted, however, that an excess water uptake by the membrane could lead to the swelling of the membrane and thus affect its thermal and morphological strength. But the synthesized membrane showed a moderate water uptake when compared to the values reported in other sources dealing with synthesized membrane (Sangeetha, 2005; Gu et al, 2006; Ni et al, 2006). Therefore, synthesized membrane from PSBR has a moderate water uptake, which makes it a good candidate for fuel cell applications. The moderate water uptake of the synthesized membrane could be attributed to the chain flexibility in comparison to Nafion<sup>®</sup>. The main chain of both the polystyrene butadiene rubber and Nafion<sup>®</sup> are well organized. The branched chains attached to the polystyrene butadiene are aromatic and flexible, whereas the Nafion<sup>®</sup> membrane has a rigid linear fluorinate chain (Woo et al, 2003).

Results presented above on the water uptake of the membrane indicated that this parameter is one of the major properties of the proton exchange membrane in a fuel cell application. If the water uptake is too low, it will affect the ionic conductivity of the membrane negatively and enhance methanol permeability. High water uptake also resulted in high ionic conductivity but the possibility of loss of dimensional stability is very high. Figure 5.27 shows the dependence of the water uptake by the composite on the amount of CNBs blended with the sulphonated polystyrene butadiene rubber. Results indicated that the water uptake of the composite membrane is influenced by the amount of CNBs blended with the polymer. Results also show that the water uptake of the composite membrane is better than that of the membrane without carbon nanoballs. The weight percentage of the water uptake by the composite membrane increases with an increase in CNBs ratio in the polymer matrix. The increase in the water uptake of the

blended membrane can be attributed to the water retention ability of the CNBs. In this study, the maximum water uptake is for the highest mass of CNBs which was close to 100% while in the literature, water uptake was in the range 30-120% (Sangeetha, 2005; Gu et al, 2006).

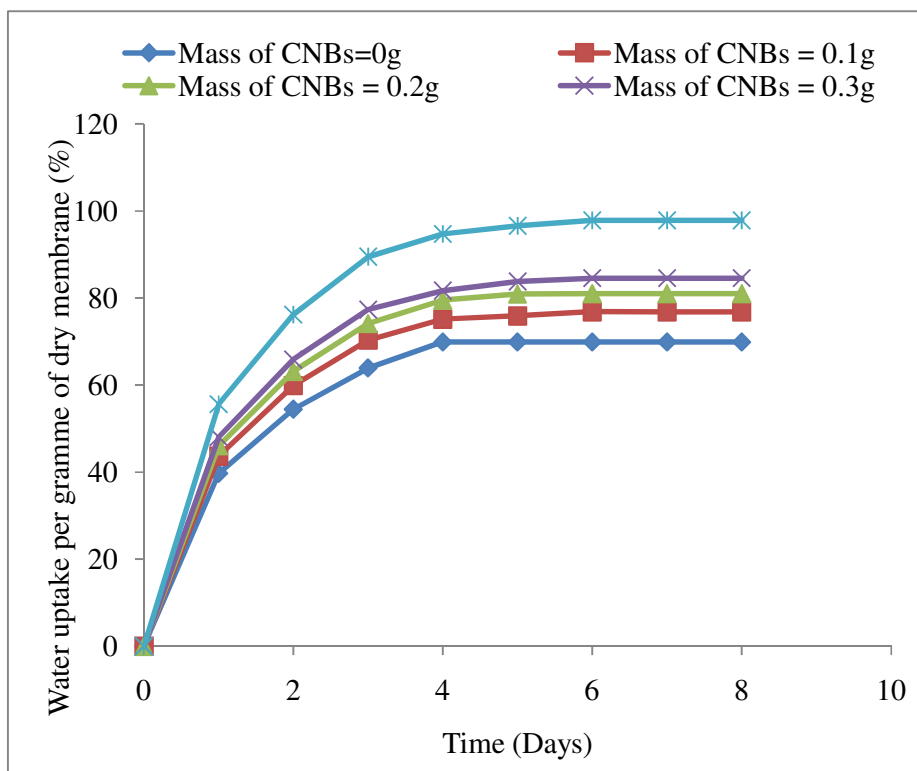


Figure 5.27: Effects of carbon nanoballs on the water uptake of the composite membranes

Desorption results; measuring the rate at which the membrane becomes dehydrated, were investigated at various temperatures and times and the results obtained are presented in Table 5.6. Results show that the membrane can hold water till 100°C for one hour. At room temperature, the percentages of water desorption by the membrane increases gradually with time and retain some of the water after 12 hours. At 40°C and 50°C, the membrane lost all its water content after 3 hours, while the water retention time at 60°C was 2 hours and 1 hour at 70, 80 and 100°C. Therefore, the higher the temperature, the

lower the water retention time of the membrane and consequently the lower the resultant performance of the membrane. Hence, it can be inferred that the membrane will require humidification, especially if the fuel cell where the membrane will be used is operating above room temperature.

The swelling ratio is the percentage change in membrane thickness per gramme of dry membrane. Figure 5.28 shows that the swelling ratio is inversely proportional to the membrane thickness, i.e. the smaller the thickness the higher the swelling ratio. This pattern of results is in agreement with the results obtained on the water uptake capacity of the membrane at different thickness as shown in Figure 5.26, where the water uptake ability of the membrane is higher at smaller thickness. Sangeetha (2005) reported that the consequence effect of excessive water uptake by the membrane with lower thickness is the swelling ratio of the membrane.

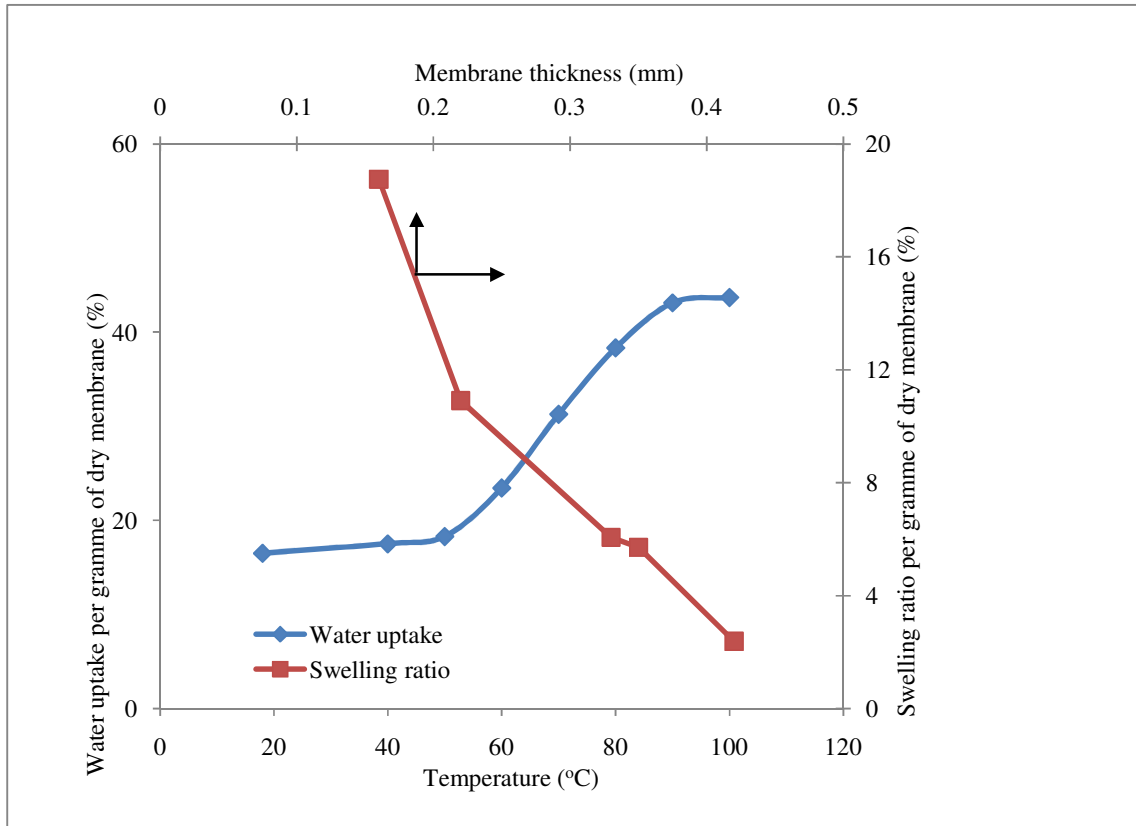


Figure 5.28: Effect of temperature and membrane thickness on water uptake and swelling ratio

Table 5.6: Effect of time and temperature on the water desorption capacity of the membrane

Time (H)	Water desorption of the membrane (%)						
	25°C	40°C	50°C	60°C	70°C	80°C	100°C
1	85.47	97.83	98.96	99.19	99.30	99.5	99.6
2	92.33	98.91	98.96	99.19	100.00	100.00	100.00
3	94.62	98.91	98.96	100.00	100.00	100.00	100.00
4	94.62	98.91	100.00	100.00	100.00	100.00	100.00
5	98.06	100.00	100.00	100.00	100.00	100.00	100.00
6	98.06	100.00	100.00	100.00	100.00	100.00	100.00
7	98.06	100.00	100.00	100.00	100.00	100.00	100.00
8	99.20	100.00	100.00	100.00	100.00	100.00	100.00
9	99.20	100.00	100.00	100.00	100.00	100.00	100.00
10	99.20	100.00	100.00	100.00	100.00	100.00	100.00
11	99.20	100.00	100.00	100.00	100.00	100.00	100.00
12	99.20	100.00	100.00	100.00	100.00	100.00	100.00

#### 5.4.5 Proton conductivity

Proton conductivity of the synthesized membranes was measured at different temperatures and membrane thickness. Prior to the measurement, the membrane samples were soaked in distilled water for hydration. A well hydrated membrane is required to achieve a desirable level of conductivity, especially in the case of a membrane that relies on sulphonic acid to conduct protons (Sangeetha, 2005). Figure 5.29 shows the hydration dependence of proton conductivity of the SPBR at different degrees of sulphonation.

Results reveal that the membrane will conduct better when it is fully rather than partially hydrated. For instance the proton conductivity of the partially hydrated membrane (10 hours hydration period) and fully hydrated at room temperature and DS of 10.48 are  $1.46 \times 10^{-3}$  and  $2.283 \times 10^{-3}$  S/cm respectively. It can be noticed from the results also that as DS increases, the difference between the proton conductivities of the partially and fully hydrated membranes decreases: this can be attributed to the fact that at high DS, IEC is also high and therefore the possibility of the membrane being fully hydrated is strong. Figure 5.29 also represents the conductivities of the membrane at different degrees of sulphonation and temperature. It can be observed from the results that the proton conductivity of the membrane was in the order of  $10^{-3}$ - $10^{-2}$  S/cm and increases with the increase in temperature and degree of sulphonation. When the degree of sulphonation increases, the polymer's hydrophilic behaviour also increases and this gives it more power to take up water during humidification. Although, the proton conductivity increases with an increase in temperature, however, care must be taken not to dehydrate the membrane when a high operating temperature is applied to the fuel cell. Humidification is therefore also necessary while using the membrane in fuel cell production.

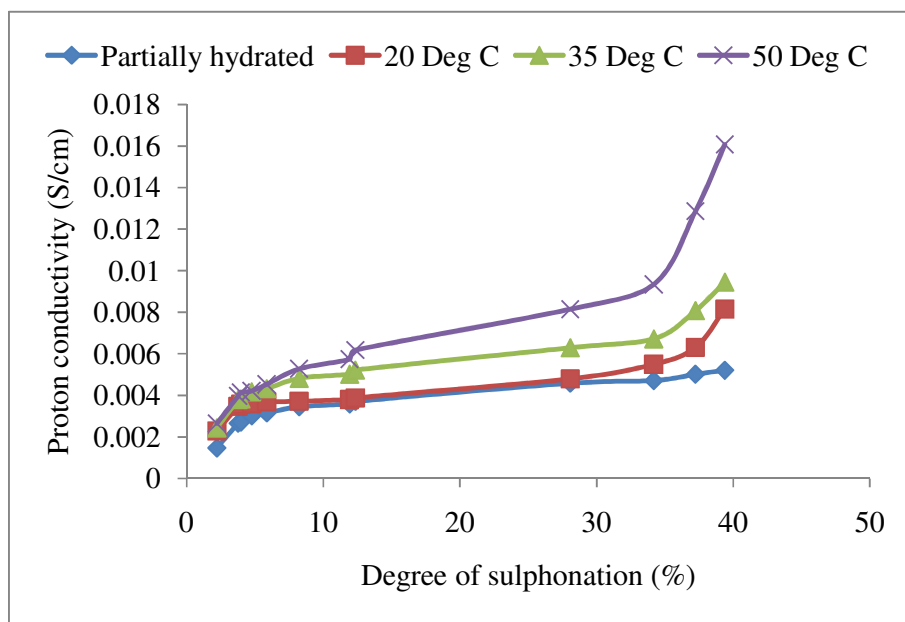


Figure 5.29: Protons conductivity of the membrane at different degrees of sulphonation and temperature.

Figure 5.30 shows the membrane thickness dependence on proton conductivity of the membrane at different DS. The conductivity of the membrane increases with an increase in DS and is inversely proportional to the membrane thickness. For instance, a membrane with the DS of 39.38% exhibits a conductivity of  $1.58 \times 10^{-2}$  and  $9.38 \times 10^{-3}$  S/cm at membrane thicknesses of  $170 \mu\text{m}$  and  $450 \mu\text{m}$  respectively. It was reported that membranes with high conductivity tend to be weak mechanically, and are often reinforced by a non conducting cloth or other similar structure (Chen et al, 2005; Mokirirn et al, 2006; Anilkumer et al, 2006; Jiang et al, 2006). Therefore, the thinnest membrane will produce the lowest internal resistance, but the thickness must be high enough to slow the molecular diffusion of gases and ensure that the membrane is strong enough for fuel cell applications. Otherwise poor current efficiency and waste of fuel gas by diffusion occur, especially during long running period.

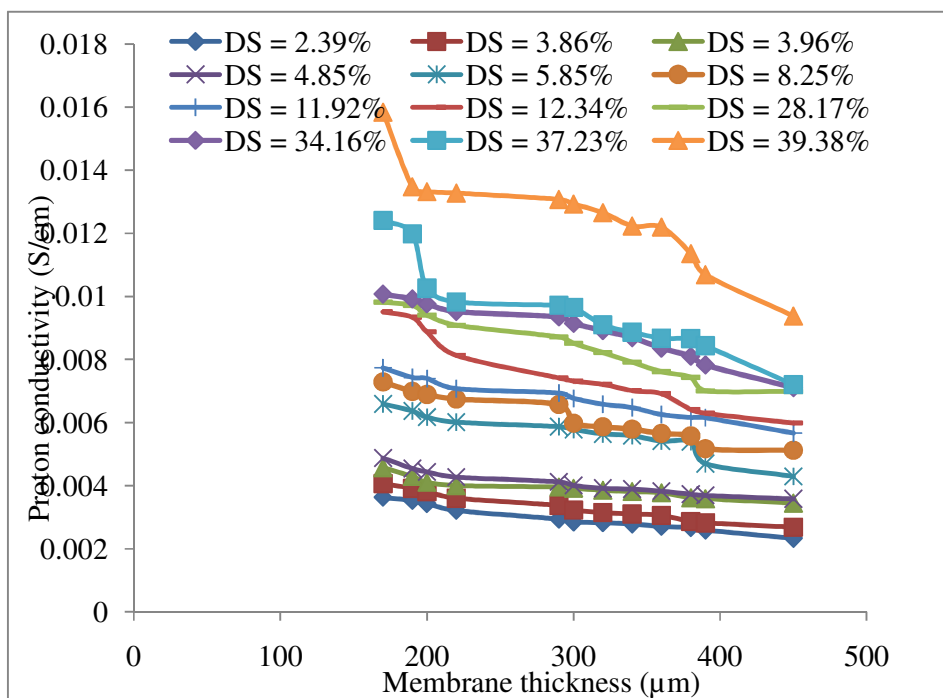


Figure 5.30: Effect of membrane thickness on the proton conductivity of the membrane at different degrees of sulphonation.

Figure 5.31 shows the proton conductivity of the synthesized SPSBR-CNBs composite membrane at different thicknesses, as a function of mass of CNBs in the composite. As shown in the Figure, the proton conductivity of the unblended membrane is lower than those blended with CNBs. The increment in the proton conductivity of the blended membrane can be attributed to the ionic cluster of CNBs around the  $\text{SO}_3\text{H}$  group in the synthesized membrane. Therefore, the blending of the membrane with CNBs is crucial to the performance of the membrane. The increase in proton conductivity of the blended membrane can be attributed to excellent water uptake due to the presence of CNBs when compared to that of an unblended membrane.

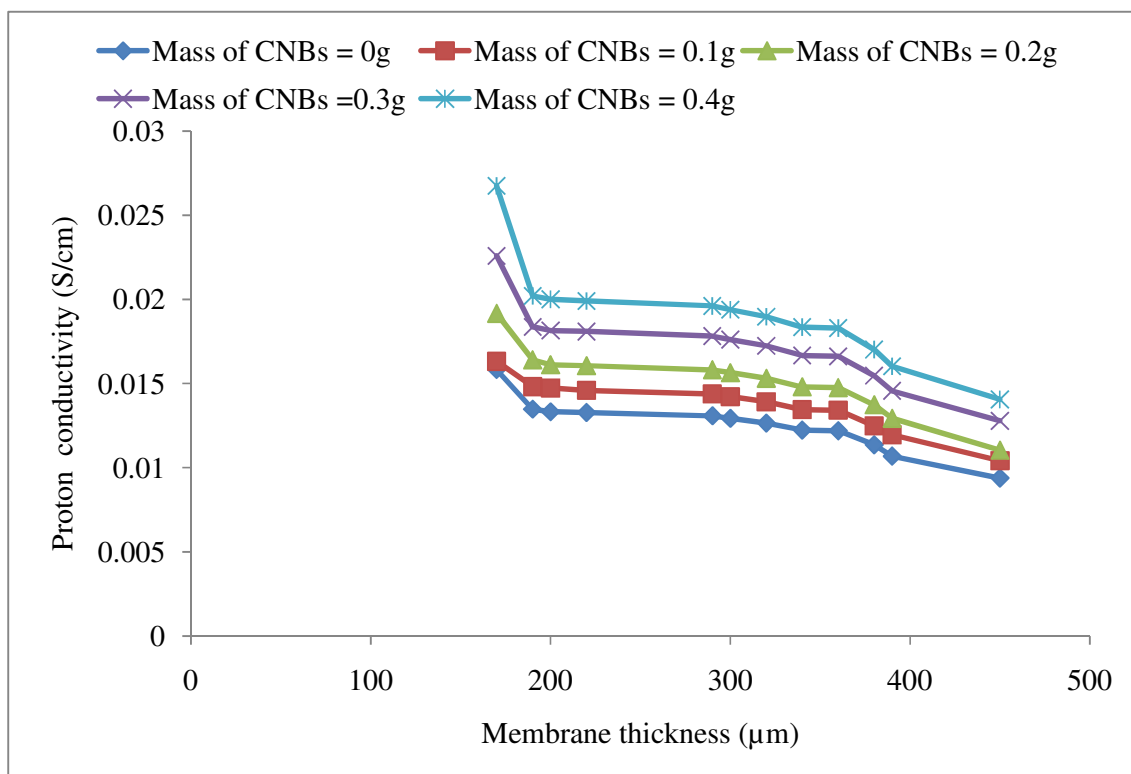
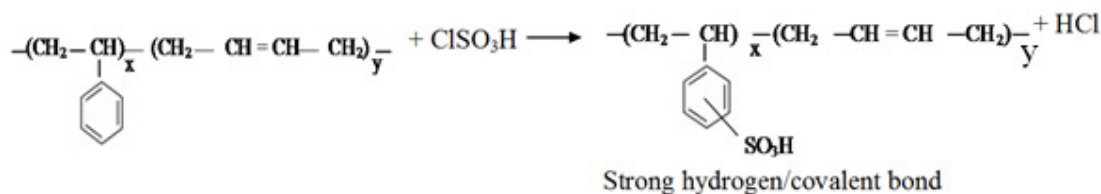


Figure 5.31: Effect of CNBs on the proton conductivity of the membrane at different membrane thicknesses.

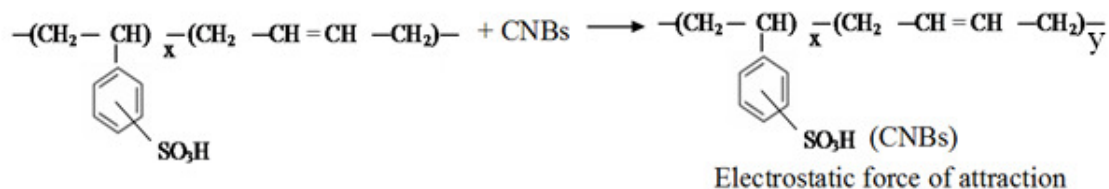
The presence of CNBs in the composite membrane form the hydration shells around the fixed covalently bonded sulphonic group which aids the water uptake capacity of the composite membrane (Haubold et al, 2001). For instance, the proton conductivity of the unblended membrane with a thickness of 200μm is  $1.3 \times 10^{-2}$  S/cm, while those of the blended membranes with same thickness are in the range of  $1.47 \times 10^{-2} - 2.0 \times 10^{-2}$  S/cm. These values increase with an increase in mass of CNBs in the composite membrane.

As shown in Figure 5.31 the CNBs substantially improve the transport of proton through the composite membrane. The CNBs particle size and stability in the polymer matrix greatly influence the conducting properties of the composite membrane. It is therefore important that the CNBs particles size be equal or less than the ionic cluster size in the

polymer membrane matrix. These particles serve as a proton hopping bridge, which is responsible for the proton conducting properties of the composite membrane. A proposed reaction mechanism between the polystyrene butadiene rubber, chlorosulphonic acid and CNBs are presented in scheme 5.3 and 5.4



Scheme 5.3: Sulphonation of polystyrene butadiene rubber



Scheme 5.4: Blending of sulphonated polystyrene butadiene rubber with CNBs

It can be proposed from schemes 5.3 and 5.4 that the nanocomposite structure of sulphonated polystyrene butadiene rubber and carbon nanoballs possesses a strong hydrogen bonding between the para position of the repeating unit and the  $\text{SO}_3\text{H}$  group as suggested by Idibie, (2009). This strong hydrogen bond leads to attachment of the  $\text{SO}_3\text{H}$  group to the styrene and electrostatic force of attraction between the  $\text{SO}_3\text{H}$  and CNBs, making it possible for the nanoparticles to blend well with the sulphonated rubber. Based on these mechanisms, the relationship between the two developed by Davis and Mott (Mahreni et al, 2009) as shown in Equations 5.3 and 5.4 were used to determine the CNBs particle diameter on the surface of the sulphonated polystyrene butadiene rubber.

$$T = A \exp(-ad) \quad (5.3)$$

Where:  $T$  = transmittance at maximum absorbance,  $A$  = inherent constant = 1,  $\alpha$  = inherent absorbance constant and,  $d$  = thickness of the membrane film:

$$(\alpha h\nu)^2 = (h\nu - E_g) \quad (5.4)$$

Where:  $h$  = plank constant =  $6.63 \times 10^{-34} \text{Js}$ ,  $\nu$  = frequency ( $\text{sec}^{-1}$ ) and,  $E_g$  = the band gap energy (eV).

The absorbance constant of the blended membrane at different masses of CNB was determined by plotting the transmission against wavelength obtained from UV-VIS spectra of the membranes blended with nanoballs. Results as presented in Figure 5.32 indicated high nanoballs content in the membrane matrix with the transmittance of all the membranes above 90% at the wavelength within the range of 700-900nm, depending on the mass of the CNBs.

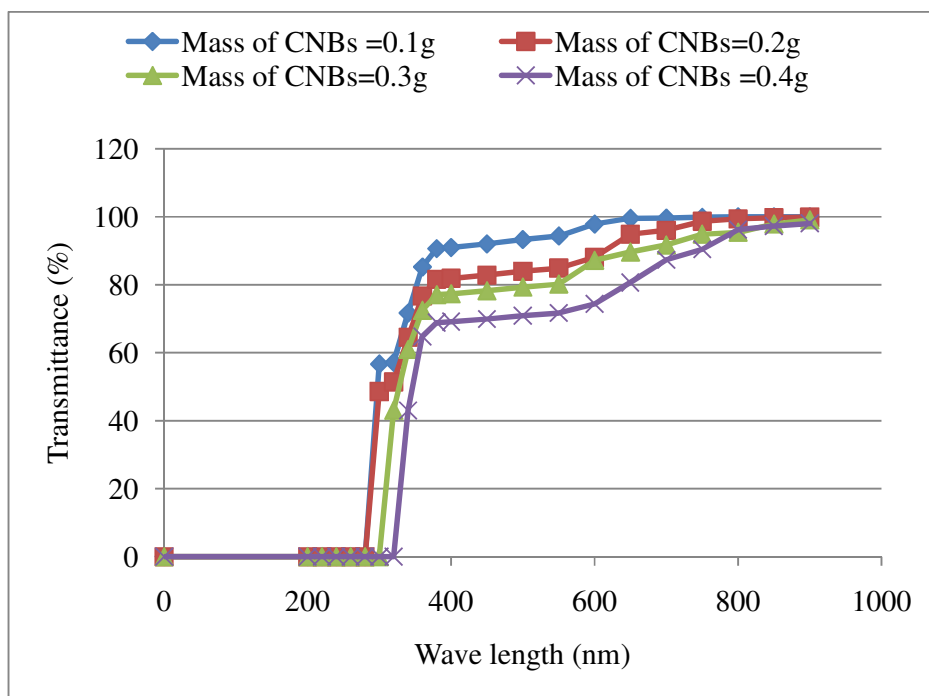


Figure 5.32: Plot of transmittance against wavelength at different mass of CNBs in the composite membranes

It can be seen from the Figure 5.32 that the blended membranes have maximum absorbance at a wavelength of 300 nm for the samples blended with 0.1g and 0.2 g of CNBs. The samples blended with 0.3 g and 0.4 g, on the other hand, attain maximum absorbance at wavelength of 320 nm and 340 nm respectively. The equivalent transmittance at these wavelengths are 56.67 %, 48.62 %, 43.07 % and 42.98% for membranes blended with 0.1g, 0.2g, 0.3g, and 0.4g of CNBs respectively. Using these values of transmittance at maximum absorbance with the values of the constant  $A = 1$  (Mahreni et al, 2009) and membrane thickness of  $117\mu\text{m}$ , the absorbance constant for each of the membrane composites was calculated and the results obtained are presented in Table 5.7. The absorbance constant determined in Equation 5.3 is used in Equation 5.4 to determine the band gap energy of the composite membrane at different masses of CNBs blended with the membrane. This was achieved from the intercept of the plot of  $(\alpha h\nu)^2$  against  $h\nu$  on the horizontal axis of the plot as presented in Figures 5.33(a-d).

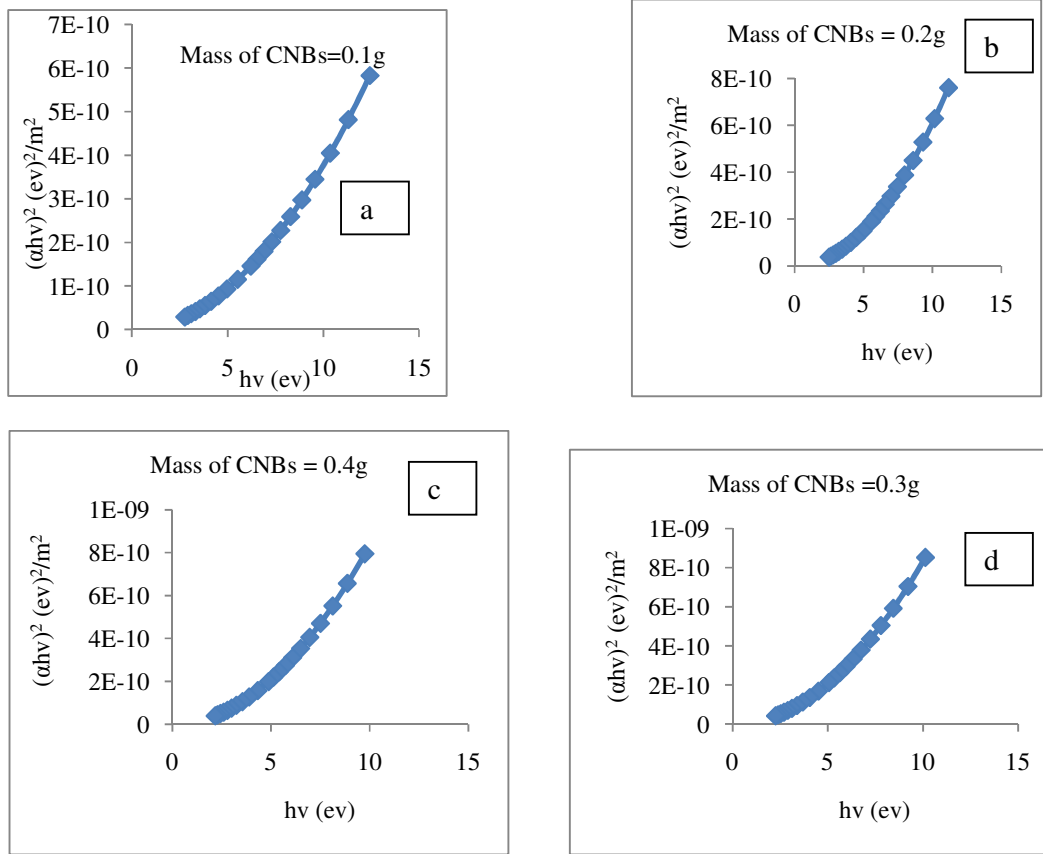


Figure 5.33: Plot of  $(\alpha hv)^2$  against  $h\nu$  at different mass of CNBs

The theoretically determined band gap energy of the membrane at different masses of CNB is presented in Table 7.17. The particle (CNBs) size in the membrane composite was then determined using the relation below (Mahreni et al, 2009):

$$E_{g, \text{nanocrystal}} = E_{g, \text{bulk}} + \frac{\kappa^2 \pi \hbar^2}{2R^2} \left( \frac{1}{m_e} + \frac{1}{m_h} \right) \quad (5.5)$$

Where  $E_{g, \text{nanocrystal}}$  = band gap energy of the composite membrane (eV)

$E_{g, \text{bulk}}$  = band gap energy of the CNBs (eV) = 1.7eV

$R$  = radius of the particle (nm)

$\kappa = (\alpha\nu)$  (sec<sup>-1</sup>)

$m_e$  = electron masses (eV) = 0.87 $m_0$  (Titantah and Lamoen, 2004)

$m_h =$  hole masses (eV) =  $0.19m_0$  (Lin et al, 1998)

$$m_0 = 8.19 \times 10^{-14} j$$

From Equation 7.38

$$(E_{g,nanocrystal} - E_{g,bulk}) = \frac{\kappa^2 \pi^2 \hbar^{*2}}{2R^2} \left( \frac{1}{m_e} + \frac{1}{m_h} \right) \quad (5.6)$$

But:

$$\hbar^* = \frac{\hbar}{2\pi} \quad (5.7)$$

Substitute equation 5.7 into Equation 5.6 to obtain:

$$(E_{g,nanocrystal} - E_{g,bulk}) = \frac{\kappa^2 \hbar^2}{2R^2} \left( \frac{1}{m_e} + \frac{1}{m_h} \right) \quad (5.8)$$

From Equation 5.8

$$R^2 = \frac{\kappa^2 \hbar^2}{2(E_{g,nanocrystal} - E_{g,bulk})} \left( \frac{1}{m_e} + \frac{1}{m_h} \right) \quad (5.9)$$

Therefore;

$$R = \sqrt{\frac{\kappa^2 \hbar^2}{2(E_{g,nanocrystal} - E_{g,bulk})} \left( \frac{1}{m_e} + \frac{1}{m_h} \right)} \quad (5.10)$$

Equation 5.10 was used to determine the particle size in the composite membrane at different masses of CNB. The results obtained as presented in Table 5.7 indicate that as the CNBs content increases, the band energy of the composite membrane reduces while the particle diameter increases. The increment in particle size relative to mass of CNBs in the composite can be attributed to the formation of the particle aggregate at a high concentration of CNBs in the composite membrane. It is also observed that the calculated particle sizes are approximately equal to the average sizes of the CNBs as observed from SEM analysis.

Table 5.7: Band energy and calculated CNBs particles diameter from UV data

Mass of CNBs (g) Blended with SPSBR	Absorbance constant	Calculated Band Energy Gap (ev) of the composite membrane	Average particle diameter from (SEM) (nm)	Calculated particle diameter from UV data (nm)
0.1	4854.06	3.066	50	43.06
0.2	6163.55	2.760	70	62.01
0.3	7199.52	2.500	80	78.31
0.4	7217.40	2.160	100	97.46

In order to confirm the rigidity of CNBs within the membrane matrix and the attachment of the sulphonic group to the membrane, the membrane samples were soaked in water for 30 days and proton conductivity was tested. The results obtained reveal that conductance values were stable, thus indicating that there was neither loss of the sulphonic acid groups attached to the membrane nor removal of the CNBs on the membrane matrix. Therefore, the CNBs and the acid group in the synthesized composite membrane were strongly attached to the membrane.

#### 5.4.6 Porosity and total solvent uptake

Figure 5.34 depicts the overall uptake of methanol solution at different degrees of sulphonation, while Figure 5.35 presents the porosity of the membrane at different membrane thicknesses. Results obtained on the uptake of methanol per sulphonic group are evaluated from Equation 3.11, showing an increase with the increase in concentration of methanol. This can be attributed to the availability of the methanol at a higher rather

than lower concentration level. Results also show that the methanol uptake per sulphonic group decreases with an increase in degree of sulphonation; this can be attributed to the decrease in equivalent weight as the degree of sulphonation increases, resulting in more sites for the distribution of the methanol within the membrane.

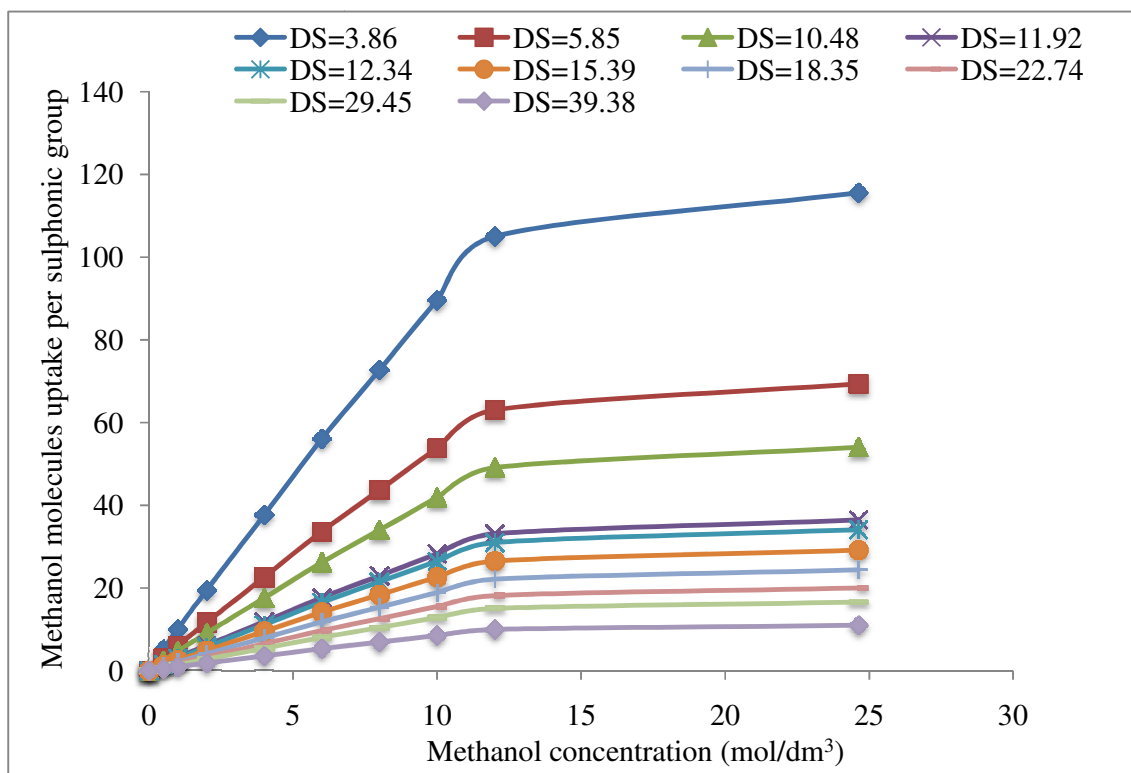


Figure 5.34: Methanol molecule uptake per sulphonic group at different concentration of methanol and degrees of sulphonation.

Figure 5.35 shows the effect of CNBs on methanol uptake per sulphonic group of the composite membrane. It can be seen from Figure 5.34 that the methanol uptake per sulphonic group in the composite membrane is lower than that of the unblended membrane. This can be attributed to the rigid electrostatic force attraction between the CNBs and SO<sub>3</sub>H group in the polymer matrix, which reduces the site for methanol uptake.

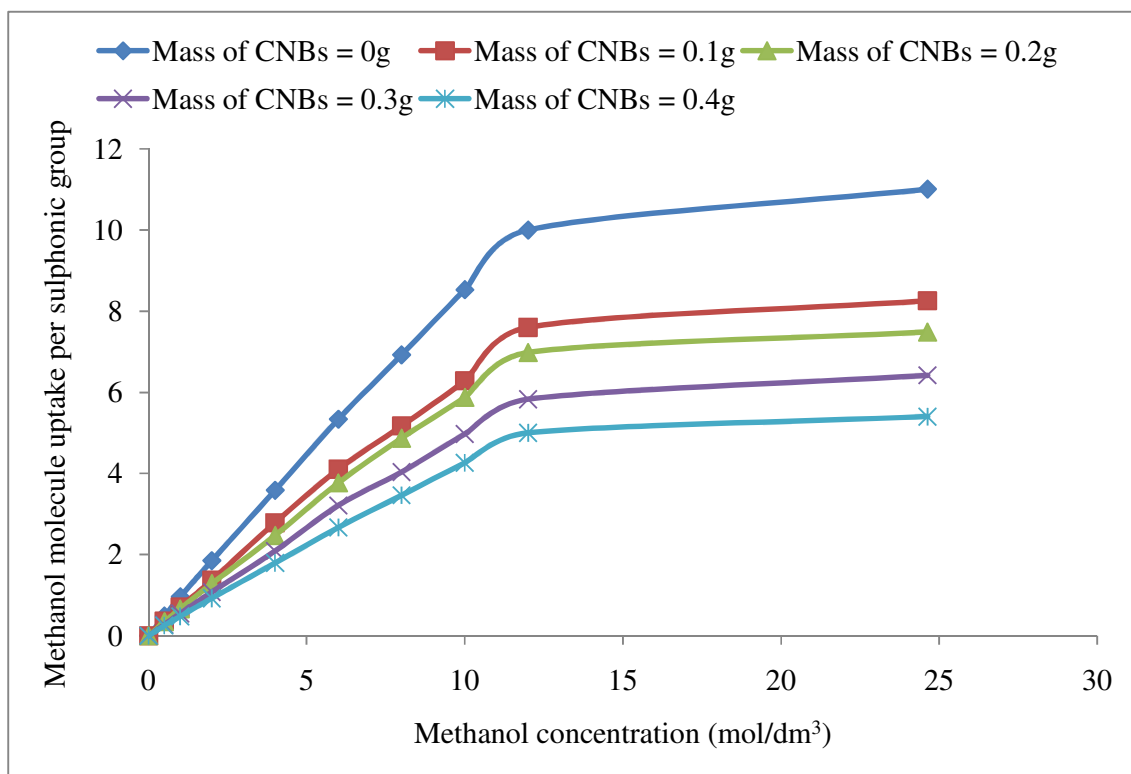


Figure 5.35: Effects of CNBs on the methanol molecule uptake per sulphonic group.

The porosity of the membrane to methanol calculated from Equation 3.7, which is weight based, increases with an increase in concentration of the methanol, as shown in Figure 5.36. The porosity of the membrane also influences the thickness of the membrane. Results obtained show that the porosity of the membrane to methanol increases with a decrease in membrane thickness. This can be attributed to the reduction in the area of the site required to hold the methanol within the membrane matrix as the thickness of the membrane decreases, and consequently results in the diffusion of methanol through the membrane which in turn results in the high porosity of the membrane. The porosity of the SPBR to methanol is less than that of Nafion<sup>®</sup>, which is in the ranges of 0.4048-0.5052, depending on the concentrations of the methanol (Sangeetha, 2005).

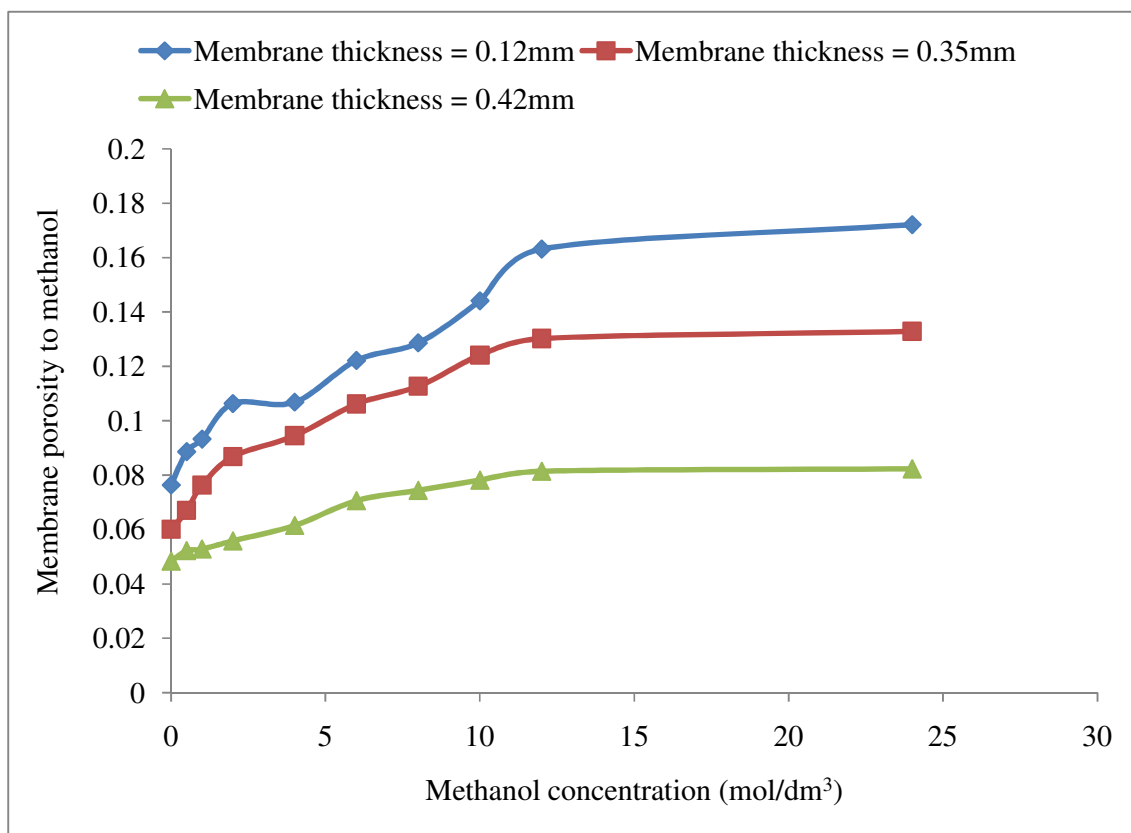


Figure 5.36: Effect of membrane thickness on the porosity of the membrane at different concentrations of methanol.

The effects of CNBs blended with the membrane on the porosity of the composite membranes are presented in Figure 5.37. It can be observed from the figure that the porosity of the composite membrane evaluated at membrane thickness 120  $\mu\text{m}$  is in the range of 0.048 – 0.124, depending on the mass of CNBs in the composite membranes and the concentration of the methanol. However, the porosity of the unblended membrane evaluated at the same thickness is in the range of 0.09 – 0.172, depending on the concentration of the methanol. The lower porosity of composite membranes can be attributed to the filling of the membrane pore by the CNBs as shown in Figure 5.37.

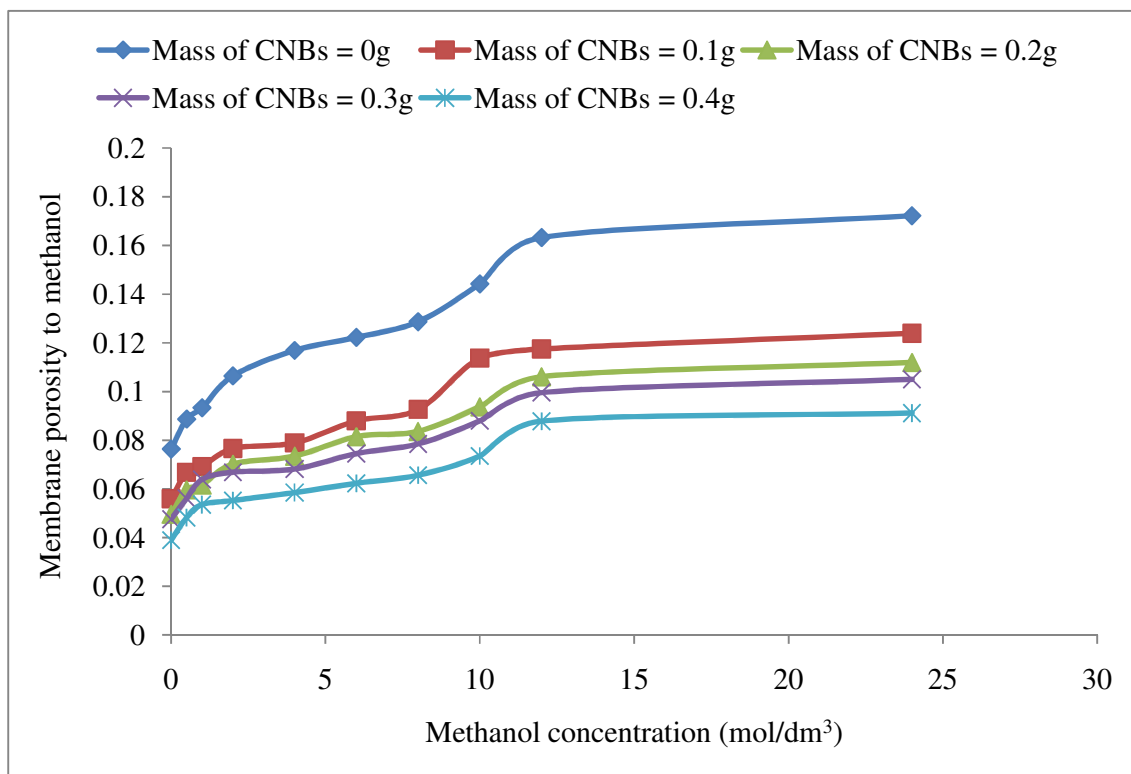


Figure 5.37: Effect of CNBs on the porosity of the membrane at different concentrations of methanol

The total uptake of methanol/water and water molecules per sulphonic acid group decreases with an increase in the concentration of methanol, as shown in Figure 5.38. Results also show that the water uptake per sulphonic acid group by the SPBR is higher than the methanol uptake per sulphonic group. Based on the results obtained from the porosity of the membrane to methanol and methanol uptake, it can be inferred that the membrane is less permeable to methanol than water. The water uptake per sulphonic group of Nafion<sup>®</sup> is almost constant (Sangeetha, 2005), while the methanol uptake increases with an increase in concentration of methanol. Kontou et al, (2007) also blame the difference between the water and methanol uptake on the possibility that the sulphonic groups in the membrane are more accessible to water than ethanol, which is

further enhanced by CNBs. Easy accessibility of the water by the sulphonic group can be attributed to the stronger interaction between the sulphonic group and water. The molecular size is another factor that influences the uptake of the solvent, the larger molecule size of methanol compared to that of water influencing the relatively small uptake of methanol compared to water.

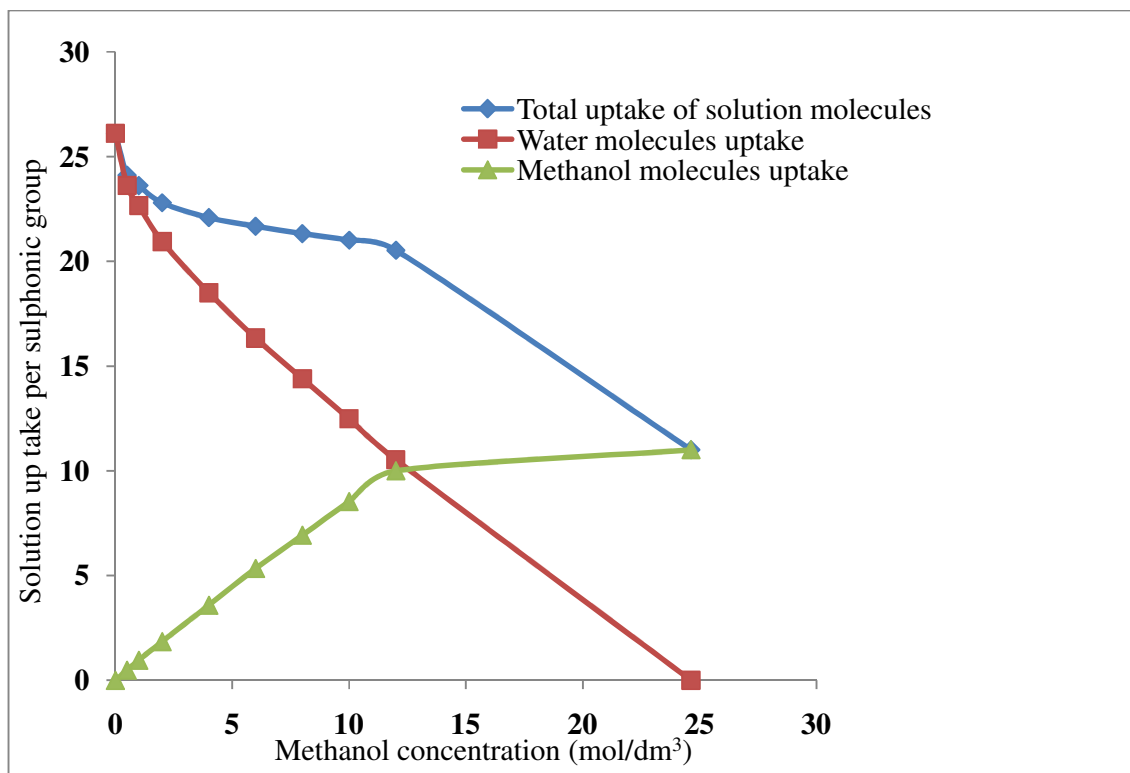


Figure 5.38: Uptake of solution molecule per sulphonic group.

#### 5.4.7 Methanol crossover

The problem of methanol permeation through proton exchange membrane (PEM) is a major constraint militating against large scale commercialization of fuel cell for energy generation, particularly direct methanol fuel cell (DMFC). This has attracted great interest in recent times (Walker et al, 1999; Fang et al, 2007). Methanol crossover (which is the capacity of the membrane to block the fuel going through the membrane) is therefore one of the qualities of the membrane that determines its performance in fuel

cell application (Han-Lang et al, 2006). The characterization of the synthesized membrane for methanol crossover is to determine the suitability of the membrane for possible application in direct methanol fuel cell; however hydrogen fuel is used in this work. Methanol crossover through the membrane leads to a decrease in the cathode potential and the energy efficiency (Hikita et al, 2001). It is therefore important to synthesize the membrane with low methanol permeability. In this study, membrane permeability was investigated using the method reported by Shen et al. (2005). Figure 5.39 shows the typical concentration changes of methanol in aqueous solution at different degrees of sulphonation and a membrane thickness of 220  $\mu\text{m}$ . The linear deviation of the results presents in Figure 5.39 can be attributed to the effects of partition coefficient and lag time which are not considered in Fick's law of diffusion.

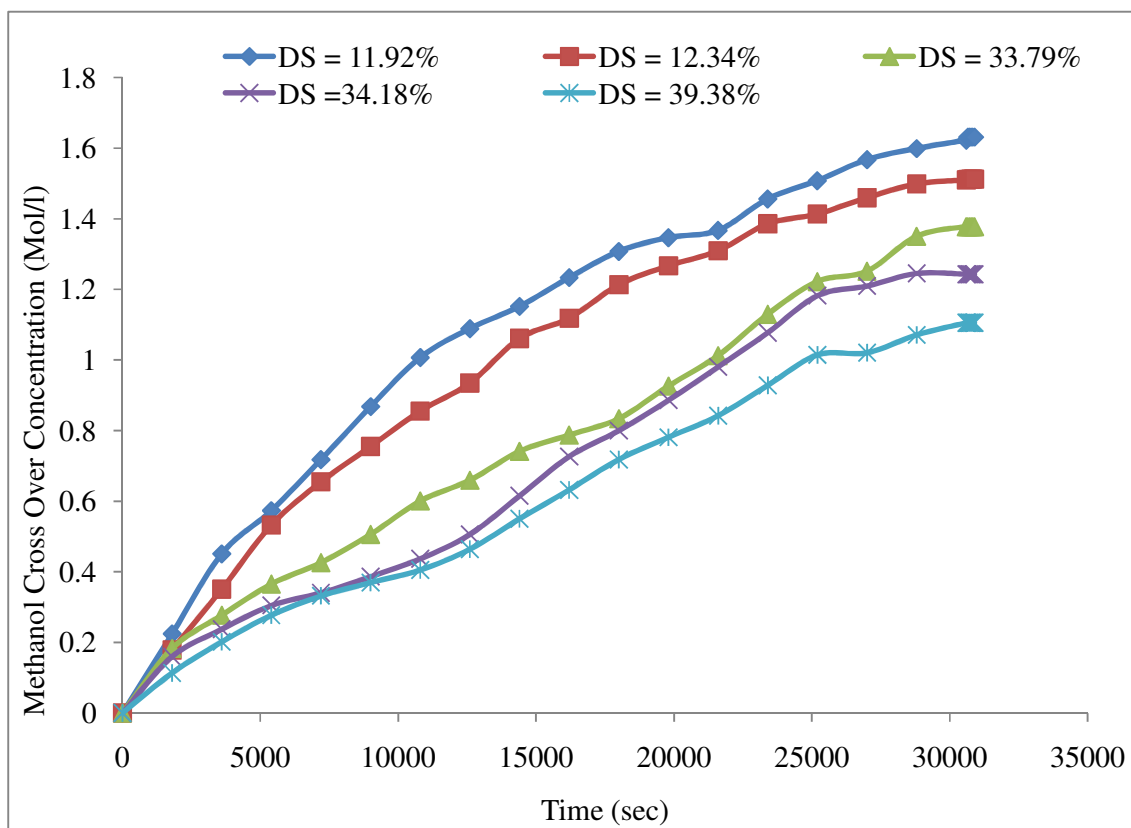


Figure 5.39: Methanol crossover concentration at different degrees of sulphonation

Results obtained as presented in Figure 5.39 reveal that at the same thickness, the membrane with a lower degree of sulphonation exhibits a higher methanol crossover, which decreases as the degree of sulphonation increases. This pattern in the results can be attributed to the decrease in equivalent weight as the degree of sulphonation increases. The reduction in equivalent weight results in more sites for the distribution of methanol within the membrane matrix, while the remaining methanol that the membrane could not hold crosses to the other side of the membrane. Figure 5.40 presents the dependence of methanol crossover on the mass of CNBs in the composite membrane. It can be observed from the results that the methanol crossover of the membrane reduces as the mass of CNBs in the composite membrane increases. This can be attributed to the reduction in the membrane pore size as the mass of CNBs increases. The presence of CNBs in the membrane also provides more sites for methanol distribution within the polymer matrix, thus reducing the quantity of methanol that diffuses through the membrane.

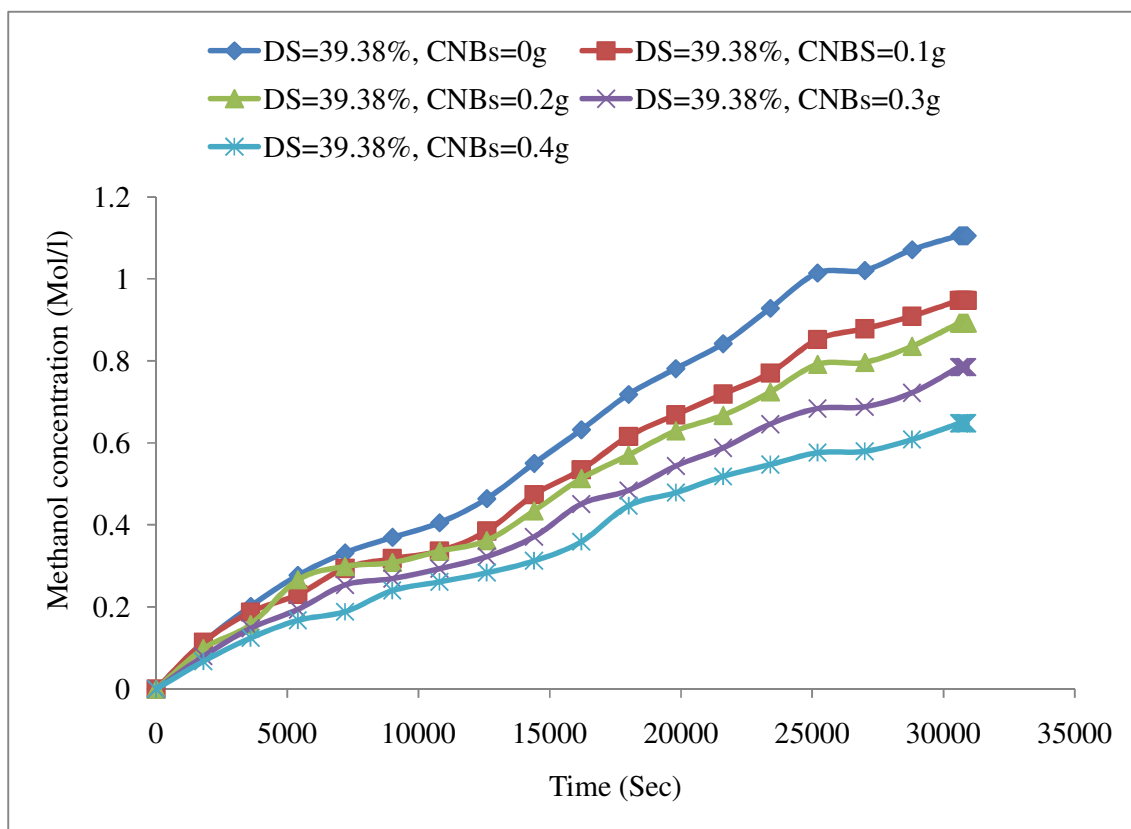


Figure 5.40: Methanol crossover concentration at different masses of CNB

The results obtained from the methanol crossover were used to determine the overall diffusion coefficient and methanol permeability using Equation 5.12 (Shen et al, 2005). To evaluate the methanol permeability of the synthesized membrane, the following assumptions were made (Shen et al, 2005):

- Methanol solution diffuses through the membrane obeying Fick's law.
- Methanol solutions at both sides of the membrane are at equilibrium as a result of stirring.
- Proportional relationship exists between methanol concentration of bulk solution and membrane wall in contact with the solution.

Based on the assumptions stated above, methanol diffuses from compartment A to B because  $C_A > C_B$ . Therefore, the methanol permeation will be obtained with the methanol concentration of compartment B with relation to time using equation 5.11

$$\frac{dC_B}{dt} = A_m \frac{\wp_{AB} K^m}{d_m V_0} (C_{A0} - 2C_B) \quad (5.11)$$

Where:  $C_A$  is the concentration of methanol in compartment A and  $C_B$  is the concentration of methanol in compartment B.  $V_0 = V_A + V_B$ , where  $V_A$  and  $V_B$  are the methanol volume in compartment A and B, respectively,  $A_m$  is the area of the membrane while  $d_m$  is the membrane thickness.

Upon integration of Equation 5.11, the relationship between the changes in concentration as a function of time was obtained as shown in Equation 5.12:

$$\frac{1}{2} \ln \frac{C_{A0}}{C_{A0} - 2C_B} = A_m \frac{\wp_{Am} K^m}{d_m V_0} t \quad (5.12)$$

Where  $\wp_{Am}$  = diffusion coefficient,  $K^m$  = Proportional constant and  $\wp_m K^m$  = overall methanol diffusion coefficient. The slope of the plot of  $\frac{1}{2} \ln \frac{C_{A0}}{C_{A0} - 2C_B}$  against time as presented in Figures 5.41 and 5.42 at different degrees of sulphonation and various masses of CNBs in the composite membrane is equal to  $A_m \frac{\wp_{Am} K^m}{d_m V_0}$ . The overall diffusion coefficient of the synthesized membrane was then determined from the slope

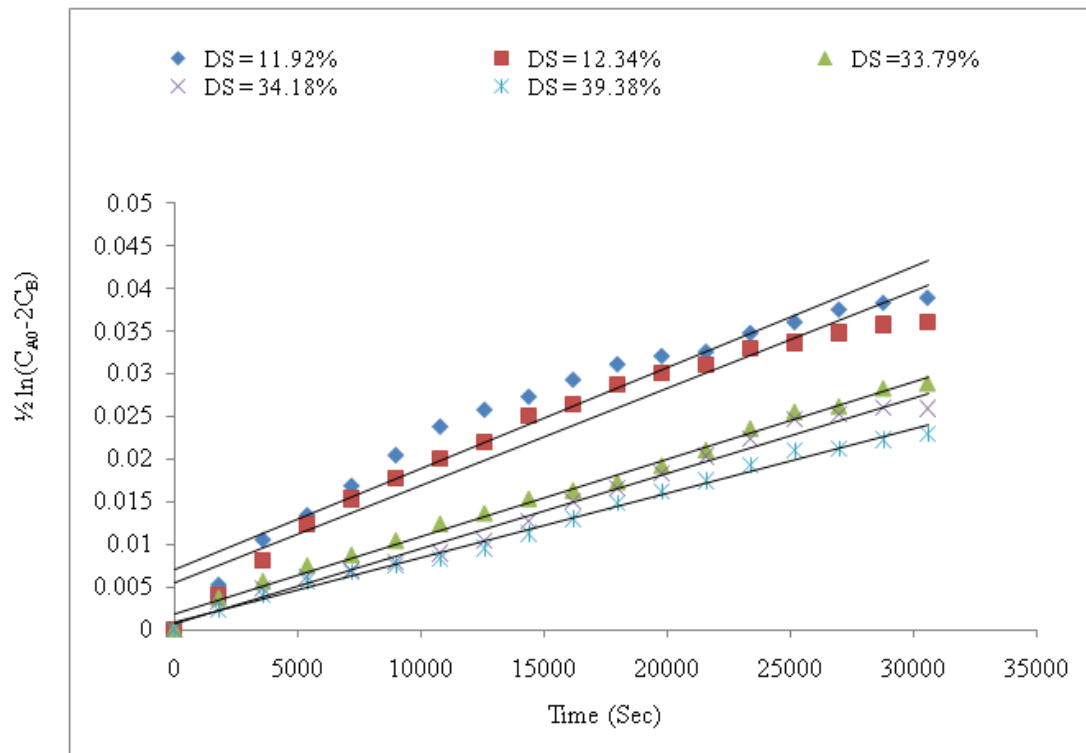


Figure 5.41: Plot of  $\frac{1}{2} \ln \frac{C_{A0}}{C_{A0}-2C_B}$  against time at different degrees of sulphonation (Marks: experiment; line: curve fitting)

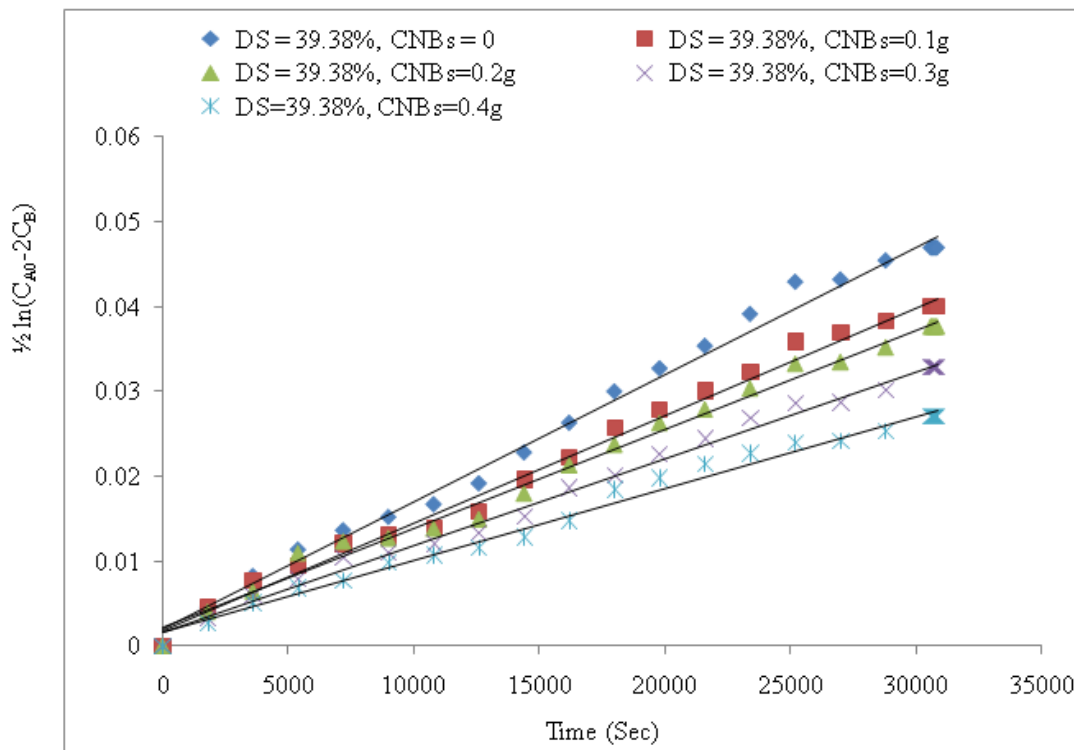


Figure 5.42: Plot of  $\frac{1}{2} \ln \frac{C_{A0}}{C_{A0}-2C_B}$  against time at different mass of CNBs (Marks: experiment; line: curve fitting)

Effects of DS on the measure of overall diffusion coefficients of the synthesized membrane at different membrane thickness are presented in Table 5.8. Results obtained show that the synthesized membrane from polystyrene butadiene rubber exhibited lower methanol diffusion coefficient compared with Nafion<sup>®</sup> 117 ( $3.42 \times 10^{-6} \text{ cm}^2/\text{s}$ ) (Shen et al, 2005). Comparing the overall diffusion coefficient with DS of the synthesized membrane, it could be observed that the membranes with lower DS have a larger methanol overall diffusion coefficient than those with higher DS.

Table 5.8: Overall diffusion coefficient of the membrane at different thickness and degree of sulphonation

DS (%)	Overall diffusion coefficient (cm <sup>2</sup> /s) × 10 <sup>-7</sup>					
	Membrane thickness (μm)					
	112	115	117	220	350	420
3.86	3.45	3.42	3.41	4.51	5.37	5.12
5.89	3.33	3.31	3.29	4.36	5.19	4.96
15.39	2.62	2.61	2.60	3.46	4.12	4.32
29.45	2.57	2.55	2.54	3.39	4.04	4.23
39.38	2.19	2.18	2.17	2.9	3.46	3.63

The overall diffusion coefficient determined from the slope of the graph shown in Figure 5.41 was used to evaluate the methanol permeation using Equation 5.13, and the results obtained at different degrees of sulphonation and membrane thickness are shown in Figure 5.43

$$J = \phi_{Am} \frac{dC_m}{dm} \quad (5.13)$$

Where:  $\phi_{Am}$  is the overall diffusion coefficient,  $dC_m$  is the concentration of methanol and  $J$  is the methanol permeation

The results presented in Figure 5.43 show that methanol permeability at the same degree of sulphonation decreases with increasing thickness. The methanol permeability of the synthesized membrane is considerably lower than that of the Nafion<sup>®</sup> 115 membrane ( $3.15 \times 10^{-6} \text{ mol cm}^2/\text{s}$ ). The methanol permeability of the synthesized membrane ranges from  $2.13 \times 10^{-7} - 7.18 \times 10^{-7} \text{ mol cm}^2/\text{s}$ , which is lower than that of Nafion<sup>®</sup>. The low methanol permeability values of the synthesized membrane are indications that the methanol crossover rate for the synthesized membrane would be drastically reduced. This will improve the performance of the DMFC utilizing the synthesized membrane over Nafion<sup>®</sup> membrane.

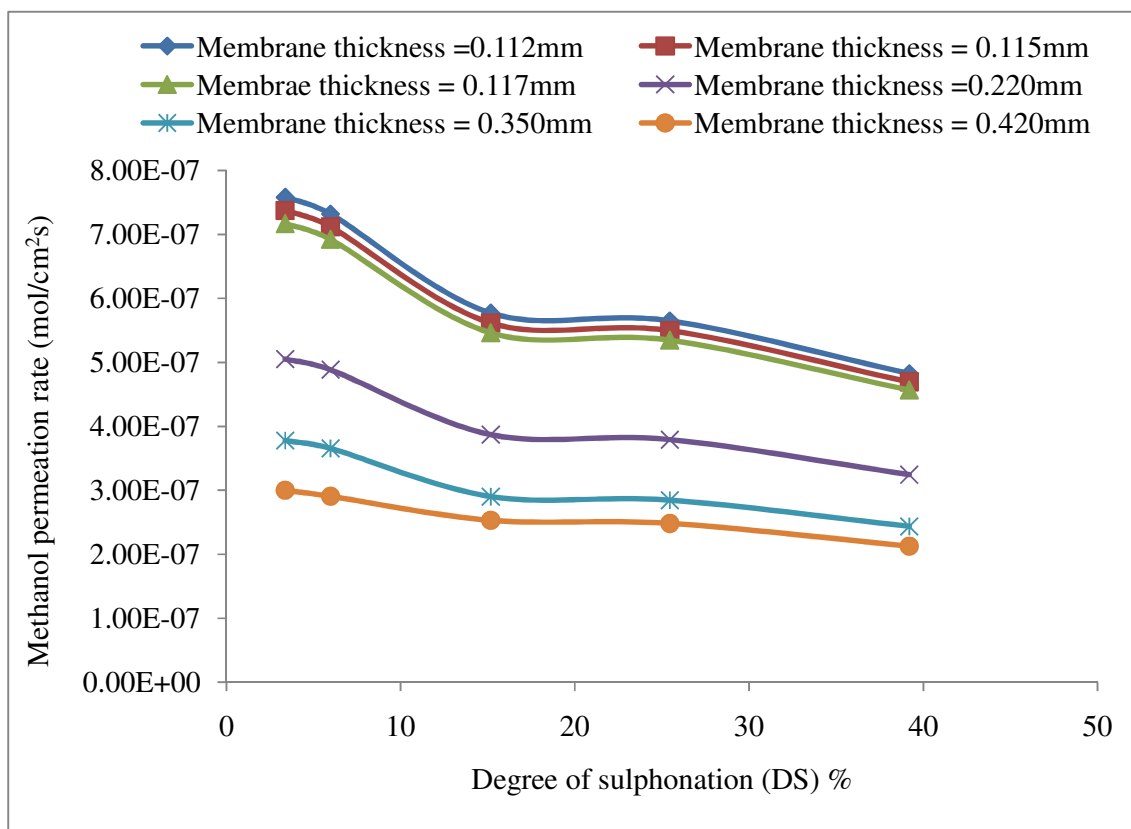


Figure 5.43: Methanol permeation at different degree of sulphonation and membrane thickness

Membranes with high permeability result in a high methanol permeating from anode to cathode where it directly reacts with oxygen, a phenomenon which leads to an efficiency reduction in the fuel cell (Matsuguchi and Takahashi, 2006). In fuel cell applications, the methanol permeation per unit area can be evaluated theoretically from Equation 5.13. Figure 5.44 presents typical theoretical evaluations of methanol permeation at different DS, membrane thickness and methanol concentration of 2 Mol/l.

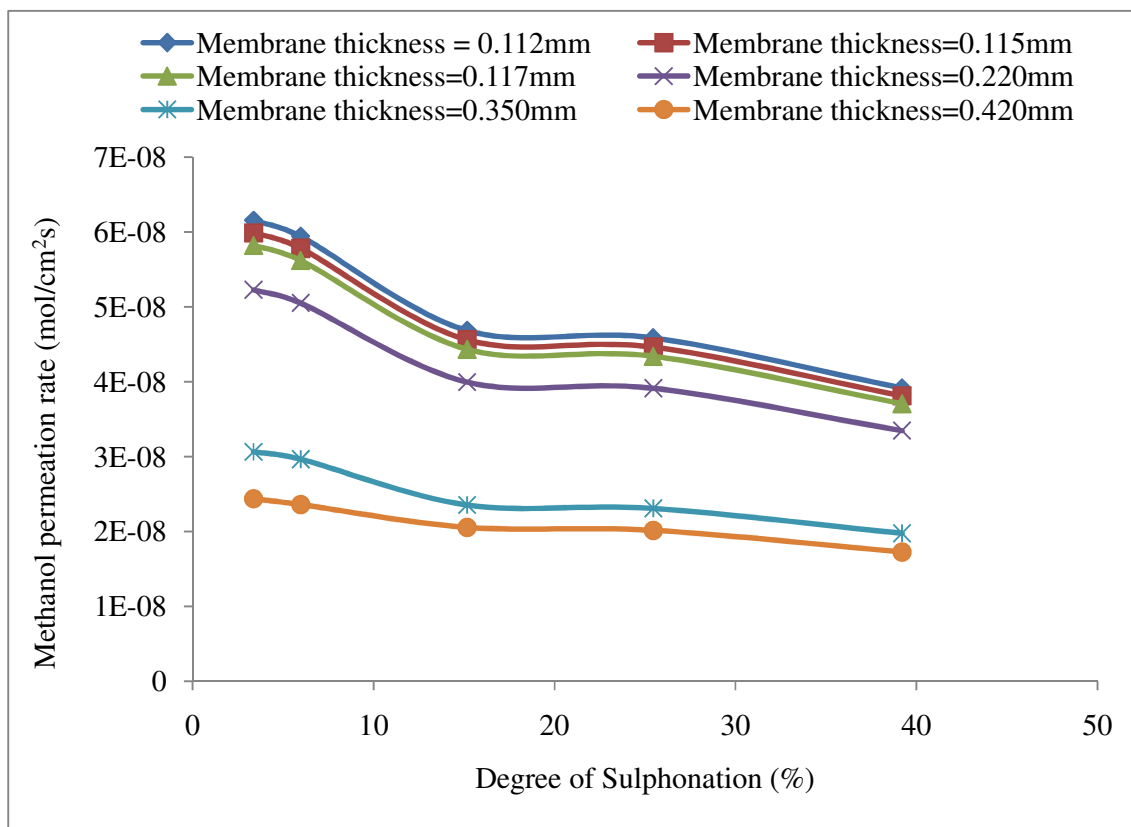


Figure 5.44: Theoretically calculated methanol permeation

Table 5.9 shows the effects of CNBs on the methanol permeability of the composite membranes. Results obtained indicate that as the mass of CNBs increases, the methanol permeability of the composite membranes decreases. This is an indication that the blending of CNBs with membrane will influence the performance of the membrane in fuel cell application. Factor ( $\phi$ ) known as a characteristic factor was also used to justify the performance of the composite membrane in the fuel cell.

Table 5.9: Characteristic factor of the composite membranes

Mass of CNBs (g)	Proton conductivity (S/cm)	Methanol permeability X 10 <sup>-7</sup> (mol/cm <sup>2</sup> s)	Characteristic factor
0	0.013275	7.329	18.11
0.1	0.014602	6.172	23.66
0.2	0.016062	5.685	28.25
0.3	0.018093	5.004	36.16
0.4	0.019912	4.124	48.29

The characteristic factor ( $\Phi$ ) which is the ratio of proton conductivity to the methanol permeability of the membrane is an effective parameter to justify the membrane performance. The decrease in the methanol permeability in the presence of high ionic conductivity should improve the cell efficiency and power density. The characteristic factor of the composite membranes was calculated using equation (Fang et al, 2007)

$$\Phi = \frac{\sigma}{P} \quad (5.14)$$

Where  $\Phi$  = characteristic factor,  $\sigma$  = proton conductivity (S/cm) and, P= methanol permeability of the membrane (mmol/cm<sup>2</sup>s).

Results as presented in Table 5.9 for the blended membrane indicate that CNBs have certain effects on the qualities of the synthesized membrane. The values obtained increase as the mass of the CNBs in the composite membranes increase: this can be attributed to the influence of the CNBs on the proton conductivity and methanol permeability of the synthesized composite membrane. Comparing the characteristic value of the synthesized membrane with that of Nafion 117 which is 8 and that of Nafion 115 which is 3 (Fang et al, 2007) reveals the following: the higher the characteristic value, the better the performance of the membrane (Bae et al, 2003). It is clear that the

characteristic factor of the synthesized composite membranes as shown in Table 5.9 is higher than that of the Nafion<sup>®</sup>. This indicates that the performance of the synthesized membrane in the fuel cell application will be superior to that of Nafion<sup>®</sup>.

### **5.5 MEA Fabrication and Testing**

Cell performance is one of the main evaluation parameters for fuel cells. During the fuel cell operation, the cell was operated at room temperature (about 25°C), with humidified hydrogen at a flow rate of 712 ml/min and pressure of 20 kPa through the anode. The humidified oxygen entered the stack through the cathode at a flow rate of 433 ml/min and 15 kPa. The Membrane Electrode Assembly (MEA) used in the fuel cell stack was fabricated by sandwiching the synthesized membrane between two electrodes and then hot pressing it at 100°C for 3 minutes at a pressure of 173.53 Psi. Electrodes used in this work were prepared by the impregnation of platinum on carbon nanotubes at varying loadings of platinum on fixed amounts of carbon nanotubes (Afolabi, 2009). This is to investigate the influence of the platinum loading on the catalyst on the performance of MEA in the fuel cell stack (Afolabi, 2009). Prior to the use of fabricated MEA in a fuel cell stack, the MEA was fully hydrated in water, since poor humidification resulted in a lower ionic conductivity. It was also observed during the experiment that the humidification of gases greatly influenced the performance of the cell. Therefore, the hydration of the membrane and humidification of the gases were undertaken so as to enhance the transference of proton from the anode side to the cathode side. In this work, the humidification temperature is equal to the cell temperature (room temperature). In order to understand the effects of the degree of sulphonation on membrane performance, MEA were prepared by using membranes with different degrees of sulphonation. During

the performance test measurement, the testing system was stabilized for more than one hour in order to obtain the constant value for all the parameters of interest. The test results obtained in a single cell stack at different degrees of sulphonation and 40 wt % catalyst electrodes are displayed in Figure 5.45. It was not surprising that increases in the degree of sulphonation resulted in the higher performance of the MEA since such an increase causes an increment in the membrane matrix of the sulphonic acid group, which in turn facilitates the proton transfer ability of the membrane. The higher the proton transfer, the higher the voltage generated and the better the power density produced. For instance, when the degree of sulphonation is equal to 8.23 %, the maximum power density produced by the membrane is approximately equal to  $0.0192 \text{ W/cm}^2$ , while at a higher degree of sulphonation (DS = 39.38%), the power density produced by the membrane is approximately equal to  $0.0737 \text{ W/cm}^2$ .

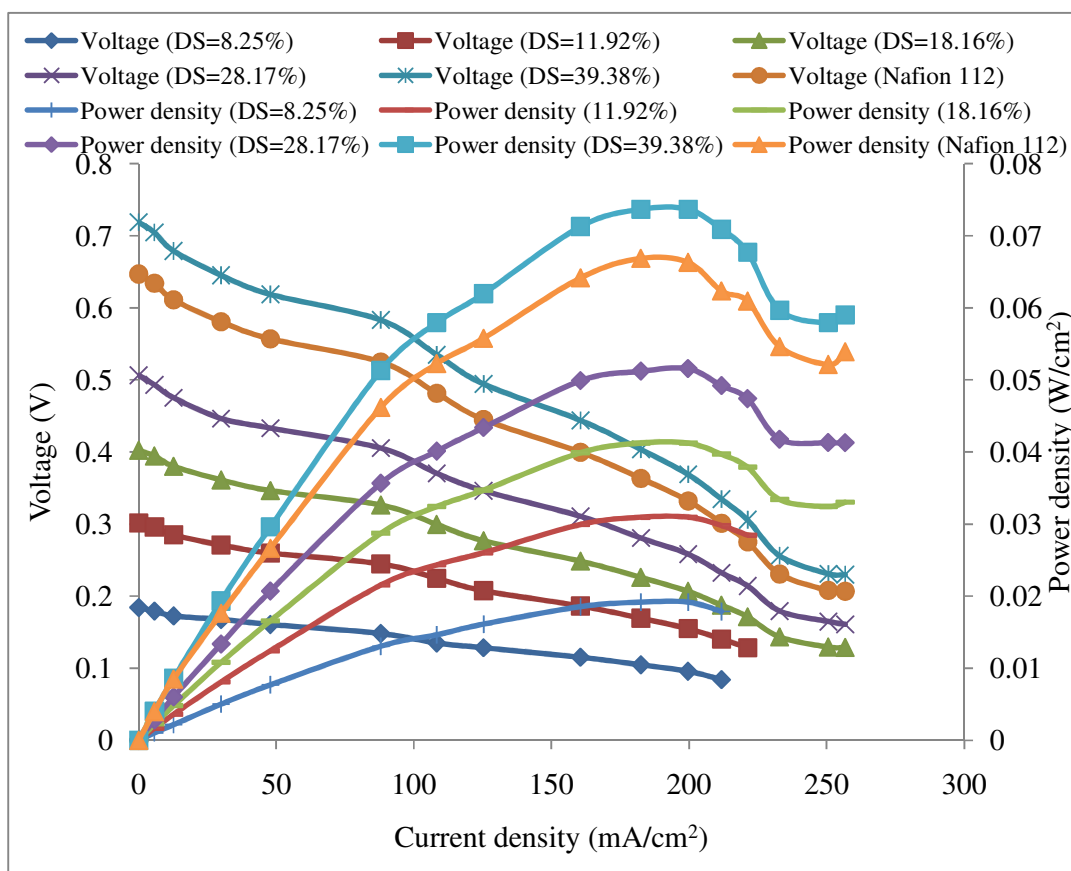


Figure 5.45: Effect of degree of sulphonation on the performance of SPSBR based MEAs.

The effect of using different loadings of catalyst electrode on the performance of the membrane in the single cell stack is explored and the results set out in Figure 5.46. In this instance the membrane is of a constant degree of sulphonation and has a varying weight of catalyst. In this research, Nafion 112 is used to compare the performance of the membrane synthesized from polystyrene butadiene rubber as shown in Figure 5.46. The comparisons of the membranes' performances were made directly on the corresponding polarization curve. As seen in Figure 5.46, the weight of catalyst influenced the performance of the synthesized membrane in the fuel cell stack. Results revealed that as the weight of catalyst increases, the performance of the membrane also increased. This is because the increment in weight of catalyst resulted in a good surface for the

electrochemical reaction in the fuel cell stack; I turn leading to the generation of voltage: however care must be taken to prevent the short circuiting of the stack. The comparison of the two MEAs prepared by sulphonated polystyrene butadiene rubber and Nafion 112 are also given in Figure 5.45. It is apparent that the use of sulphonated polystyrene butadiene rubber resulted in a higher performance at constant 40 % weight of catalyst. Nafion 112 produced a maximum power density of  $0.0669 \text{ W/cm}^2$ , while the use of a membrane synthesized from PSBR resulted in a maximum power density of  $0.0737 \text{ W/cm}^2$  (approximate values). This difference corresponds to about 10.16 % improvement in power density.

The improvement of the membrane blended with carbon nanoballs (SPSBR-CNBs composite membrane) has already been shown in various analysis conducted on the composite membrane and none blended membrane. It is therefore important to prove the superiority of the composite membrane over non-blended membrane in a fuel cell stack, by testing and comparing both in a single cell stack at room temperature. The results obtained are shown in Figure 5.46.

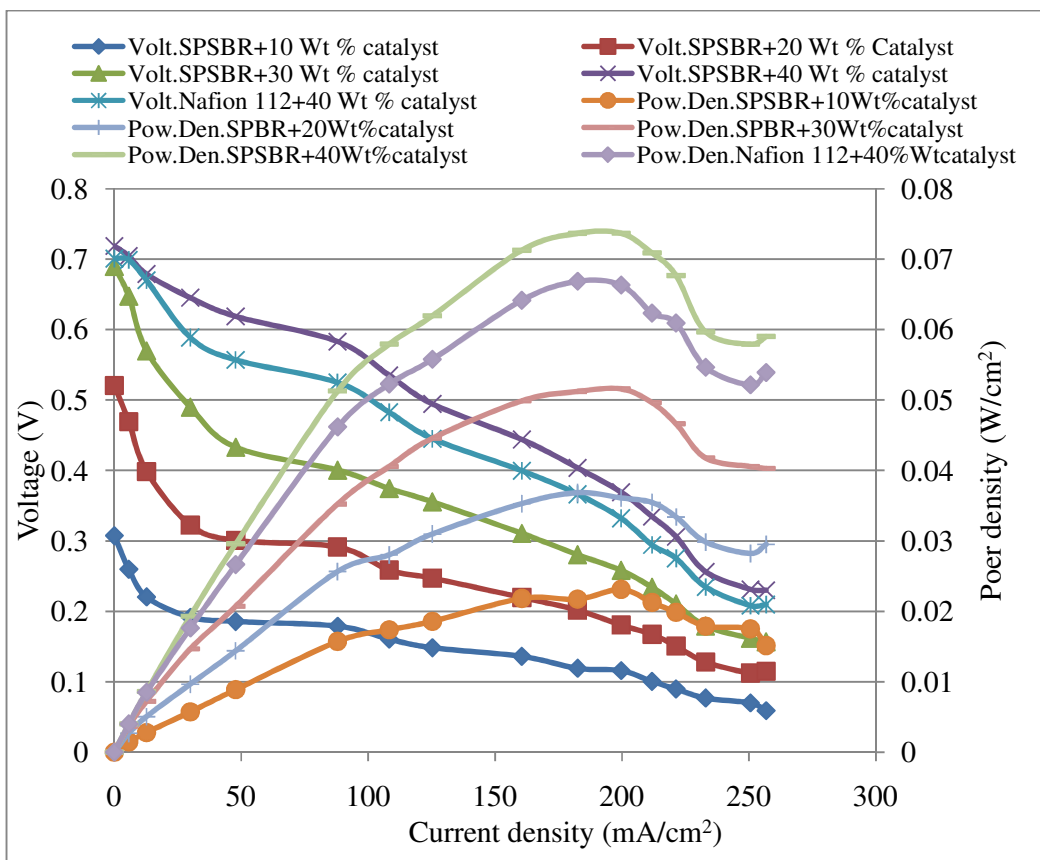


Figure 5.46: Effect of catalyst loading on the performance of SPSBR and Nafion 122 based MEAs.

From Figure 5.47, it becomes clear that the membranes blended with CNBs exhibit a superior performance to non-blended membrane. The former gives a maximum power density in the range of 0.0737-0.0971 W/cm<sup>2</sup>, depending on the mass of CNBs, which is about 6.9-31.75 % higher than the latter as shown in Table 5.10. The better performance of the blended membrane can be attributed to the hydrophilic properties of carbon nanoballs, which contribute to the proton conductivity of the composite membranes. Therefore, the use of CNBs as proton conducting fillers enhances the global proton conductivity of the composite membranes.

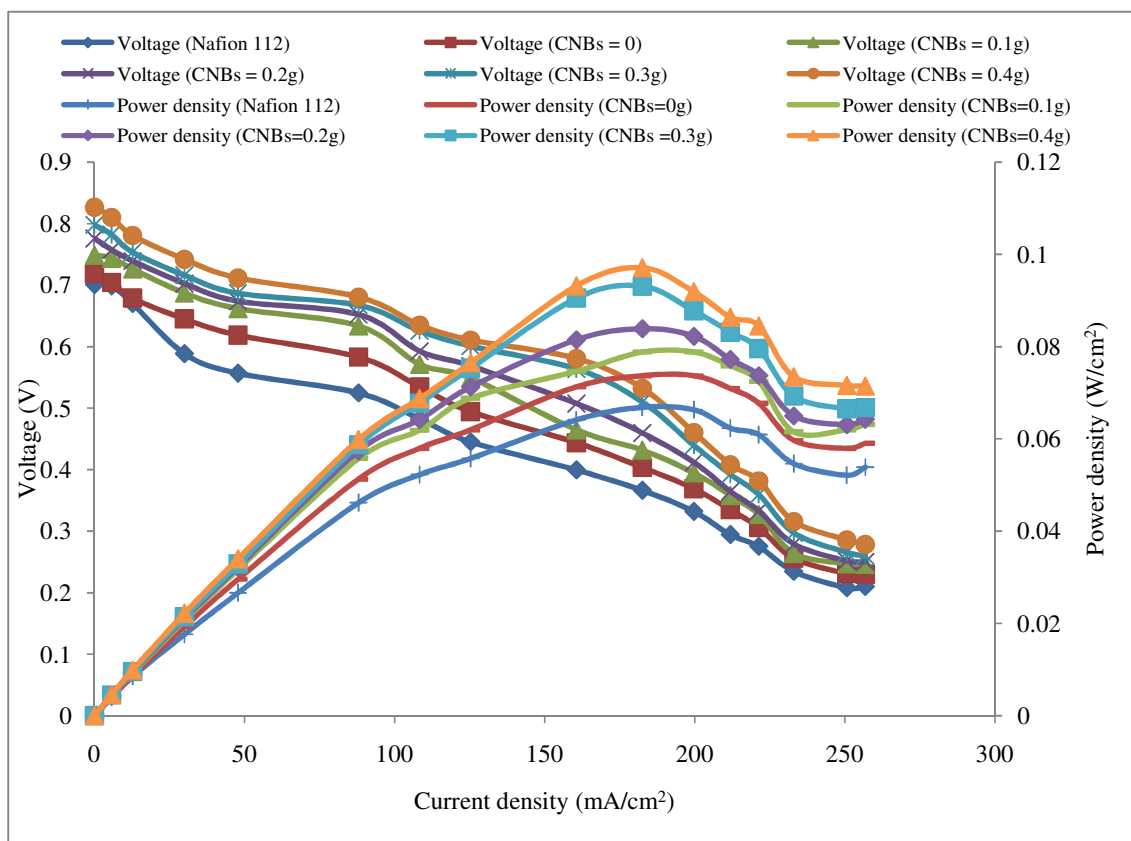


Figure 5.47: Influence of CNBs on the performance of the SPSBR based MEAs

Table 5.10: Effects of mass of CNBs on the performance of SPSBR based MEAs

Mass of CNBs (g)	Maximum power density (W/cm <sup>2</sup> )	Percentage increment relative to non-blended (%)
Nafion 112	0.067	
0	0.074	
0.1	0.079	6.92
0.2	0.0834	13.84
0.3	0.093	26.32
0.4	0.097	31.75

Apart from measuring the current density –voltage polarization curve, the durability in terms of performance of the MEA with time is another major parameter used in evaluating the performance of the membrane in the fuel cell. The MEA fabricated with Nafion 112, synthesized and blended membrane long term stability in the fuel cell stack was tested for a period of 600 minutes and the results obtained are presented in Figure 5.48. It can be observed here that the blended membranes are more stable and durable than non blended membrane, which in turn better in stability than Nafion 112 which is the commercially available membrane. However, due to experimental limitation, the durability test was done for 10 hours.

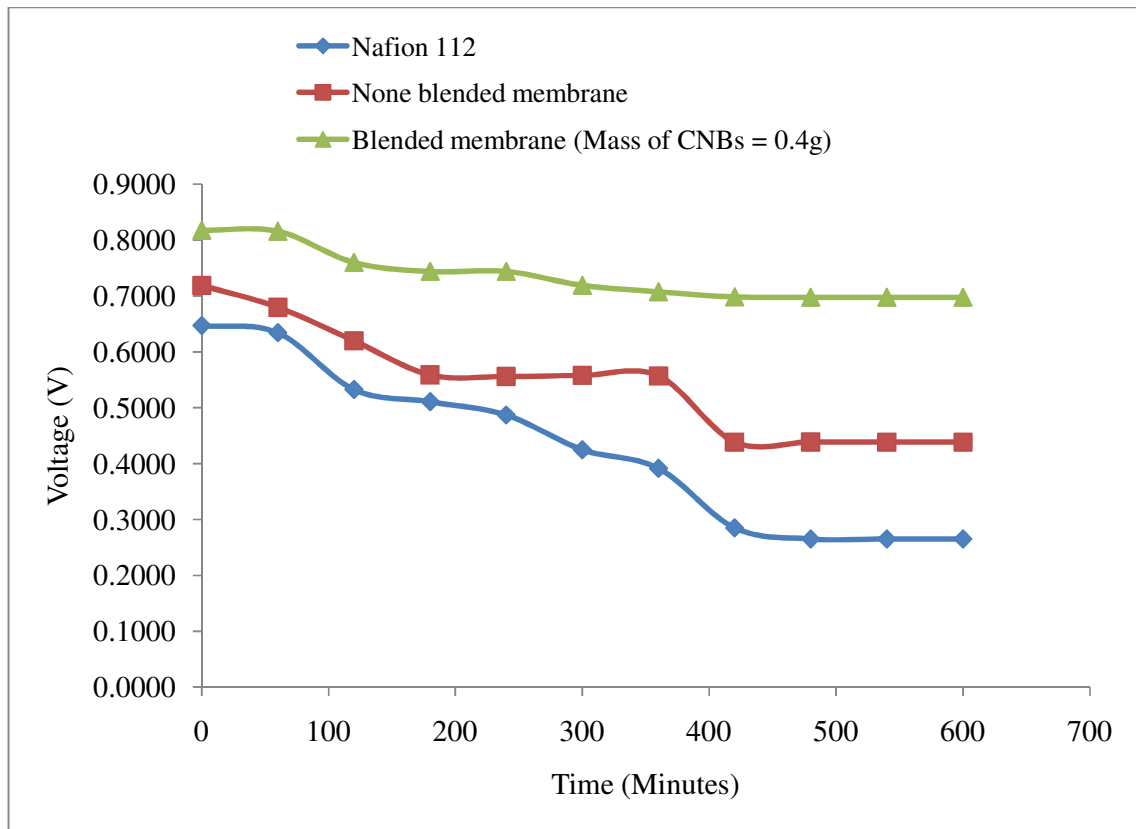


Figure 5.48: Durability of blended and non-blended membrane in a fuel cell stack.

Experimental data was fit to the existing equation of polarization curve from a single cell stack. This equation developed based on the theory of electrochemical reaction (Mahreni et al, 2009)

Iyuke et al., (2003) stated in their work that in low and medium temperature fuel cells, activation overvoltage is the most important irreversibility and cause of voltage drop; these phenomena occur at the oxygen-reducing cathode. Therefore, overvoltage in the fuel cell can be attributed to kinetics which is a function of current density that is directly proportional to the reaction rate in the fuel cell. The cell potential (E) and current density (i) of the fuel cell are related by equation 5.14, thus:

$$E_0 = E + \Delta V \quad (5.14)$$

where,  $E_0$  = open circuit voltage (V),  $E$  = cell voltage (V) and,  $\Delta V$  = overvoltage (V)

From equation 5.14:

$$E = E_0 - \Delta V \quad (5.15)$$

Relationship between over voltage and current density is described by Tafel equation as:

$$\Delta V = A \ln \frac{lni}{lni_0} \quad (5.16)$$

where,  $A$  = Tafel constant (V),  $i_0$  = exchange current density ( $A/cm^2$ )

From equation 5.16, therefore:

$$\Delta V = A \ln i - A \ln i_0 \quad (5.17)$$

Substitute equation 5.17 into 5.15 to obtain:

$$E = E_0 - A \ln i - A \ln i_0 \quad (5.18)$$

Selvarani et al (2007) blame the linear variation of over potential with load current density to the effect of ohmic resistance. It is therefore important to consider the effect of ohmic resistance in the model. Equation 5.18 then becomes,

$$E = E_0 - A \ln i - A \ln i_0 - iR \quad (5.19)$$

Mahreni et al, 2009 considered the effect of flooding on the cell potential, equation 7.54 then becomes;

$$E = E_o - Alni - Alni_0 - iR - \gamma \exp(\omega i) \quad (5.20)$$

Where;  $\gamma$  = flooding constant =  $11.43i^2 - 3.245i + 1.18$

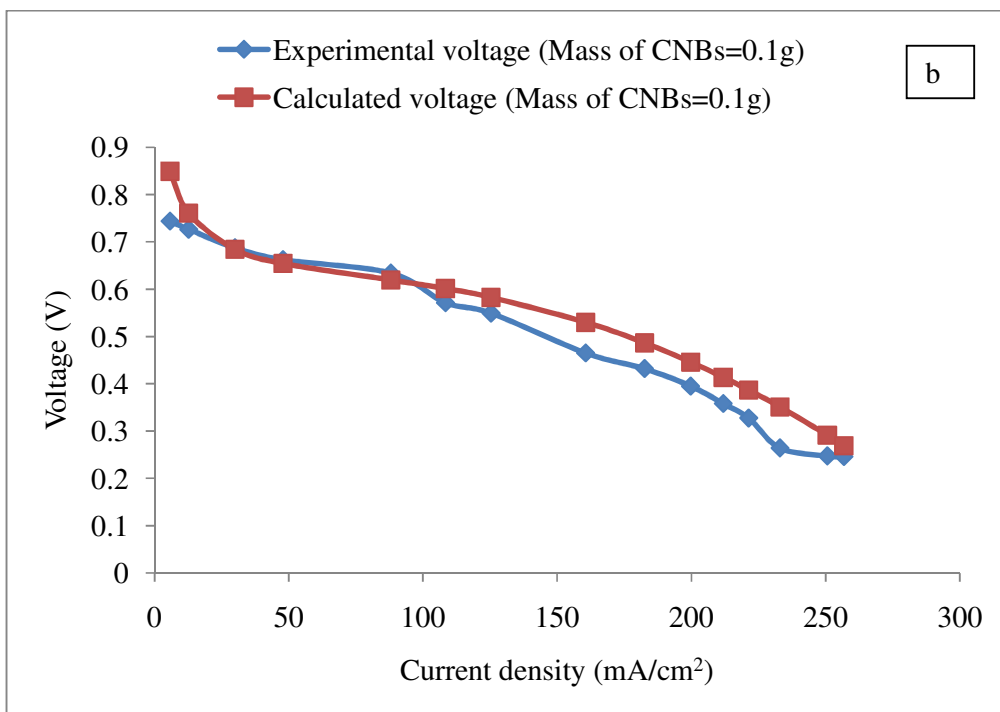
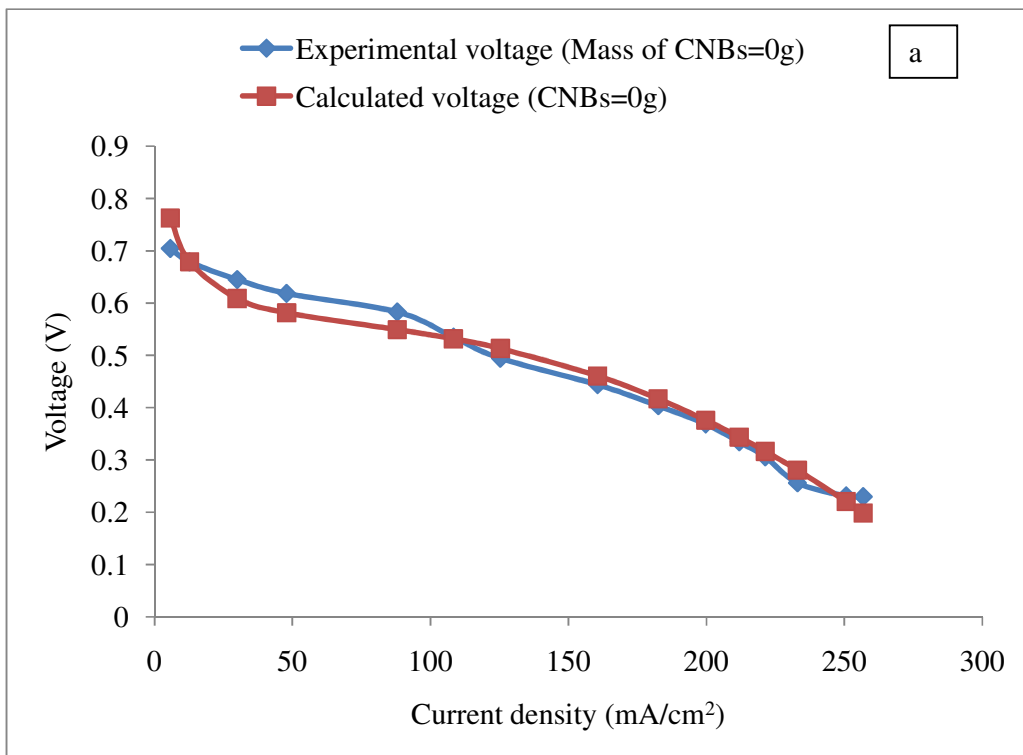
$\omega$  = fitting constant (0.01)

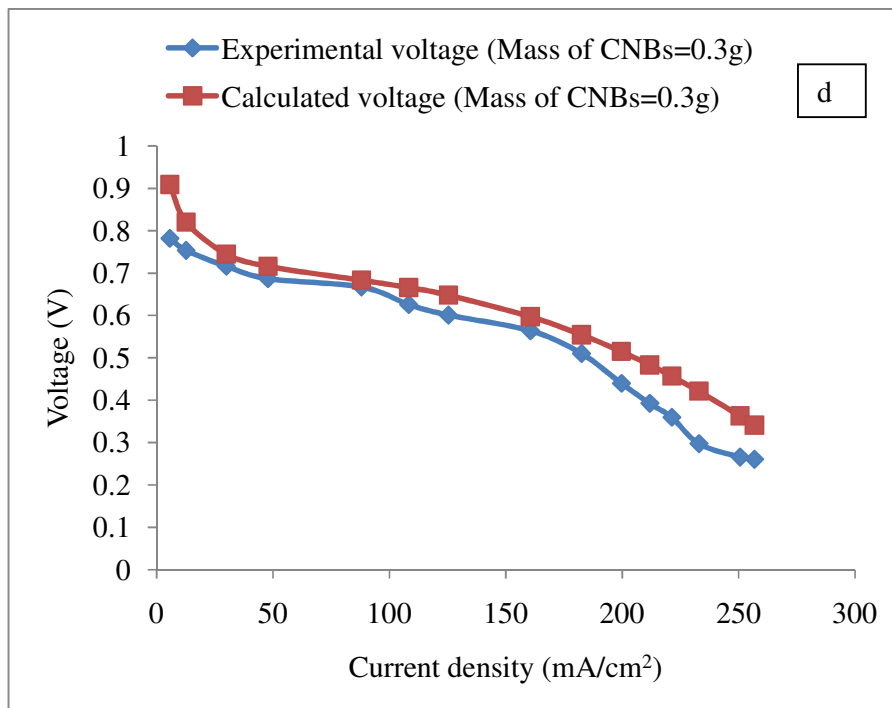
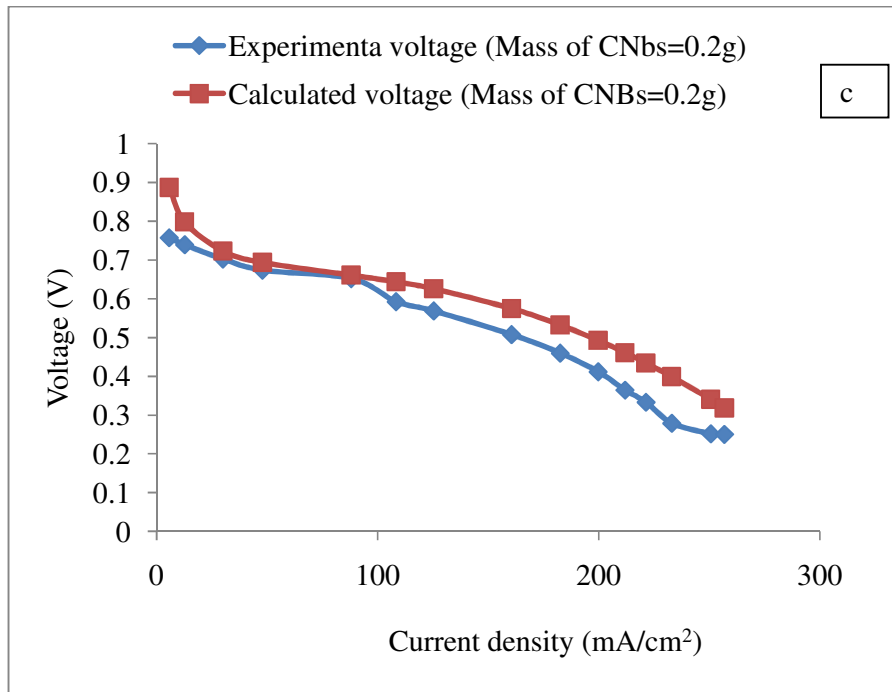
Equation 5.20 is the fit equation for the performance of MEA in a single cell stack. The kinetic parameters for the performance of MEA are presented in Table 5.11. These parameters are obtained from the slope of the polarization curve, while the membrane resistances are obtained from the impedance curve and the flooding parameters and fitting constant are obtained by fitting the data to the equation.

Table 5.11: Electrochemical kinetic parameters for the single fuel cell stack at different mass of carbon nanoballs in the membrane.

Mass of CNBs (g)	$E_0$ (V)	A (V)	R ( $\Omega\text{cm}^2$ )	$i_o$ ( $\text{A}/\text{cm}^2$ )
0	0.719	0.12592	0.573	0.0118
0.1	0.749	0.133589	0.521	0.0135
0.2	0.776	0.133543	0.474	0.0124
0.3	0.798	0.130706	0.421	0.0121
0.4	0.827	0.133607	0.382	0.0119

It can be observed from Table 5.11 that the resistance decreases with increasing the mass of CNBs contents of the composite membrane. This result also confirms the ability of the blended membrane to reduce MEA resistance and thus facilitates proton conduction of the membrane. Equation 5.20 was used to predict the potential of the fuel cell stack at different masses of CNBs in the membrane composites. The results obtained are presented together with experimental results for comparison in Figure 5.49.





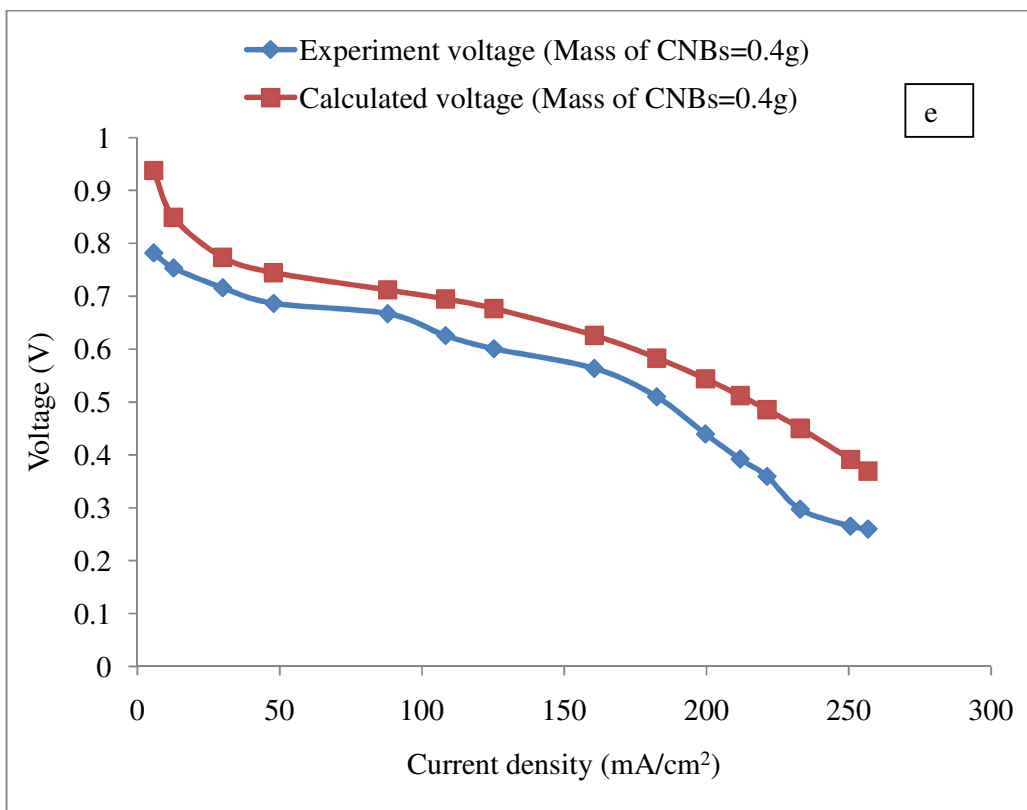


Figure 5.49: Experimental and calculated potential at different current density (a) mass of CNBs = 0g (b) mass of CNBs = 0.1g (c) mass of CNBs = 0.2g (c) mass of CNBs = 0.3g (d) mass of CNBs = 0.4g

The statistical analyses of the calculated and experimental results as shown in Table 5.11 indicate that the calculated results conform well to the experimental results, with slight variation. This variation can be attributed to inconsistency in the flooding parameters. It can be inferred from the performance test of the MEA in a single fuel cell stack at room temperature that the composite membrane presents a better performance than the non blended membrane which in turn present better performance than Nafion 112.

Table 5.11: Error analysis for the calculated and experimental results

<b>Mass of CNBs (g)</b>	<b>Standard error</b>	<b>Correlation coefficient</b>	<b>Standard deviation</b>
0	0.028	0.987	0.164
0.1	0.033	0.983	0.173
0.2	0.032	0.983	0.175
0.3	0.033	0.982	0.175
0.4	0.030	0.985	0.17

In conclusion therefore, results of various analysis obtained revealed that the synthesized membrane possesses better qualities (solvent uptake, methanol permeability and thermal stability) in comparison to the Nafion 112 which is the commercially available membrane. Results also revealed that blending of membrane with CNBs improve the qualities of the membrane with more than 50% increase in proton conductivity. Performance evaluation of the synthesized membrane in a single fuel cell stack also indicates that the blended membrane exhibited a superior performance to none blended membranes, which in turn better in performance than the Nafion 112.